

Leibniz-Institut für Meereswissenschaften

# Production and Emissions of Oceanic Nitrous Oxide

Dissertation  
zur Erlangung des Doktorgrades  
der Mathematisch-Naturwissenschaftlichen Fakultät  
der Christian-Albrechts-Universität  
zu Kiel

vorgelegt von

Alina Freing

Kiel

2009

Referent: PD Dr. habil. Hermann W. Bange  
Korreferent: Prof. Dr. Douglas W. R. Wallace

Tag der mündlichen Prüfung: 02.11.2009  
Zum Druck genehmigt: 02.11.2009

gez. Prof. Dr. rer. nat. Lutz Kipp  
– Dekan –

It is the task of scientists to clear away the mysteries, on the understanding that they find them back a bit further on. But still, it is agreeable to have progressed a little.

*Henri Poincaré*



## This thesis is based on the following manuscripts:

1. **Manuscript:** Freing, A., D. W. R. Wallace, T. Tanhua, S. Walter, and H. W. Bange(2009), North Atlantic production of nitrous oxide in the context of changing atmospheric Levels, *Global Biogeochemical Cycles*, 23, GB4015, doi: 10.1029/2009GB003472.

**Contribution:** Alina Freing performed the calculations, evaluated the data and wrote the paper. Douglas W. R. Wallace and Hermann W. Bange assisted with input to the manuscript and revision. Toste Tanhua provided the tracer data, assisted with the TTD calculations and reviewed the manuscript. Sylvia Walter provided the N<sub>2</sub>O data and reviewed the manuscript.

2. **Manuscript:** Freing, A., D. W. R. Wallace, T. Tanhua, S. Walter, and H. W. Bange, North Atlantic Nitrous Oxide Emissions, *manuscript*, 2009.

**Contribution:** Alina Freing performed the calculations, evaluated the data and wrote the paper. Douglas W. R. Wallace and Hermann W. Bange assisted with input to the manuscript and revision. Toste Tanhua provided the tracer data. Sylvia Walter provided the N<sub>2</sub>O data.

3. **Manuscript:** Freing, A., D. W. R. Wallace, T. Tanhua, and H. W. Bange, Global Subsurface Nitrous Oxide Production, *manuscript*, 2009.

**Contribution:** Alina Freing performed the calculations, evaluated the data and wrote the paper. Douglas W. R. Wallace and Hermann W. Bange assisted with input to the manuscript and revision. Toste Tanhua assisted with the TTD calculations and reviewed the manuscript.



# Contents

<b>Zusammenfassung</b>	<b>1</b>
<b>Summary</b>	<b>3</b>
<b>1 Introduction</b>	<b>5</b>
1.1 Nitrous Oxide . . . . .	7
1.2 Distribution of N <sub>2</sub> O . . . . .	14
1.3 Sensitivities to Change . . . . .	18
1.4 Thesis Outline . . . . .	23
<b>2 North Atlantic Production of Nitrous Oxide</b>	<b>25</b>
2.1 Methods . . . . .	26
2.2 Results & Discussion . . . . .	35
2.3 Conclusions . . . . .	45
<b>3 North Atlantic Nitrous Oxide Emissions</b>	<b>47</b>
3.1 Methods . . . . .	47
3.2 Results & Discussion . . . . .	51
3.3 Conclusions . . . . .	68
<b>4 Global Subsurface Nitrous Oxide Production</b>	<b>71</b>
4.1 Methods . . . . .	71
4.2 Results & Discussion . . . . .	79
4.3 Conclusions . . . . .	91
<b>5 Conclusions and Outlook</b>	<b>93</b>
<b>Acknowledgements</b>	<b>99</b>
<b>Bibliography</b>	<b>101</b>





# Zusammenfassung

Die Zielsetzung dieser Arbeit war es, mit Hilfe vorhandener in-situ  $\text{N}_2\text{O}$ - und Tracer-Daten aus dem zentralen Nord-Atlantik die  $\text{N}_2\text{O}$ -Produktion und bestehende Zusammenhänge zwischen der  $\text{N}_2\text{O}$ -Produktion und anderen (chemischen) Parametern zu untersuchen. Transit Time Distributions (TTD) wurden benutzt, um die Konzentration von biologisch produziertem  $\text{N}_2\text{O}$  ( $[\text{N}_2\text{O}]_{xs}$ ) abzuschätzen und  $\text{N}_2\text{O}$ -Produktionsraten für den Nord-Atlantik zu berechnen. Bisher benutzte Methoden haben die Equilibrium-Konzentration von  $\text{N}_2\text{O}$  um 8% – 13% überschätzt, was zu einer verzerrten Darstellung der quantitativen Charakteristiken der viel benutzen Beziehung zwischen dem (biologischen) Sauerstoff-Verbrauch (AOU) und  $[\text{N}_2\text{O}]_{xs}$  geführt hat. Es wurden neue Parametrisierungen für die  $\text{N}_2\text{O}$ -Produktion durch Nitrifizierung entwickelt, die linear vom (biologischen) Sauerstoff-Verbrauch (AOU) und exponentiell von der Temperatur bzw. der Tiefe abhängen. Diese Parametrisierungen lassen sich auch zur Berechnung der  $\text{N}_2\text{O}$ -Produktion durch Nitrifizierung in Sauerstoff-Minimum-Zonen verwenden.

Mittels der Nord-Atlantik-Daten wurden ebenfalls der Fluss von  $\text{N}_2\text{O}$  in die Mischungsschicht durch diapyknische Vermischung ( $F_{grad}$ ) und der durch Gasaustausch bedingte  $\text{N}_2\text{O}$ -Fluss in die Atmosphäre ( $F_{gase}$ ) ausgerechnet. Der mittlere jährliche Fluss in die Mischungsschicht ist deutlich kleiner, als die mittleren jährlichen  $\text{N}_2\text{O}$ -Emissionen. Ein möglicher Grund dafür ist die Saisonalität von  $p\text{N}_2\text{O}/F_{gase}$ , da sich die Differenz deutlich reduziert, wenn man statt eines simplen Mittelwerts der extrapolierten täglichen (meist aus dem Sommer stammenden) Flüsse einen über einen vollständigen Jahresgang integrierten Fluss zur Abschätzung von  $F_{gase}$  verwendet. Letzteres liefert einen jährlichen  $\text{N}_2\text{O}$ -Fluss von  $-2 \pm 1 \mu\text{mol m}^{-2}$  (LM86) bzw.  $10 \pm 2 \mu\text{mol m}^{-2}$  (W92) vom Ozean in

die Atmosphäre, der dem geschätzten  $F_{grad}$  von  $3 \pm 1 \mu\text{mol m}^{-2}$  vergleichbar ist. Obwohl der Jahresgang von  $p\text{N}_2\text{O}$  im Vergleich mit  $p\text{CO}_2$  keinen Hinweis auf eine biologische Beeinflussung von  $\text{N}_2\text{O}$  in der Mischungsschicht liefert, kann eine  $\text{N}_2\text{O}$ -Quelle in der Mischungsschicht als Ursache für die restliche Differenz zwischen  $F_{grad}$  und  $F_{gase}$  wegen einer mangelhaften saisonalen/geographischen Auflösung nicht ausgeschlossen werden. Im Vergleich mit einer jährlichen  $\text{N}_2\text{O}$ -Produktion von  $14 \pm 10 \mu\text{mol m}^{-2}$  unterhalb der Mischungsschicht (berechnet für die Stationen von M60/5) würde eine  $\text{N}_2\text{O}$ -Produktion von  $7 \pm 2 \mu\text{mol m}^{-2} \text{yr}^{-1}$  einen signifikanten Anteil der gesamten ozeanischen  $\text{N}_2\text{O}$ -Produktion stellen.

Eine jährliche  $\text{N}_2\text{O}$ -Produktion unterhalb der Mischungsschicht von  $3.1 \pm 0.9 \text{ Tg N}$  bzw.  $3.4 \pm 0.9 \text{ Tg N}$  wurde mit Hilfe unserer Parametrisierungen, Gitter-Daten und einer Abschätzung der  $\text{N}_2\text{O}$ -Produktion/des  $\text{N}_2\text{O}$ -Abbaus durch Denitrifizierung ( $\sim 7\%$  der Produktion durch Nitrifizierung) abgeschätzt. Die jährliche Remineralisationsrate von organischem Kohlenstoff wurde auf Basis der geschätzten jährlichen Sauerstoff-Verbrauchsrate auf  $17.6 \text{ Pg}$  geschätzt. Der Vergleich unserer neuen, datenbasierten Abschätzung der  $\text{N}_2\text{O}$ -Produktion mit Literaturwerten kommt zu einem ähnlichen Ergebnis wie der Vergleich der verschiedenen Flüsse im Nord-Atlantik: es besteht eine gewisse Diskrepanz zwischen der jährlichen  $\text{N}_2\text{O}$ -Produktion unterhalb der Mischungsschicht und existierenden, auf Parametrisierungen des Gasaustauschs basierenden Abschätzungen der globalen ozeanischen  $\text{N}_2\text{O}$ -Emissionen. Mögliche Ursachen für diese Diskrepanz, wie zum Beispiel eine durch eine Extrapolation über längere Zeitspannen und/oder einen Jahresgang bedingte systematische Verzerrung der abgeschätzten Gasaustausch-Emissionen oder eine  $\text{N}_2\text{O}$ -Quelle in der Mischungsschicht, werden diskutiert.

# Summary

The aim of this study was to analyse an existing dataset of in-situ North Atlantic Ocean  $\text{N}_2\text{O}$  and tracer data in order to investigate  $\text{N}_2\text{O}$  production and its relationship to other (chemical) parameters. Transit time distributions (TTD) calculated from these data were used to estimate the concentration of biologically produced  $\text{N}_2\text{O}$  ( $[\text{N}_2\text{O}]_{xs}$ ) and  $\text{N}_2\text{O}$  production rates in the central North Atlantic Ocean. Previously used approaches were found to have overestimated the oceanic equilibrium  $\text{N}_2\text{O}$  concentrations by 8% – 13% resulting in a biased description of the widely used relationship between apparent oxygen utilisation (AOU) and  $[\text{N}_2\text{O}]_{xs}$ . A new parameterisation of  $\text{N}_2\text{O}$  production during nitrification depending linearly on AOU and exponentially on temperature/depth was developed and was applied to calculate  $\text{N}_2\text{O}$  production due to nitrification in the entire ocean.

The dataset was also used to calculate both the  $\text{N}_2\text{O}$  flux to the mixed layer by diapycnal mixing and the  $\text{N}_2\text{O}$  emissions to the atmosphere with standard gas exchange models for the central North Atlantic Ocean. The mean annual  $\text{N}_2\text{O}$  flux to the mixed layer ( $F_{grad}$ ) was found to be significantly smaller than the mean annual  $\text{N}_2\text{O}$  flux across the air-sea interface due to gas exchange ( $F_{gasex}$ ). A possible reason for this is the seasonality of surface  $p\text{N}_2\text{O}/F_{gasex}$ , and the difference was significantly reduced when a seasonally-resolved integrated air-sea flux estimate was used to estimate  $F_{gasex}$  instead of a simple extrapolated mean of (primarily summertime) daily fluxes. It results in a net annual ocean-atmosphere  $\text{N}_2\text{O}$  flux of  $-2 \pm 1 \mu\text{mol m}^{-2}$  (LM86) and  $10 \pm 2 \mu\text{mol m}^{-2}$  (W92), respectively, which compare well to the annual mean  $F_{grad}$  of  $3 \pm 1 \mu\text{mol m}^{-2}$ . Even though the seasonal cycle of  $p\text{N}_2\text{O}$  compared to that of  $p\text{CO}_2$  shows no conclusive evidence of a biological control on mixed layer  $\text{N}_2\text{O}$ , the possibility of a  $\text{N}_2\text{O}$  source in

the mixed layer causing the remaining difference between  $F_{grad}$  and  $F_{gasex}$  cannot be ruled out due to insufficient seasonal/latitudinal data coverage. Compared to an annual subsurface  $N_2O$  production of  $14 \pm 10 \mu\text{mol m}^{-2}$  calculated at the stations of M60/5, a mixed layer production of  $N_2O$  of  $7 \pm 2 \mu\text{mol m}^{-2} \text{ yr}^{-1}$  would constitute an important contribution to oceanic  $N_2O$  production.

A global annual subsurface  $N_2O$  production of  $3.1 \pm 0.9 \text{ Tg N}$  and  $3.4 \pm 0.9 \text{ Tg N}$ , respectively, was estimated using the developed parameterisations on gridded data and together with a data-based estimate of the  $N_2O$  yield due to denitrification ( $\sim 7\%$  of the production due to nitrification). A global annual organic carbon remineralisation rate of  $17.6 \text{ Pg}$  was estimated based on a global estimate of the apparent oxygen utilisation rate. The results agree with the findings for the North Atlantic Ocean, showing that there is a discrepancy between the subsurface  $N_2O$  yield and existing global ocean-atmosphere flux estimates based on gas exchange parameterisations. Possible reasons for this, such as a systematic bias in gas-exchange estimates due to extrapolation over long time periods and/or seasonal variability or a  $N_2O$  source in the mixed layer, are discussed.

# Chapter 1

## Introduction

Human activities including the burning of fossil fuels are known to influence our climate by changing the concentration of greenhouse gases in Earth's atmosphere [Forster *et al.*, 2007]. Changing the abundance and concentration of greenhouse gases in the atmosphere affects climate by altering the radiative balance of the Earth. Overall, since the industrial revolution ( $\sim 1750$ ) these effects have exerted a warming influence. This anthropogenic impact on climate greatly exceeds any impact wielded by natural processes such as solar radiation changes and volcanic eruptions [Forster *et al.*, 2007].

The IPCC's Fourth Assessment Report distinguishes four principal greenhouse gases [Forster *et al.*, 2007]: carbon dioxide ( $\text{CO}_2$ ), methane ( $\text{CH}_4$ ), nitrous oxide ( $\text{N}_2\text{O}$ ) and the halocarbons. Based on its radiative forcing,  $\text{N}_2\text{O}$  is ranked fourth among this group of the so-called long-lived greenhouse gases. However, as atmospheric  $\text{N}_2\text{O}$  shows a continuing increase and the atmospheric concentrations of important halocarbons are slowly decreasing,  $\text{N}_2\text{O}$  is expected to take over third place in this ranking [Forster *et al.*, 2007].  $\text{N}_2\text{O}$  is emitted to the atmosphere as a result of human activities such as fertiliser use and fossil fuel burning [Forster *et al.*, 2007]. Natural processes in soils and the oceans also release  $\text{N}_2\text{O}$  [Forster *et al.*, 2007].

The effectiveness of the different greenhouse gases is evaluated using the concept of global warming potentials. The global warming potential (GWP) is defined as the ratio of the time-integrated radiative forcing from a pulse emission of 1 kg of some compound  $X$  relative to that of 1 kg of the reference gas  $\text{CO}_2$  [Houghton

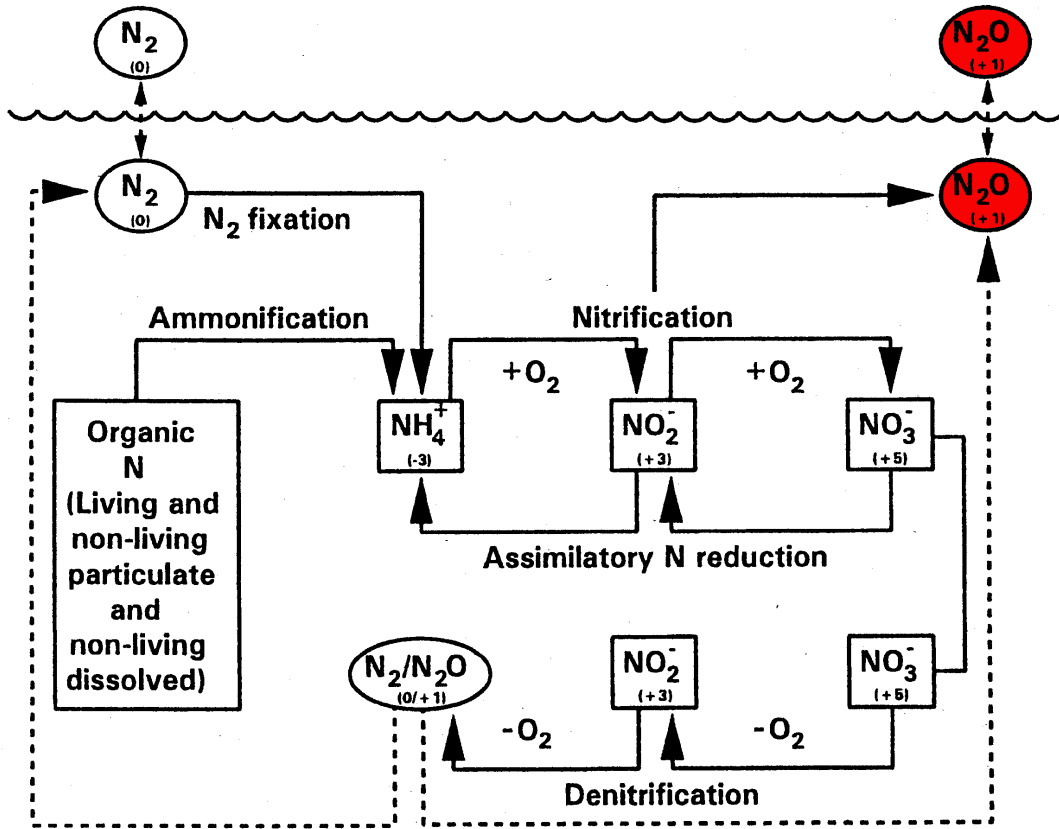


Figure 1.1: The marine nitrogen cycle [Karl *et al.*, 2002]. Oxidation numbers of N are given in brackets.

*et al.*, 1990], i.e.

$$\text{GWP}_X = \frac{\int_0^{TH} a_X [X(t)] dt}{\int_0^{TH} a_{\text{CO}_2} [\text{CO}_2(t)] dt}, \quad (1.1)$$

where  $TH$  is the time horizon,  $a_X$  and  $a_{\text{CO}_2}$  are the radiative efficiency due to a unit increase in atmospheric abundance of  $X$  and  $\text{CO}_2$ , respectively, and  $[X(t)]$  and  $[\text{CO}_2(t)]$  are the time-dependent decay in abundance of the instantaneous release of  $X$  and  $\text{CO}_2$ , respectively.

---

Mean global tropospheric mixing ratio in 2005	319 ppb
Preindustrial mixing ratio in 1750	270 ppb
Annual tropospheric growth rate in the 1990s	0.8 - 1.1 ppb
Atmospheric lifetime	114 yr
100 yr global warming potential	$298 \times \text{CO}_2$

---

Table 1.1: Some characteristics of  $\text{N}_2\text{O}$ , Table modified from *Forster et al.* [2007].

## 1.1 Nitrous Oxide

### 1.1.1 Climatic relevance

The importance of  $\text{N}_2\text{O}$  for the chemistry of the atmosphere was discovered 1970 by Paul Crutzen [Crutzen, 1970].  $\text{N}_2\text{O}$  influences the Earth's climate both directly and indirectly:

1. In the troposphere it acts as a greenhouse gas like  $\text{CO}_2$ , directly contributing to global warming. As a greenhouse gas it is vastly more effective than e.g.  $\text{CO}_2$  as its global warming potential on a 100-year-basis is about 300 times larger than that of  $\text{CO}_2$  [Forster et al., 2007, Table 1.1]. However, atmospheric concentrations of  $\text{N}_2\text{O}$  are much lower than those of  $\text{CO}_2$ , making  $\text{N}_2\text{O}$  overall a less important greenhouse gas than  $\text{CO}_2$ .
2. Due to a relatively long atmospheric lifetime of 114 years [Forster et al., 2007, Table 1.1],  $\text{N}_2\text{O}$  can reach up to the stratosphere, where it acts as the major source for nitric oxide radicals (NO), which are involved in one of the main ozone ( $\text{O}_3$ ) reaction cycles [Crutzen and Schmailzl, 1983; Forster et al., 2007], resulting in ozone depletion.

Since the industrial revolution the concentration of  $\text{N}_2\text{O}$  in the atmosphere has increased rapidly by about 18% [Forster et al., 2007, Table 1.1]. The historical development of atmospheric  $\text{N}_2\text{O}$  is illustrated in Figure 1.2.

Anthropogenic activities contribute to enhanced  $\text{N}_2\text{O}$  emissions, both by direct emissions and indirectly by the stimulation of  $\text{N}_2\text{O}$  producing processes in both terrestrial and aquatic ecosystems resulting from the agricultural nitrogen input

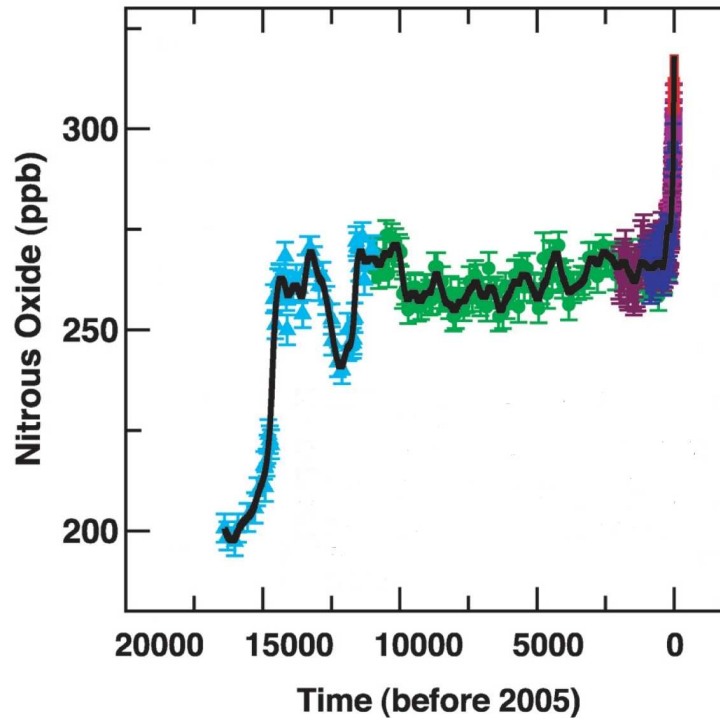


Figure 1.2:  $\text{N}_2\text{O}$  atmospheric mixing ratios (ppb) versus time before 2005 (years), modified from *Jansen et al.* [2007]. Data from Dome C [*Flückiger et al.*, 2002, green circles], H15 [*Machida et al.*, 1995, pink triangles], Law Dome [*MacFarling Meure et al.*, 2006, purple diamonds], South Pole Firn [*Battle et al.*, 1996, light purple circles], GRIP Transition [*Flückiger et al.*, 1999, light blue triangles], GRIP/Eurocore [*Flückiger et al.*, 1999, dark blue squares], and NOAA/CMDL [*Prinn*, 2005, red rectangles]. The black curve shows a spline interpolation of the data.

[*Mosier et al.*, 1998]. The impacts and feedbacks on the nitrogen cycle, on other important biogeochemical systems and on the Earth's climate are still only poorly understood.

### 1.1.2 Sources and Sinks

Sources of  $\text{N}_2\text{O}$ , both natural and anthropogenic, are illustrated in Figure 1.3. The dominant natural sources are believed to be soils and oceans, while anthropogenic sources mostly result from agricultural and industrial activity involving



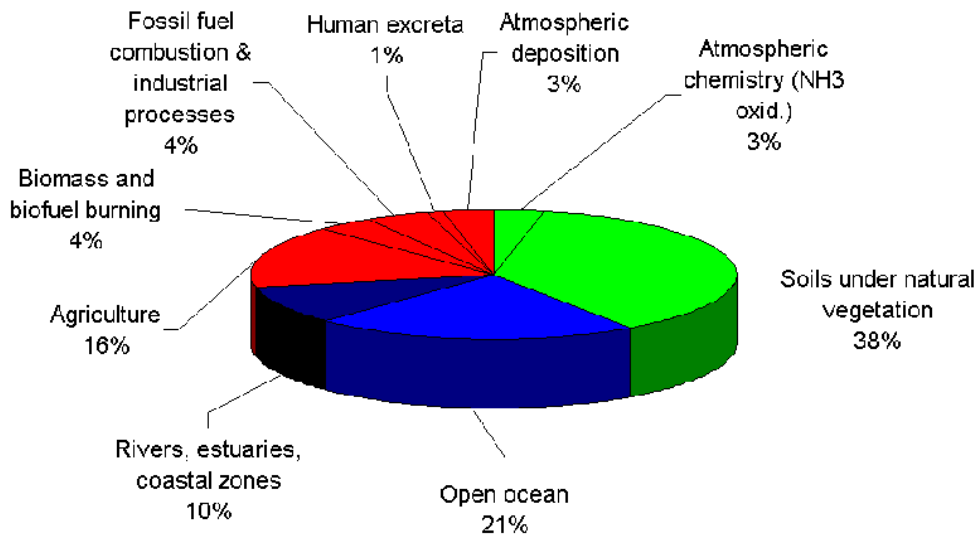


Figure 1.3: Sources of atmospheric N<sub>2</sub>O [Denman *et al.*, 2007].

the Haber-Bosch-process. It is worth noting, that the error margins associated with the N<sub>2</sub>O budget and the respective contributions are large (up to 50%).

### 1.1.3 Marine N<sub>2</sub>O

Nitrous oxide is biologically produced in the ocean and the resulting oceanic N<sub>2</sub>O emissions play a major role for the atmospheric N<sub>2</sub>O budget [e.g. Denman *et al.*, 2007; Bange, 2006, Figure 1.3].

According to the Fourth Assessment report of the IPCC [Denman *et al.*, 2007], open ocean and coastal areas make up ~21% and ~10% of the total sources of atmospheric N<sub>2</sub>O of 17.7 Tg N yr<sup>-1</sup>, respectively. The definition of coastal ocean is that of the respective estimates used, i.e. that of Nevison *et al.* [2004, MATLAB coastal database, [www.mathworks.com](http://www.mathworks.com)] and Kroeze *et al.* [2005, only rivers and estuaries].

The reasons for the considerable ranges of uncertainty (up to 50%) for the various existing estimates of the global N<sub>2</sub>O inventory and, especially, the global emissions result include [Bange, 2008]:

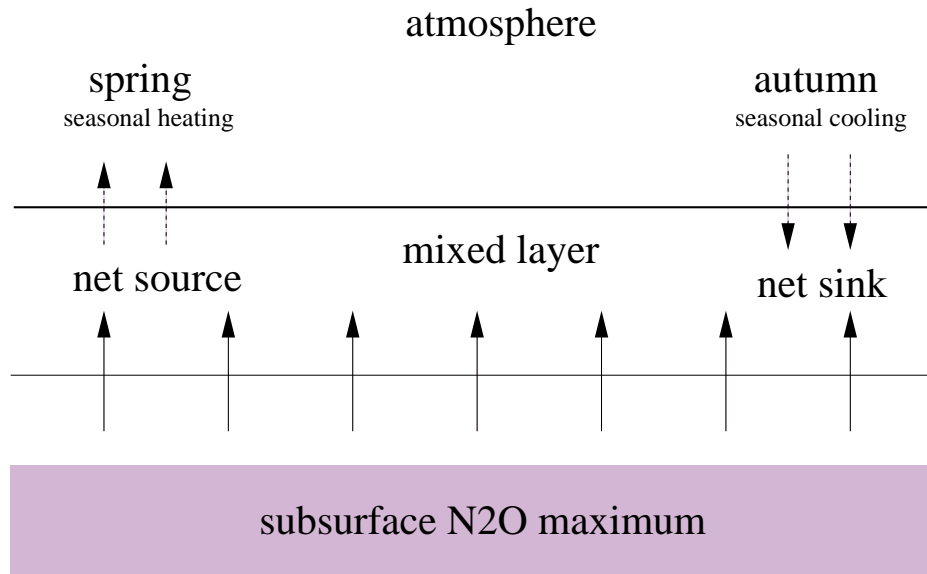


Figure 1.4: The seasonal behaviour of the mixed layer as an apparent source or sink. Solid arrows represent transport from the deep ocean into the mixed layer via diapycnal mixing and diffusion, dashed arrows represent transport via gas exchange across the air-sea interface.

1. Different methodological approaches (mainly empirical models or extrapolation of measured data).
2. The application of different air-sea gas exchange parameterisations.
3. Different classifications for coastal areas.

#### 1.1.4 Regional Marine Sources and Sinks

Overall, the ocean is a net source of N<sub>2</sub>O [Denman *et al.*, 2007]. On a regional level, the picture is less clear. Upwelling regions, estuaries and coastal regions in general have been identified as strong sources of N<sub>2</sub>O [e.g. Bange *et al.*, 1996; Rhee *et al.*, 2009]. Considering there is a clear subsurface N<sub>2</sub>O maximum almost everywhere in the world ocean and thus a gradient in direction of the surface, there is a permanent N<sub>2</sub>O flux into the mixed layer. As denitrification, the

only known mechanism consuming  $\text{N}_2\text{O}$  in the ocean, only occurs in suboxic environments (cf. Section 1.1.5.3), it seems unlikely that any oceanic region supports permanent ingassing of  $\text{N}_2\text{O}$ . However, changes of solubility induced by relatively fast changes in temperature in the mixed layer in spring and autumn, respectively, can cause the mixed layer to temporarily act as an apparent source or sink for  $\text{N}_2\text{O}$  (cf. Chapter 3), as is illustrated in Figure 1.4. For example, *Nevison et al.* [2003] found the North Atlantic Ocean to be sink of  $\text{N}_2\text{O}$  based on  $p\text{N}_2\text{O}$  surface data.

In areas of deep convection,  $\text{N}_2\text{O}$  from the atmosphere can enter the deep ocean. This assertion is supported by the findings of *Walter et al.* [2006], who showed  $\text{N}_2\text{O}$  profile data without any clear subsurface maximum from the cold-temperate North Atlantic Ocean. These regions have been found to be sinks for atmospheric  $\text{N}_2\text{O}$  by *Bange and Andreae* [1999]. However, on centennial timescales,  $\text{N}_2\text{O}$  is only temporarily removed from the atmosphere via deep convection as it probably gets into contact with the atmosphere again in the course of transport due to thermohaline circulation.

Anoxic zones are probably the only permanent sinks for dissolved  $\text{N}_2\text{O}$  within the ocean, as the only known process decomposing  $\text{N}_2\text{O}$  in the ocean is denitrification (cf. Section 1.1.5.3).

### 1.1.5 Production

$\text{N}_2\text{O}$  is microbially produced via nitrification and denitrification, two main biological processes within the nitrogen cycle (see Figure 1.1). They are widely accepted to be the main production mechanisms [*Bonin et al.*, 2002; *Bouwman et al.*, 1995; *Kroeze and Seitzinger*, 1998].  $\text{N}_2\text{O}$  can occur as a by-product during nitrification and as an intermediary during denitrification (see Figure 1.5). However, the exact metabolism used for  $\text{N}_2\text{O}$  production during nitrification, the net behaviour of denitrification and their respective contribution to the global  $\text{N}_2\text{O}$  inventory remain unclear [*Kroeze and Seitzinger*, 1998; *Codispoti et al.*, 2001; *Popp et al.*, 2002; *Punshon and Moore*, 2004; *Yamagishi et al.*, 2005].

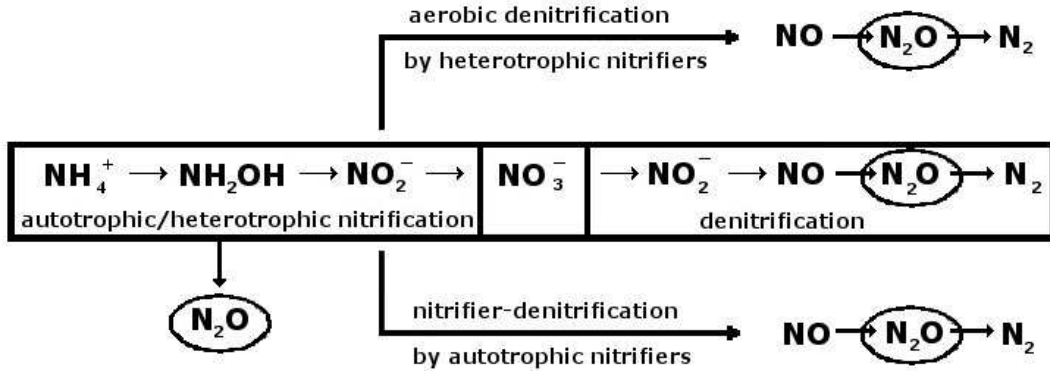
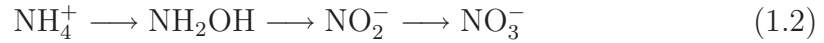


Figure 1.5: Possible production pathways of  $\text{N}_2\text{O}$  during nitrification and denitrification [Walter, 2006].

### 1.1.5.1 Bacterial Nitrification

Nitrification is the oxidation of ammonium via hydroxylamine and nitrite to nitrate:



Both autotrophic and heterotrophic bacteria can perform nitrification. This relation of  $\text{N}_2\text{O}$  production to the remineralisation of organic matter was first reported by *Yoshinari* [1976].  $\text{N}_2\text{O}$  is not a mandatory intermediate of nitrification. During autotrophic nitrification it can be formed via the pathways  $\text{NH}_2\text{OH} \rightarrow \text{N}_2\text{O}$  and  $\text{NO}_2^- \rightarrow \text{NO} \rightarrow \text{N}_2\text{O}$ . The second pathway is either used by heterotrophic organisms via aerobic denitrification or by autotrophic organisms via nitrifier-denitrification [Bange, 2008, and references therein]. The enzymes involved in the heterotrophic reaction sequence are different from those involved in the autotrophic pathway. Nitrification is a generally aerobic process, however, *Goreau et al.* [1980] found that  $\text{N}_2\text{O}$  yields are enhanced under suboxic conditions.

### 1.1.5.2 Archaeal Nitrification

Archaea have been found to be capable of nitrification [Könneke et al., 2005], especially the archaean group crenarcheota also seems to play an important role for nitrification [Wuchter et al., 2006] throughout the ocean [DeLong, 2003]. An

ammonia monooxygenase similar to that of bacteria has been found in archaea [Nicol and Schleper, 2006; Treusch *et al.*, 2005]. Thus they are of interest as potential producers of N<sub>2</sub>O, however, so far there is no experimental evidence of something similar to a hydroxylamine oxidoreductase in archaea, which would facilitate the production of N<sub>2</sub>O.

### 1.1.5.3 Bacterial Denitrification

Denitrification is the reduction of nitrate to gaseous nitrogen (N<sub>2</sub>), i.e. it effectively results in a loss of fixed nitrogen compounds:



Denitrifying organisms are found among bacteria [Cabello *et al.*, 2004; Chen *et al.*, 2002; Shapleigh, 2001]. Most bacterial denitrifiers are facultative aerobic heterotrophs. N<sub>2</sub>O-reductase, the enzyme responsible for reducing N<sub>2</sub>O to molecular nitrogen is the most oxygen-sensitive enzyme involved in denitrification [Tiedje, 1988; Knowles, 1982]. Denitrification can thus produce or consume N<sub>2</sub>O, depending on the surrounding conditions: it produces N<sub>2</sub>O at the interface between suboxic and anoxic waters, where only the N<sub>2</sub>O-reductase is inhibited by the remaining oxygen [Knowles, 1982], and it consumes N<sub>2</sub>O under anoxic conditions when the complete process of denitrification is performed [Elkins *et al.*, 1978; Cohen and Gordon, 1978].

The magnitude of the net N<sub>2</sub>O production or loss due to denitrification remains unclear. The zones supporting production via denitrification by inhibiting N<sub>2</sub>O-reductase naturally often occur close to zones with even lower oxygen concentrations. Within these, N<sub>2</sub>O-reductase is no longer inhibited and it is therefore likely that at least part of the N<sub>2</sub>O produced by denitrification will be consumed again by denitrification on rather short timescales.

A significant N<sub>2</sub>O consumption attributed to denitrification was first observed by Cohen and Gordon [1978] and Cohen [1978] in the oxygen minimum zone in the subsurface waters of the Eastern Tropical North Pacific Ocean and the anoxic waters of the Saanich Inlet basin (off Vancouver Island).

#### 1.1.5.4 Anammox

Via anaerobic ammonium oxidation (Anammox), molecular nitrogen is produced by bacteria by reducing nitrite and oxidising ammonium [Kuypers *et al.*, 2003]:



Recently this process has received increasing attention, amongst other things as a potential production pathway of  $\text{N}_2\text{O}$  [e.g. *Devol*, 2008; *Francis et al.*, 2007]. But so far,  $\text{N}_2\text{O}$  has only been found to be produced in relatively small quantities during nitric oxide detoxification ( $\text{NO}_2^- \longrightarrow \text{NO} \longrightarrow \text{N}_2\text{O}$ ), which seems to be performed by certain bacteria as a side reaction during the anammox process [Kartal *et al.*, 2007]. The question whether anammox is a significant production pathway for  $\text{N}_2\text{O}$  remains unresolved.

## 1.2 Distribution of $\text{N}_2\text{O}$

### 1.2.1 $\text{N}_2\text{O}$ in the Water Column

The distribution of  $\text{N}_2\text{O}$  in the water column depends on the surrounding oxygen conditions. In oxic environments,  $[\text{N}_2\text{O}]$  profiles usually display a distinct subsurface maximum and a good correlation between  $[\text{N}_2\text{O}]$  and the apparent oxygen utilisation (AOU), which is interpreted as evidence for  $\text{N}_2\text{O}$  production via nitrification [Yoshinari, 1976; Cohen and Gordon, 1978]. A  $[\text{N}_2\text{O}]$  profile typical for oxic conditions and production via nitrification is shown in Figure 1.6(a).

In suboxic conditions, where denitrification can produce  $\text{N}_2\text{O}$  [Tiedje, 1988; Knowles, 1982],  $[\text{N}_2\text{O}]$  profiles usually display two distinct subsurface maxima, which are decoupled from AOU. A typical profile is shown in Figure 1.6(b). In anoxic waters, the  $\text{N}_2\text{O}$  in the water column can be consumed by denitrification [Elkins *et al.*, 1978; Cohen and Gordon, 1978]. A typical profile is shown in Figure 1.6(c).

### 1.2.2 $\text{N}_2\text{O}$ in the World Ocean

Nevison *et al.* [1995] used a global data set of 60,286 surface  $\Delta p\text{N}_2\text{O}$  measurements and globally extrapolated these to a  $2.8^\circ \times 2.8^\circ$  grid using a relaxation

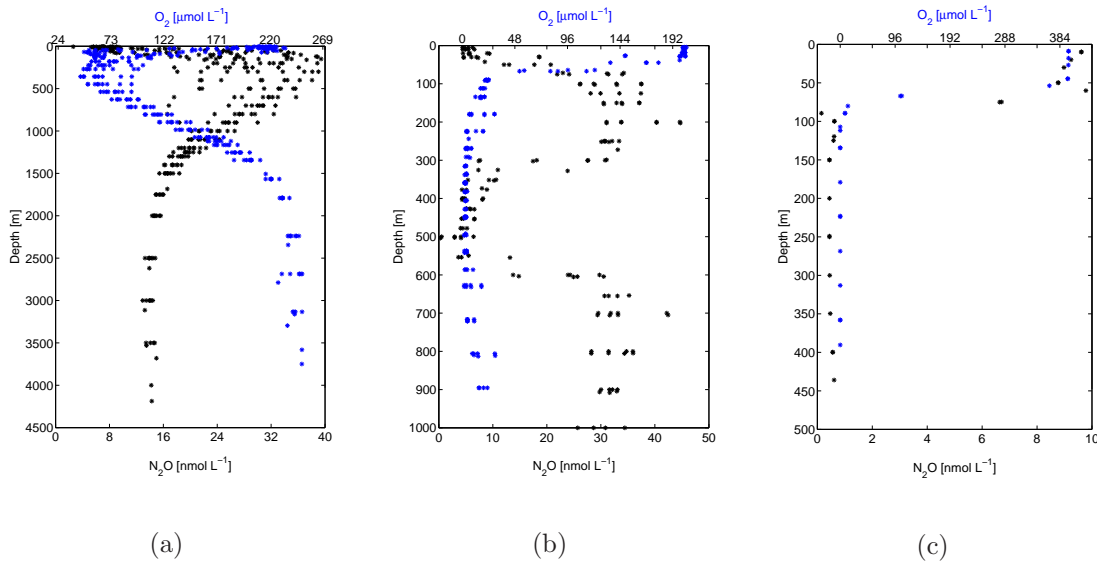


Figure 1.6:  $N_2O$  concentration ( $\text{nmol L}^{-1}$ ) and dissolved oxygen concentration ( $\mu\text{mol L}^{-1}$ ) versus depth (m) for oxic ((a), Tropical Atlantic), suboxic ((b), Eastern Tropical Pacific off Peru) and anoxic ((c), Baltic Sea) conditions.

scheme together with a diffusion-type equation. In the Southern Ocean and near the Equator zonal neighbours were preferentially weighted over meridional neighbours to account for the primarily zonal nature of the ocean currents in these regions. The extrapolation results were coupled to modelled gas transfer coefficients. They estimate a global  $N_2O$  source of about 4 (1.2–6.8)  $\text{Tg N yr}^{-1}$ . They found the Southern Ocean, particularly the 40–60°S latitude band, to be the strongest  $N_2O$  source as large winds coincide with large  $N_2O$  surface supersaturations. While they also found the North Pacific, the equatorial upwelling and the coastal upwelling zones to be strong sources, they found the North Atlantic and parts of the subtropical gyres to be weak sinks in winter and weak sources in summer. The latter seems unlikely, considering the shape of a typical  $N_2O$  depth profile (cf. Figure 1.6(a)). They acknowledge large uncertainties in their estimate and a distinct summertime bias in the employed dataset. In the high latitudes only 14–17% of the data were collected in winter time. In tropical latitudes, the data were biased towards spring and summer. *Nevison et al.* also extract monthly  $\Delta pN_2O$  maps from their globally extrapolated dataset, which lead them

to suggest that in some regions, like the coastal waters of Antarctica, the seasonal cycle of  $\Delta p\text{N}_2\text{O}$  is predominantly controlled by mixing effect, whereas in the North Atlantic and in the subtropical gyres the seasonal cycle of  $\Delta p\text{N}_2\text{O}$  is mainly controlled by thermal effects.

*Suntharalingam and Sarmiento* [2000] used an ocean general circulation model together with a  $\text{N}_2\text{O}$  source function to investigate whether a simple  $\text{N}_2\text{O}$  parameterisation is sufficient to explain the observed subsurface  $\text{N}_2\text{O}$  distribution. They assumed zero  $\text{N}_2\text{O}$  production in the euphotic zone and loss via gas exchange. They found that an  $\text{N}_2\text{O}$  function which parameterises production using a scalar relationship between  $\text{N}_2\text{O}$  production and  $\text{O}_2$  consumption and accounting for depth variations of this relationship best fits the observational data of *Butler et al.* [1988]. However, they concede that their model is unable to account for the more complex  $\text{N}_2\text{O}$  cycling mechanism in suboxic and anoxic zones. As the parameterisation of  $\text{N}_2\text{O}$  depends on the  $\text{O}_2$  consumption, the modelled  $\text{O}_2$  distribution is an important control on the  $\text{N}_2\text{O}$  distribution. The authors discuss the “warm thermocline” problem, which leads to an underestimation of  $[\text{O}_2]$  by the model. This problem is addressed by using AOU instead of  $[\text{O}_2]$ . Also, they remark that model simulations indicate that waters ventilating the deep ocean are undersaturated with respect to oxygen when leaving the ocean surface, which implies that the associated modelled AOU is overestimating biological oxygen utilisation. They show a globally averaged depth profile of oxygen and AOU, but the general distribution of  $\text{O}_2$ , especially with respect to suboxic zones is not discussed. They conclude from their calculations that the majority of  $\text{N}_2\text{O}$  formation occurs in the upper ocean. Their best estimate of the global open ocean water column  $\text{N}_2\text{O}$  source is  $3.85 \text{ Tg N yr}^{-1}$ . *Suntharalingam and Sarmiento* note that anomalous features of localised high  $\text{N}_2\text{O}$  in the southern high latitudes, which are in disagreement with the observations of *Weiss et al.* [1992], are due to the circulation model, which produced zones of intense deep convection and thus elevated new production.

To address the issue of  $\text{N}_2\text{O}$  cycling in suboxic zones, *Suntharalingam et al.* [2000] used a slightly modified version of the  $\text{N}_2\text{O}$  source function used by *Suntharalingam and Sarmiento* [2000] to investigate the significance of enhanced  $\text{N}_2\text{O}$  production in low oxygen regions and the transport from these regions. The



source function retains its scalar dependence on oxygen consumption but a second function is added, to simulate high  $\text{N}_2\text{O}$  yields under low-oxygen conditions. They use the features of the  $\text{N}_2\text{O}$  source function postulated by *Codispoti et al.* [1992] and the data of *Goreau et al.* [1980] to parameterise this second function. Denitrification is not modelled explicitly as a sink for  $\text{N}_2\text{O}$ , but when oxygen levels drop below  $1 \mu\text{mol L}^{-1}$  the  $\text{N}_2\text{O}$  production rate drops linearly off to zero. This parameterisation heavily depends on the modelled  $[\text{O}_2]$  distribution. The authors concede that the two distinct oxygen minimum zones observed north and south of the Equator in the Eastern Tropical are not well delineated in the model. While the model reproduces the oxygen minimum zones in the Arabian Sea, it also predicts oxygen minimum zones in the Bay of Bengal and the northeast Indian Ocean, which cannot be found in observational data. They admit that the modelled oxygen minimum zones, both in the Indian and the Pacific Ocean, are more extensive than in reality, which is likely to overestimate  $\text{N}_2\text{O}$  production in and  $\text{N}_2\text{O}$  transport from these regions. The global  $\text{N}_2\text{O}$  source is constrained and fixed to be equivalent to  $3.6 \text{ Tg N yr}^{-1}$ . Three different cases are modelled: (1) The entire source originates from the low-oxygen regions, i.e. the second part of the source function. (2) Half the source originates from the low-oxygen regions and half follows the original source function, i.e. is simply linearly related to oxygen consumption. (3) One quarter of the source originates from the low-oxygen regions and three quarters follow the simple linear relationship with oxygen consumption. The model results were validated against surface data [*Weiss et al.*, 1992] and depth profiles [*Butler et al.*, 1988]. Case (3) and to a lesser extent case (2) agreed reasonably well with the observations. It is worth noting that the case which agreed particularly well with upper ocean observations overestimated deep ocean  $\text{N}_2\text{O}$  production. They concluded that  $\text{N}_2\text{O}$  formed in low-oxygen zones contributes 25% – 50% to the total oceanic source most of which is directly ventilated to the atmosphere. They found that only a small fraction of this  $\text{N}_2\text{O}$  is transported poleward. They remark, however, that poleward transport generally seems to be underestimated by the underlying ocean general circulation model, the extent of the tropical low oxygen zones is overestimated and that the  $\text{N}_2\text{O}$  database used for model validation is sparse in certain regions of potential significance.

*Nevison et al.* [2003] use a data set of subsurface  $\text{N}_2\text{O}$  from a range of oceanic regions and the laboratory data of *Goreau et al.* [1980] to develop a parameterisation of the  $\text{N}_2\text{O}$  yield per mole  $\text{O}_2$  consumed. This parameterisation is coupled to a global dissolved  $\text{O}_2$  climatology and ocean carbon model output. The dataset was supplemented with  $[\text{O}_2]$  data from selected World Ocean Circulation Experiment (WOCE) cruises. They estimate a total oceanic  $\text{N}_2\text{O}$  inventory of  $610 - 840 \text{ Tg N}$  and a global interior ocean production rate of  $5.8 \pm 2 \text{ Tg N yr}^{-1}$ . Consumption of  $\text{N}_2\text{O}$ , probably by denitrification, only occurs in the oxygen minimum zones in the Eastern Tropical Pacific and in the Arabian Sea. They found that observed  $\Delta\text{N}_2\text{O}$ -AOU correlation slopes are often strongly influenced by mixing. While their results are consistent with nitrification being the main production mechanism of oceanic  $\text{N}_2\text{O}$ , they concede that denitrification and/or coupled nitrification/denitrification cannot be ruled out as a significant source because these mechanisms may be responsible for producing some of the  $\text{N}_2\text{O}$  that is exported from the Eastern Tropical Pacific. It should be noted, that *Suntharalingam et al.* found no significant advective transport of  $\text{N}_2\text{O}$  out of the oxygen minimum zones.

## 1.3 Sensitivities to Change

Even some seemingly basic things about  $\text{N}_2\text{O}$  are not yet completely understood, however, what we know so far already indicates that the ocean-atmosphere  $\text{N}_2\text{O}$  flux is potentially very sensitive to changing conditions. Especially, some of these sensitivities of the oceanic  $\text{N}_2\text{O}$  source and its potentially influential effects on a changing climate motivated this study, which aims to better understand characteristic features of the  $\text{N}_2\text{O}$  distribution and better constrain the oceanic source.

### 1.3.1 Changes in the Meridional Overturning Circulation

It has been suggested, that changes in the large-scale ocean circulation and abrupt climate change are correlated and that this correlation can be used to predict the change in the meridional overturning circulation in response to anthropogenically

induced climate change [e.g. *Alley, 2007; Broecker, 1997*, and references therein]. As sites of elevated  $\text{N}_2\text{O}$  emissions, like e.g. coastal upwelling regions, are also determined by transport of  $\text{N}_2\text{O}$  rich water to the surface, these changes in transport might affect the local and the global source strength. Additionally, changing circulation might result in less frequent ventilation of some areas, affecting the extent of and the overall oxygen concentration in the oxygen-minimum zones (cf. Section 1.3.4).

The relationship between changes in ocean circulation and changing atmospheric  $\text{N}_2\text{O}$  concentrations as well as its controlling mechanisms have been investigated by two paleo modelling studies. *Goldstein et al. [2003]* used a zonally averaged three basin ocean circulation model and a data-based  $\text{N}_2\text{O}$  production rate of one molecule  $\text{N}_2\text{O}$  per  $10^4$  molecules  $\text{O}_2$  consumed. The modelled distribution of  $[\text{O}_2]$ , however, is not discussed. Their model did not include a representation of denitrification, neither as a source nor as a sink. They simulated a fresh water pulse to the North Atlantic causing a breakdown of the Atlantic thermohaline circulation. They identified three effects relevant for atmospheric  $\text{N}_2\text{O}$ , a decrease in new production, an increased storage of  $\text{N}_2\text{O}$  in the deep ocean and a salinity-induced solubility effect. However, these effects only resulted in a drawdown of atmospheric  $\text{N}_2\text{O}$  of 10 ppb, while the ensuing rise took place over 1000 years. The discrepancies between these model results and ice core data of *Flückiger et al. [1999]*, which show a drawdown of 25 – 30 ppb and an abrupt rise, led *Goldstein et al.* to suggest a reduction of oceanic emissions is not solely responsible for the observed reduction of atmospheric  $\text{N}_2\text{O}$  during the Younger Dryas (12,700 – 11,550 before present).

In contrast, *Schmittner and Galbraith [2008]* used the full three dimensional model of *Schmittner et al. [2008]* and the parameterisation given by *Nevison et al. [2003]*, which is only based on considerations of nitrification, to investigate abrupt changes in the Atlantic meridional overturning circulation. The modelled distribution of  $[\text{O}_2]$ , which is an important control of  $[\text{N}_2\text{O}]$  in the parameterisation chosen, is not discussed. The modelled  $\text{N}_2\text{O}$  amplitudes of 15 – 40 ppb were much larger than those found by *Goldstein et al.* and in good agreement with ice-core data [*Flückiger, 2004*]. While *Flückiger [2004]* suggested, that there might be a potentially causal relationship between an observed  $\text{N}_2\text{O}$  increase and the rapid

warming in Greenland, model results of *Schmittner and Galbraith* indicate the contrary. They precluded N<sub>2</sub>O effects on climate and found that the recovery of N<sub>2</sub>O concentrations is related to the long-term adjustment of upper ocean nitrate and oxygen inventories after the collapse of the Atlantic meridional overturning circulation. They concluded, that changes in ocean sources could have dominated glacial variability of atmospheric N<sub>2</sub>O on millennial timescales, emphasising the role of ocean circulation and biogeochemical cycling for atmospheric greenhouse gas concentrations.

### 1.3.2 Large Scale Ocean Fertilisation

N<sub>2</sub>O has also received some attention in connection with large scale iron fertilisation experiments, which are being considered as a strategy for CO<sub>2</sub> mitigation. *Jin and Gruber* [2003] conducted a modelling study, using a suite of three dimensional coupled physical-biogeochemical models and the N<sub>2</sub>O model of *Suntharalingam et al.* [2000]. The modelled [O<sub>2</sub>] distribution, which strongly controls the [N<sub>2</sub>O] distribution by means of the parameterisation chosen, is not discussed in any detail. It is mentioned that low oxygen zones occur in the tropical Indian and Pacific Ocean and the zonally integrated volume of water with less than 50 μmol kg<sup>-1</sup> is given. The effect of fertilisation on this integrated volume is discussed. They found that the potential feedback of large scale long-time iron fertilisation experiments is substantial and can completely offset the radiative benefit caused by the intended CO<sub>2</sub> drawdown. Iron fertilisation is particularly effective in the Southern Ocean, causing a reduction of atmospheric CO<sub>2</sub> of more than 60 ppm over 100 years. However, at the same time, atmospheric N<sub>2</sub>O increases by nearly 23 ppb, offsetting 13 ± 6% of the radiative benefit. Fertilising the tropical areas even results in an N<sub>2</sub>O-induced offset of 40 ± 20% of the radiative benefits due to increasing the volume of suboxic water masses. Short scale fertilisation experiments display an N<sub>2</sub>O-induced offset of 115 ± 34% of the radiative benefits. There is, however, contrasting experimental evidence concerning the effects of iron fertilisation. While *Law and Ling* [2001] found an accumulation of N<sub>2</sub>O in the pycnocline during SOIREE, *Walter et al.* [2005] found no accumulation during EIFeX. They suggest that the export of organic matter might have been so rapid

that the nitrifying bacteria could not adapt quickly enough. Therefore existing modelling studies might lack important features controlling the enhancement of N<sub>2</sub>O production and these model results should be viewed with caution.

### 1.3.3 Atmospheric Nitrogen Deposition

*Duce et al.* [2008] analyse the impact of atmospheric anthropogenic nitrogen on the open ocean. They emphasise the potential importance of the growing quantity of reactive atmospheric anthropogenic nitrogen, which is deposited to the ocean surface and approaches the importance of nitrogen fixation as a source of marine reactive nitrogen. Especially in nitrate-limited surface waters, the fertilisation induced by this extra reactive nitrogen can lead to enhanced primary productivity. They find that deposition of atmospheric anthropogenic nitrogen may account for up to 3% of the annual new oceanic primary productivity, but up to one third of the productivity generated in response to external input of nitrogen to the ocean. This fertilisation could account for up to one tenth of the uptake of atmospheric anthropogenic carbon by the ocean. However, according to *Duce et al.* the anthropogenic nitrogen deposited to the ocean might be responsible for the production of up to 1.6 Tg of N<sub>2</sub>O per year, thus offsetting up to two thirds of the radiative benefits induced by the drawdown of atmospheric carbon. It should be noted, that their results are based on the very simplistic assumption that the N<sub>2</sub>O production is related linearly to the nitrogen supply.

### 1.3.4 Increase in Volume of the Suboxic Zones

There is evidence, that the tropical oxygen minimum zones in the world ocean are increasing in volume [*Stramma et al.*, 2008]. This would result in an expansion of the zones supporting denitrification, which would probably have an impact on the production and decomposition of N<sub>2</sub>O. Whether it would have a net positive or net negative effect on N<sub>2</sub>O production remains unclear as the net behaviour of denitrification and its controlling mechanisms are not yet fully understood (cf. Section 1.1.5.3). As N<sub>2</sub>O yields during nitrification have been found to be enhanced under low oxygen conditions in a lab study [*Goreau et al.*, 1980], this increase in volume will probably also lead to increased production of N<sub>2</sub>O due to

nitrification.

### 1.3.5 Ocean Warming

There is evidence that the oceans are warming [e.g *Levitus et al.*, 2005; *Barnett et al.*, 2005]. As marine autotrophic and heterotrophic processes display sensitivities to temperature (to varying degrees), ocean warming might result in changes of the bacterial community structure and hence in changes of N<sub>2</sub>O production. Changes in ocean temperature also affect the solubility of N<sub>2</sub>O. Rising ocean temperature implies that the N<sub>2</sub>O long-term storage capacity of the deep ocean will be reduced. Additionally, this effect will temporarily strengthen the N<sub>2</sub>O source as apparent supersaturations created by warming water masses after their last contact with the atmosphere will increase the ocean-atmosphere gradient when these water masses finally get into contact with the atmosphere again. This strengthening effect will disappear again once the temperature change levels off and the system reaches equilibrium again. Also, non-uniform warming could induce enhanced stratification of the water column. This could potentially diminish the oceanic N<sub>2</sub>O source by keeping N<sub>2</sub>O rich water from intermediate depths from reaching the air-sea interface.

### 1.3.6 Eutrophication of Coastal Zones

Coastal zones probably contribute to a significant degree to the total oceanic emissions of N<sub>2</sub>O [*Denman et al.*, 2007]. They are fertilised to an increasing degree by river run-off carrying a high load of organic nitrogen. This fertilisation may lead to enhanced primary production and thus enhanced nitrification and N<sub>2</sub>O formation. Additionally, the changing flux of organic material reaching the sediments might change O<sub>2</sub> concentrations in the sediment, changing N<sub>2</sub>O production in turn. And unlike in the open ocean, the shallow depths of coastal regions allow for N<sub>2</sub>O produced in the sediments to reach the atmosphere.

## 1.4 Thesis Outline

Since the industrial revolution, the concentration of  $\text{N}_2\text{O}$  in the atmosphere has steadily increased [Forster *et al.*, 2007]. However, the important oceanic source of atmospheric  $\text{N}_2\text{O}$  is still poorly constrained [see compilation of estimates in Denman *et al.*, 2007; Bange, 2006]. This study aims to calculate data-based  $\text{N}_2\text{O}$  production rates to investigate regional patterns and controlling factors of the subsurface  $\text{N}_2\text{O}$  production. The subsurface  $\text{N}_2\text{O}$  yield is compared to the ocean-atmosphere flux of  $\text{N}_2\text{O}$  in order to better constrain the oceanic  $\text{N}_2\text{O}$  source.

In Chapter 2, transit time distributions (TTD) calculated from tracer data together with in-situ measurements of  $\text{N}_2\text{O}$  are used to estimate the concentration of biologically produced  $\text{N}_2\text{O}$  and  $\text{N}_2\text{O}$  production rates in the central North Atlantic Ocean. This approach to estimation of  $\text{N}_2\text{O}$  production rates integrates the effects of potentially varying production/decomposition mechanisms along the transport path of a water mass. A new parameterisation of  $\text{N}_2\text{O}$  production during nitrification depending linearly on AOU and exponentially on temperature/depth was developed, which can be applied to calculate  $\text{N}_2\text{O}$  production due to nitrification in the entire ocean including oxygen minimum zones.

In Chapter 3, the in-situ measurements of  $\text{N}_2\text{O}$  from the North Atlantic Ocean are used to calculate both the  $\text{N}_2\text{O}$  flux to the mixed layer and the  $\text{N}_2\text{O}$  flux across the air-sea interface due to gas exchange. The influence of the seasonal  $p\text{N}_2\text{O}$  cycle on the discrepancy between both flux estimates is investigated. Other potential explanations for the two different flux estimates are discussed.

In Chapter 4 the parameterisations developed in Chapter 2 are used together with global gridded World Ocean Atlas temperature [Locarnini *et al.*, 2006], salinity [Antonov *et al.*, 2006], oxygen [Garcia *et al.*, 2006] data and global gridded GLODAP CFC-12 data [Key *et al.*, 2004] to calculate the annual subsurface  $\text{N}_2\text{O}$  yield and the amount of organic carbon which is remineralised. The results are compared to existing global ocean-atmosphere flux estimates in order to facilitate the development of tighter constraints for the  $\text{N}_2\text{O}$  budget. The slight discrepancy between production and ocean-atmosphere flux estimates and its potential reasons and implications are discussed.





## Chapter 2

# North Atlantic Production of Nitrous Oxide in the Context of Changing Atmospheric Levels

In the ocean, the excess of  $\text{N}_2\text{O}$  over the atmosphere equilibrium concentration ( $[\text{N}_2\text{O}]_{xs}$ ) is a measure to diagnose the production of  $\text{N}_2\text{O}$  in different water masses [Nevison *et al.*, 1995, 2003]. It is defined as

$$[\text{N}_2\text{O}]_{xs} = [\text{N}_2\text{O}]_{insitu} - [\text{N}_2\text{O}]_{eq}, \quad (2.1)$$

where  $[\text{N}_2\text{O}]_{insitu}$  is the in-situ concentration of  $\text{N}_2\text{O}$  and  $[\text{N}_2\text{O}]_{eq}$  is the concentration of  $\text{N}_2\text{O}$  in equilibrium with the atmosphere at the time of the last atmospheric contact.

For the preindustrial ocean and water masses ventilated before 1800,

$$[\text{N}_2\text{O}]_{eq} = [\text{N}_2\text{O}]_{eq}^{preind} = X_{\text{N}_2\text{O}_{preind}} P H_{T,S}, \quad (2.2)$$

where  $X_{\text{N}_2\text{O}_{preind}}$  is the preindustrial atmospheric mixing ratio of  $\text{N}_2\text{O}$ ,  $P$  is the atmospheric pressure and  $H_{T,S}$  is the temperature- and salinity-dependent solubility of  $\text{N}_2\text{O}$  in seawater [Weiss and Price, 1980].

For water masses which were fully or partially ventilated by water originating at the sea surface since 1800, the calculation of  $[\text{N}_2\text{O}]_{eq}$  is more complicated. For these water masses the effect of the anthropogenic increase of the  $\text{N}_2\text{O}$  atmospheric mixing ratio needs to be considered, and an atmospheric mole fraction

for the time of the last contact of the water mass with the atmosphere has to be estimated. This implies that the “age” of the water mass has to be determined. However, water masses are generally mixtures of fractions with different origins and, usually, different ages.

In most previous studies used for such calculations, e.g. *Nevison et al.* [2003]; *Butler et al.* [1989]; *Yoshinari* [1976], the contemporary atmospheric mole fraction has been used, independent of the “real” age of the sampled water masses. This procedure is well suited for calculating  $N_2O_{xs}$  for near-surface waters, but ignores the effect of variable water mass age and hence the variable atmospheric mole fraction involved in establishing initial “equilibrium”  $N_2O$  concentrations for the deeper layers of the ocean. *Nevison et al.* [2003] acknowledge that the use of only the contemporary atmospheric mole fraction introduces an uncertainty of 10 – 15% in the estimate of  $[N_2O]_{xs}$ . To address this issue, a water mass age dependent method to calculate  $[N_2O]_{xs}$  was introduced for the first time by *Walter et al.* [2006]. They used three separate atmospheric mole fractions based on roughly estimated water mass ages in order to calculate  $N_2O$  equilibrium concentrations. With this approach the calculated equilibrium concentration of  $N_2O$  for water masses below the thermocline was lower than calculated using the contemporary  $N_2O$  mole fraction. This paper introduces an improved approach to calculating  $[N_2O]_{xs}$  by using transit time distributions (TTD) for water samples in which  $N_2O$  was measured. The TTD concept allows an age distribution to be estimated for a sampled water mass on the basis of measurements of transient tracers such as CFCs [*Waugh et al.*, 2003]. TTDs make it possible to estimate relative age distributions of a water mass which can then be applied to calculate an effective value for  $[N_2O]_{eq}$ . Moreover, the calculated age provides means to calculate *in-situ* nitrous oxide production rates.

## 2.1 Methods

### 2.1.1 Study Area

The data presented here were collected in the mid-latitude North Atlantic Ocean during spring 2004 on board the German research vessel RV Meteor [*Tanhua*

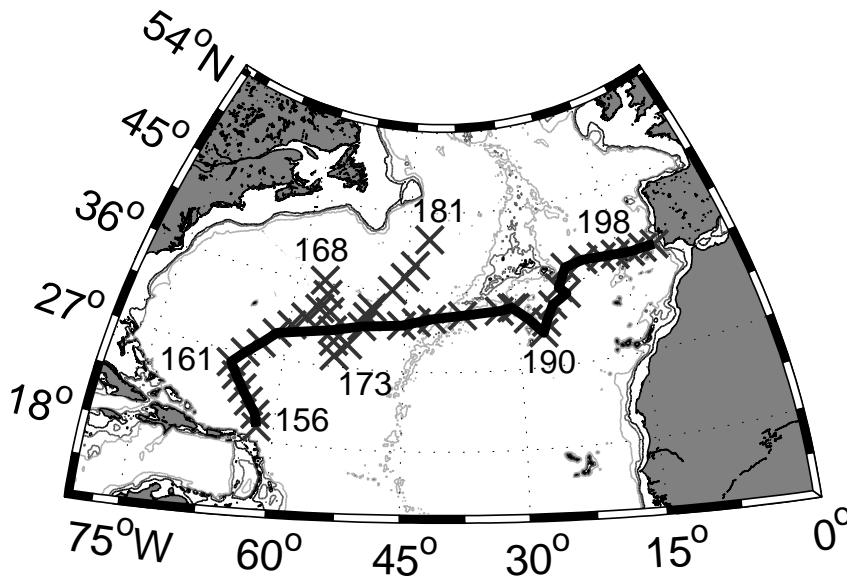


Figure 2.1: Cruise track of the M60/5 cruise in 2004. The crosses mark individual stations, the stations used for the W-E section in Figure 2.5 are joined with the solid line. Selected station numbers are indicated.

*et al.*, 2006; *Walter et al.*, 2006]. The cruise track of the Meteor cruise 60/5 was from Martinique to Lisbon, with a northernmost station at 42°N, 42°W and the cruise therefore included sampling of both the subtropical and cold-temperate gyre, as well as the western and eastern basins (see Figure 2.1). Most stations were repeat samplings of stations from the Transient Tracers in the Ocean Program (TTO-NAS) in 1982.

### 2.1.2 N<sub>2</sub>O, SF<sub>6</sub> and CFC Measurements

Water samples for N<sub>2</sub>O analysis were collected at 37 stations in triplicate from various depths, taken with a 24-Niskin-bottle rosette, equipped with a CTD-sensor. Samples were then analysed gas-chromatographically using an electron capture detector. The analytical method applied for N<sub>2</sub>O analysis is described in detail by *Walter et al.* [2006]. For the two-point calibration procedure we used standard gas mixtures with  $311.8 \pm 0.2$  ppb and  $346.5 \pm 0.2$  ppb N<sub>2</sub>O in synthetic air, which have been calibrated against the NOAA (National Oceanic and

Atmospheric Administration, Boulder, Co.) standard scale in the laboratories of the Air Chemistry Division of the Max Planck Institute for Chemistry, Mainz, Germany. The overall relative mean analytical error is estimated to be  $\pm 1.8\%$ .  $\text{N}_2\text{O}$  concentrations are denoted by brackets and are generally reported in  $\text{nmol kg}^{-1}$ . All measured profiles are displayed in Figure 2.2(a).

The determination of  $\text{SF}_6$  was performed by purge-and-trap gas chromatography with electron capture detection [Tanhua *et al.*, 2005]. The analytical precision was  $\pm 1.5\%$ , the detection limit was estimated to be  $0.05 \text{ fmol kg}^{-1}$  ( $\sim 0.15$  ppt), and a sampling blank (determined from analyses of deep water samples in the eastern basin) of the same magnitude has been subtracted from the data. The  $\text{SF}_6$  data were calibrated against an air standard prepared at CMDL, Boulder, CO, and recalibrated to the GMD2000 scale ([http://www.cmdl.noaa.gov/hats/standard/SF6\\\_scale.htm](http://www.cmdl.noaa.gov/hats/standard/SF6\_scale.htm)).

The CFC measurements were made on an analytical system similar to that described by Bullister and Weiss [1988] and are reported on the SIO98 scale [Prinn *et al.*, 2000]. The analytical precision was  $0.7\%$  for CFC-12, and a sampling blank of  $0.007 \text{ pmol kg}^{-1}$  (determined as the median value of 18 deep water samples in the eastern basin) has been subtracted from the data.

The salinity and temperature dependent solubility of the CFC-12,  $\text{SF}_6$  and  $\text{N}_2\text{O}$  are calculated from their respective solubilities [Bullister *et al.*, 2002; Warner and Weiss, 1985; Weiss and Price, 1980], and we have assumed an atmospheric pressure of 1 atmosphere over the surveyed area. In this way, tracer concentrations can be compared directly to the time-varying atmospheric histories of these compounds [Maiss and Brenninkmeijer, 1998; Walker *et al.*, 2000].

### 2.1.3 The Atmospheric History of $\text{N}_2\text{O}$

In order to estimate the background  $\text{N}_2\text{O}$  signal in the ocean we need to know the time dependent history of atmospheric concentrations. For this work, we have used a synthesis of ice-core and firn data [Machida *et al.*, 1995; Battle *et al.*, 1996] merged with air measurements. The data are available at <http://daac.ornl.gov> [Holland *et al.*, 2005]. We assume a constant atmospheric mixing ratio of  $\text{N}_2\text{O}$  of 275 ppb prior to year 1800 and used a polynomial fit of the data (Figure

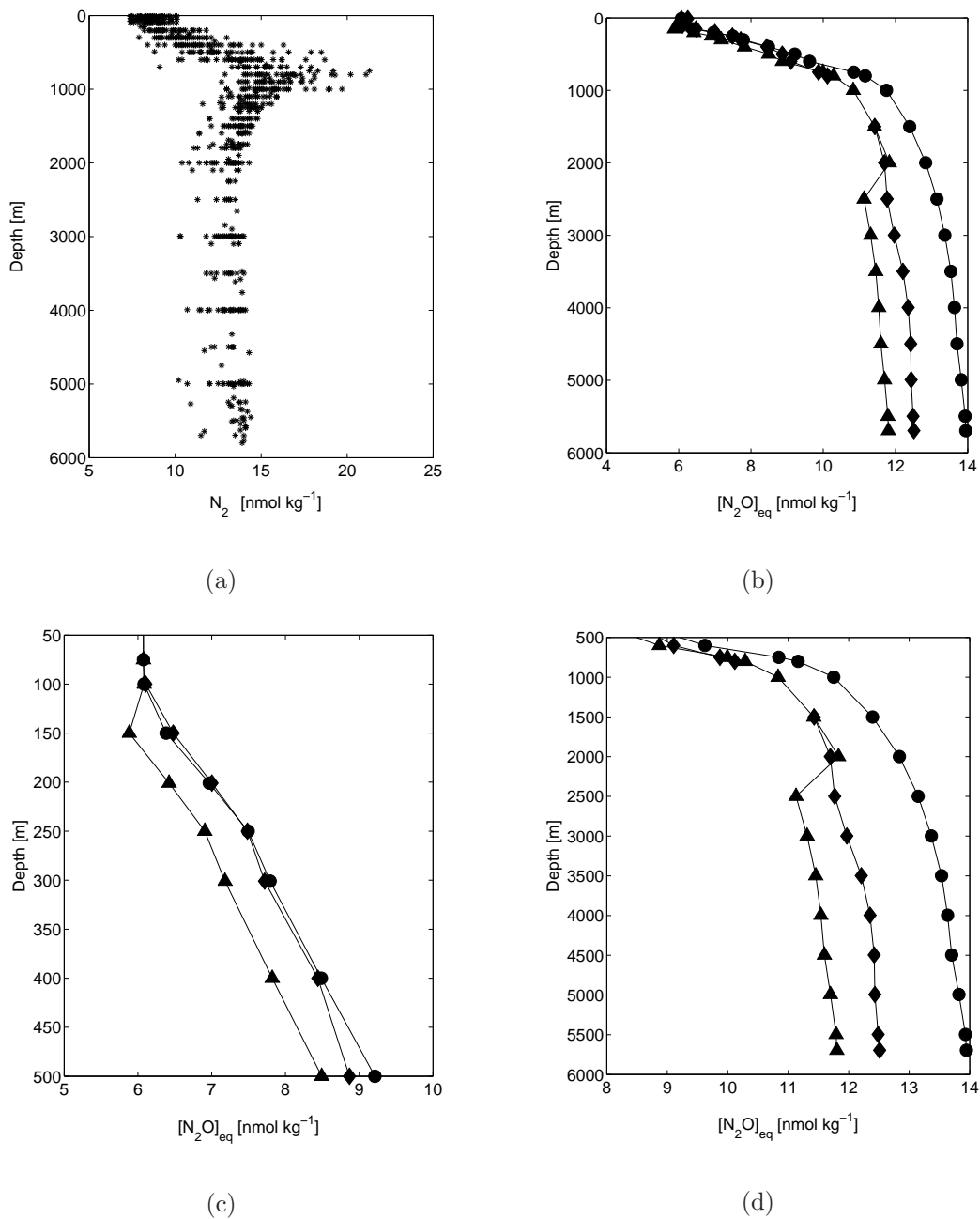


Figure 2.2: 2.2(a): In-situ  $\text{N}_2\text{O}$  concentrations ( $\text{nmol kg}^{-1}$ ) versus depth (m). 2.2(b): Comparison of profiles at station #156 of  $[\text{N}_2\text{O}]_{eq}$  ( $\text{nmol kg}^{-1}$ ) vs. depth (m) for the “contemporary” (circles), “layer” (triangles) and “TTD” (diamonds) approach. 2.2(c): 0 – 500 m section of 2.2(b). 2.2(d): 500 – 2500 m section of 2.2(b).

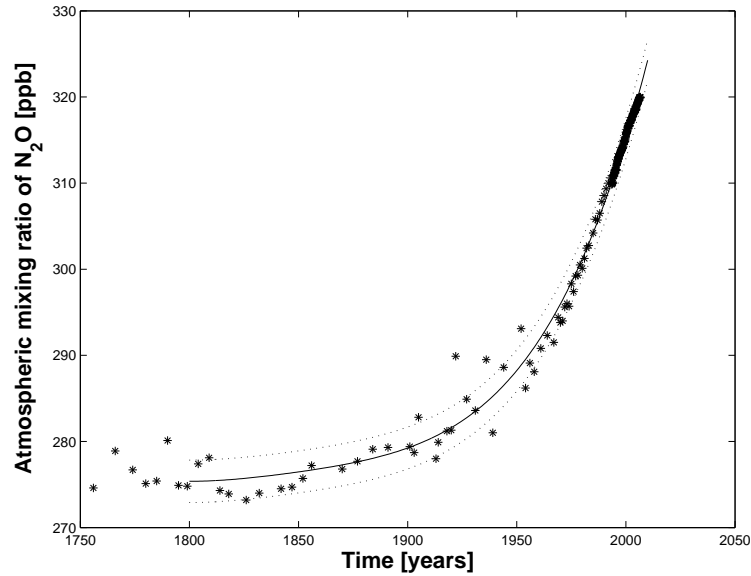


Figure 2.3: The in-situ air measurements, firn measurements, and ice-core data we used for reconstructing the atmospheric history of  $\text{N}_2\text{O}$  (*Machida et al.* [1995]; *Battle et al.* [1996]). The best fit we used for the analysis (see Equation 2.3) is shown as a black line, the dotted lines represent 95% confidence intervals for an individual observation.

2.3) from 1800 to the present day. The atmospheric mixing ratio of  $\text{N}_2\text{O}$  ( $X_{\text{N}_2\text{O}}$ ) in  $\text{nmol mol}^{-1}$  was calculated as

$$X_{\text{N}_2\text{O}}(t) = -0.0004t^3 + 1.0520t^2 - 1288.6261t + 592247.9514, \quad (2.3)$$

where  $t$  denotes the sampling year,  $1800 < t < 2008$ .

#### 2.1.4 Transit Time Distributions (TTD)

Following *Waugh et al.* [2003], it is assumed that the age distribution (TTD) of a water parcel, produced by different transport pathways and mixing, can be described as an inverse Gaussian function.

Since this function is a Green's function, it can be used to calculate the concentration  $c$  of a conservative tracer at any given point in space  $r$  and any given time  $t$ :

$$C(r, t) = \int_0^{\infty} c_0(t - t')G(r, t')dt', \quad (2.4)$$

where  $c_0$  is the input function of the tracer at the sea surface and  $G(r, t')$  is the TTD.

To uniquely determine an inverse Gaussian age distribution one needs to determine its two parameters  $\Gamma$ , the mean age, and  $\Delta$ , the width of the distribution. In order to estimate these from observations of a single transient tracer, such as CFC-12 or SF<sub>6</sub>, one needs to make an assumption about the ratio of  $\Gamma$  and  $\Delta$ .

*Waugh et al.* [2004] showed that a ratio of  $\Gamma/\Delta = 1$  is consistent with the distribution of a range of different tracers, and *Tanhua et al.* [2008] confirmed that this value is appropriate for the mid-latitude North Atlantic Ocean from the M60/5 cruise.

The TTD is then given by:

$$G(t) = \sqrt{\frac{\Gamma^3}{\pi 4\Delta^2 t^3}} \exp\left(\frac{-\Gamma(t - \Gamma)^2}{4\Delta^2 t}\right), \quad (2.5)$$

### 2.1.5 Calculation of Excess N<sub>2</sub>O

Three different approaches have been used to calculate  $[\text{N}_2\text{O}]_{eq}$  and hence  $[\text{N}_2\text{O}]_{xs}$ .

- (1) The “contemporary” approach:  $[\text{N}_2\text{O}]_{eq}$  was calculated based on the contemporary atmospheric dry mole fraction of N<sub>2</sub>O, e.g. [*Nevison et al.*, 2003; *Butler et al.*, 1989; *Yoshinari*, 1976]. The problem is that the “contemporary” atmospheric dry mole fraction of N<sub>2</sub>O has increased every year since c. 1800.
- (2) The “layer” approach used by *Walter et al.* [2006]: Given that equilibration time for N<sub>2</sub>O between the ocean surface layer and the atmosphere is fast (c. 3 weeks) relative to the atmospheric growth rate [*Najjar*, 1992],  $[\text{N}_2\text{O}]_{eq}^{layer}$  in the mixed layer was calculated using the contemporary atmospheric N<sub>2</sub>O value [*Jansen et al.*, 2007, 319 ppb for the year 2005]. For depths greater than 2000m  $[\text{N}_2\text{O}]_{eq}^{layer}$  was calculated using the tropospheric preindustrial value of 270 ppb [*Flückinger et al.*, 1999] as, generally, tropical Atlantic deep waters below 2000 m are older than 200 years [*Broecker and Peng*, 2000].

For the depth range between the upper thermocline and 2000 m an average of the current and the preindustrial atmospheric value was used (294 nmol mol<sup>-1</sup>). Hence:

$$[\text{N}_2\text{O}]_{eq}^{layer} = \begin{cases} 319 H_{T,S} P \text{ for mixed} \\ \text{layer samples} \\ 294 H_{T,S} P \text{ for samples} \\ \text{between thermo-} \\ \text{cline and 2000 m} \\ 270 H_{T,S} P \text{ for samples} \\ \text{deeper than} \\ \text{2000 m} \end{cases} \quad (2.6)$$

where  $H_{T,S}$  is the solubility of N<sub>2</sub>O in seawater [Weiss and Price, 1980] and  $P$  is the atmospheric pressure.

- (3) The “TTD” approach introduced here: CFC-12 and SF<sub>6</sub> data from the M60/5 cruise were used to calculate the transit time distribution, the TTD. *Tanhua et al.* [2008] have shown that use of SF<sub>6</sub> results in a more reliable estimation of TTDs for younger water masses. Hence SF<sub>6</sub> data (if available) were used for samples from “younger” water masses and CFC-12 data were used for all other samples, where “young waters” are defined as having CFC-12 values larger than 450 pmol mol<sup>-1</sup>.

The equilibrium N<sub>2</sub>O concentration was then calculated as the integral of the different fractions multiplied by their respective equilibrium concentrations, where the atmospheric mixing ratios were calculated using the sampling year and the polynomial fit as described in Equation 2.3.

$$[\text{N}_2\text{O}]_{eq}^{TTD}(t) = \int_0^\infty H_{T,S} X_{\text{N}_2\text{O}}(t - t') G(t') dt', \quad (2.7)$$

where  $t$  is the sampling year,  $H_{T,S}$  is the solubility of N<sub>2</sub>O in seawater [Weiss and Price, 1980],  $X_{\text{N}_2\text{O}}$  is the atmospheric history of N<sub>2</sub>O (see Equation 2.3) and  $G$  is the calculated transit time distribution (see Equation 2.5).

The 95%-confidence intervals for an individual observation associated with the atmospheric history used for the “TTD” approach are indicated in Figure



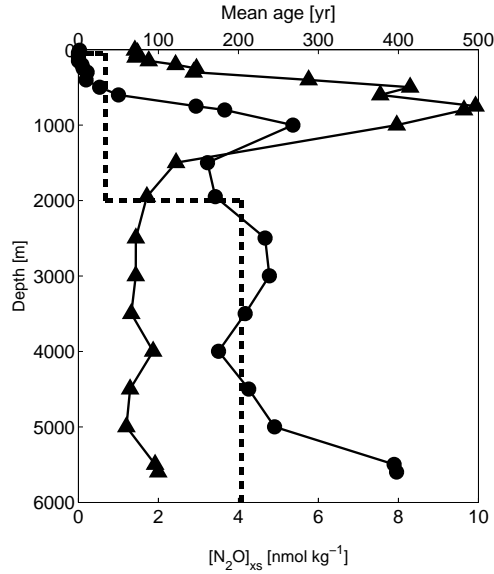


Figure 2.4:  $[\text{N}_2\text{O}]_{xs}$  ( $\text{nmol kg}^{-1}$ , denoted by triangles) and mean age according to the “TTD” approach (years, denoted by circles) versus depth (m) at station #158. Dashed lines indicate the mean age assumed by the “layer” approach.

2.3. Within these bounds the fitted values differ by less than 2.5 ppb from the extreme observations. A difference of 2.5 ppb leads to a difference in  $[\text{N}_2\text{O}]_{eq}$  and  $[\text{N}_2\text{O}]_{xs}$  of  $0.06 - 0.1 \text{ nmol kg}^{-1}$  for a range of suitable temperatures.

This calculation of  $\text{N}_2\text{O}$ OPR is based on the assumption that  $\text{N}_2\text{O}$  starts off at equilibrium with the atmosphere, which is not necessarily true for every water mass. *Körtzinger et al.* [2004] observed, however, that  $\text{O}_2$  was uniformly distributed at close-to-equilibrium concentrations even within an extremely deep winter-mixed layer (1400 m) in the Labrador Sea. As  $\text{N}_2\text{O}$  displays similar solubility characteristics as  $\text{O}_2$  it is likely to be the same for  $\text{N}_2\text{O}$ . An undersaturation/supersaturation of 2% has approximately the same quantitative effect on  $[\text{N}_2\text{O}]_{eq}$  as has the uncertainty of the atmospheric history. Additionally, it is assumed that  $[\text{N}_2\text{O}]_{xs}$  is not significantly altered by mixing of water with different temperatures, salinities and hence  $\text{N}_2\text{O}$  solubilities. The uncertainty thus introduced only attains the range of the uncertainty introduced by the atmospheric history ( $\sim 0.1 \text{ nmol kg}^{-1}$ ) if water masses differing by  $5^\circ - 10^\circ\text{C}$  in temperature are mixed. Therefore it is negligible.

The results of these three approaches are compared in Section 2.2.1 below.

### 2.1.6 Apparent N<sub>2</sub>O Production Rate

An apparent N<sub>2</sub>O production rate (N<sub>2</sub>OPR) was calculated as

$$\text{N}_2\text{OPR} = \frac{[\text{N}_2\text{O}]_{xs}}{\bar{t}}, \quad (2.8)$$

where  $\bar{t}$  is the mean age of the water sample calculated from the sample's TTD. To exclude any undue influence of short-term seasonal variations affecting the near-surface ocean in the estimated mean age, production rates were only calculated for samples with a mean age of at least one year. This explicitly excludes mixed layer samples.

A mean N<sub>2</sub>OPR for a water sample based on a history of advection, mixing and N<sub>2</sub>O production is not necessarily equivalent to a local or instantaneous N<sub>2</sub>O production rate. However, scaling by the mean age is a way of averaging the N<sub>2</sub>O production and attaching less weight to singular influential events. This means in particular that short-lived features of the N<sub>2</sub>O production rate cannot be represented this way but will be averaged out.

### 2.1.7 Apparent Oxygen Utilisation Rate

The apparent oxygen utilisation rate (AOUR) was estimated in a similar fashion:

$$\text{AOUR} = \frac{[\text{AOU}]}{\bar{t}}, \quad (2.9)$$

where  $\bar{t}$  is the mean age of the water sample calculated with the TTD method. As for N<sub>2</sub>O production rates, apparent oxygen utilisation rates were only calculated for samples with a mean age of at least one year.

## 2.2 Results & Discussion

### 2.2.1 Comparison of Different Approaches for $[\text{N}_2\text{O}]_{eq}$ Calculation

The effect of using different approaches to calculate  $[\text{N}_2\text{O}]_{eq}$  is shown in Figure 2.2. In surface waters, all three methods agree, as all methods employ the contemporary atmospheric  $\text{N}_2\text{O}$  mole fraction to calculate the  $\text{N}_2\text{O}$  background for this layer.

The TTD method is likely to be the quantitatively most appropriate method of calculating  $[\text{N}_2\text{O}]_{eq}$  and  $[\text{N}_2\text{O}]_{xs}$  as it uses a more sophisticated approach to age estimation. However, as noted earlier the TTD approach still cannot determine where, and when the excess  $\text{N}_2\text{O}$  was produced. The measured  $\text{N}_2\text{O}$  concentration represents an integrated estimate of  $[\text{N}_2\text{O}]_{xs}$ , which was produced along the transport path and mixing history of the water parcel. Figure 2.4 shows exemplary profiles of mean age and  $[\text{N}_2\text{O}]_{xs}$  versus depth. The uncertainty introduced by the approach amounts to  $0.06 - 0.1 \text{ nmol kg}^{-1}$  for a range of suitable temperatures (see Section 2.1.5).

The “layer” approach uses only three different atmospheric mixing ratios and is therefore a very rough approach to dealing with the atmospheric change displayed in Figure 2.3. As a result, application of this method produces sharp and unrealistic steps in background  $\text{N}_2\text{O}$  profiles (see Figures 2.2(c), 2.2(d)). In addition, this method also appears to slightly overestimate the age of water masses found below 2000m in comparison to the TTD approach. This arises from the approach’s failure to account for mixing with “younger” waters enriched in  $\text{N}_2\text{O}$ . It is worth noting, that for the “layer” approach the value of 294 ppb used for the intermediate layer differs by 24 ppb for the year 2004. This difference, which will most likely continue to increase due to the changing atmospheric mole fraction, leads to a difference in  $[\text{N}_2\text{O}]_{eq}$  and  $[\text{N}_2\text{O}]_{xs}$ , respectively, of  $0.5 - 1.2 \text{ nmol kg}^{-1}$  for a range of suitable temperatures.

Figure 2.2(c) shows that the commonly used “contemporary” approach systematically overestimates  $[\text{N}_2\text{O}]_{eq}$  by  $8\% - 13\%$  and thus underestimates  $[\text{N}_2\text{O}]_{xs}$  below the mixed layer, making it inappropriate for quantitative assessment of  $\text{N}_2\text{O}$  pro-

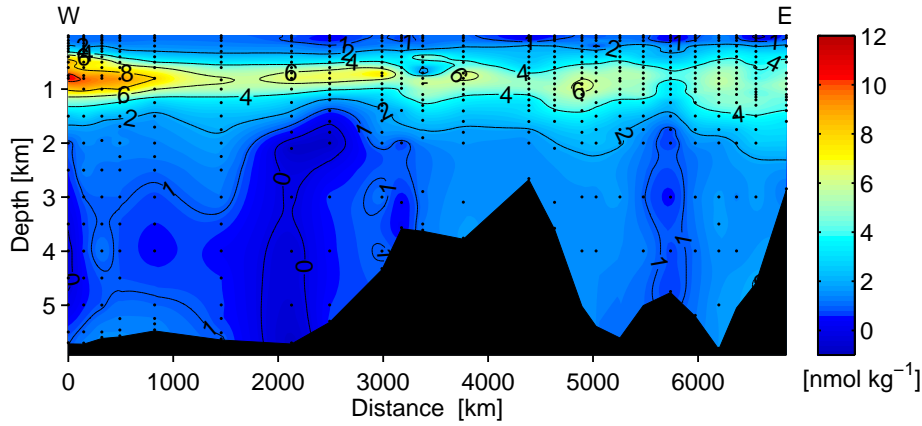


Figure 2.5: Section of excess  $\text{N}_2\text{O}$  ( $\text{nmol kg}^{-1}$ ) calculated with the TTD method. For exact location of the section, see Figure 2.1.

duction in deeper parts of the water column. Depending on the actual age of the water mass concerned, the “contemporary” approach can lead to a difference in  $[\text{N}_2\text{O}]_{eq}$  and  $[\text{N}_2\text{O}]_{xs}$ , respectively, of up to  $1 - 2 \text{ nmol kg}^{-1}$  for a range of suitable temperatures.

### 2.2.2 Excess $\text{N}_2\text{O}$ Concentrations

The measured  $[\text{N}_2\text{O}]$  profiles (Figure 2.2(a)) display a distinct peak around 700 – 1000 m, which has no equivalent in the  $[\text{N}_2\text{O}]_{eq}$  profiles (Figure 2.2(d)), and must therefore be the result of in-situ production. Figure 2.5 shows  $[\text{N}_2\text{O}]_{xs}^{TTD}$  along a west to east transect in the mid-latitude North Atlantic. In line with the results displayed in Figure 2.2, maximum values of  $[\text{N}_2\text{O}]_{xs}^{TTD}$  of  $6 - 12 \text{ nmol kg}^{-1}$  were found around 700 – 1000 m indicating that this part of the water column has accumulated a significant amount of  $\text{N}_2\text{O}$ .

The  $[\text{N}_2\text{O}]_{xs}^{TTD}$  peak appears to be slightly shallower and to be more pronounced in the western basin compared to the eastern basin. At shallower depth there is a clear difference in the magnitude of the  $[\text{N}_2\text{O}]_{xs}$  maximum between the eastern and the western basins. Maximum concentrations in the western basin reach up to  $12 \text{ nmol kg}^{-1}$ , whereas maximum concentrations in the eastern basin only attain about  $7 \text{ nmol kg}^{-1}$ . It should be noted that most stations sampled in the western basin were located further south of those sampled in the eastern basin

(see Figure 2.1).

$[\text{N}_2\text{O}]_{xs}$  in waters deeper than 2000 m is at  $1.9 \pm 0.5 \text{ nmol kg}^{-1}$  slightly elevated in the eastern basin compared to  $1 \pm 0.9 \text{ nmol kg}^{-1}$  in the western basin. A paired t-test rejects the hypothesis that both samples originate from a distribution of equal mean and equal variance at the 1%-significance level, but the overall level of excess  $\text{N}_2\text{O}$  accumulation in the deep waters of either basin remains very low.

### 2.2.3 The $[\text{N}_2\text{O}]_{xs}/\text{AOU}$ -Relationship

Maximum  $[\text{N}_2\text{O}]_{xs}$  coincides with maximum AOU concentrations. This indicates that the production of  $\text{N}_2\text{O}$  is due to nitrification consistent with the view of nitrification as the dominant production pathway of  $\text{N}_2\text{O}$  in the North Atlantic Ocean [Walter *et al.*, 2006; Nevison *et al.*, 2003; Oudot *et al.*, 2002; Yoshinari, 1976].

The fact that  $[\text{N}_2\text{O}]_{eq}$  is overestimated by 8% – 13% by the previously used “contemporary” approach implies that the earlier and widely reported correlations between apparent oxygen utilisation (AOU) and  $[\text{N}_2\text{O}]_{xs}$  are probably a distorted image of the true relationship between these quantities. While this distortion will not affect the interpretation of positive  $\text{N}_2\text{O}_{xs}/\text{AOU}$  correlations as qualitative indicators for the production of  $\text{N}_2\text{O}$  via nitrification, it may have an impact on the use of the quantitative characteristics of the relationship for the parameterisation of  $\text{N}_2\text{O}$  in models [e.g., Schmittner and Galbraith, 2008; Goldstein *et al.*, 2003; Suntharalingam and Sarmiento, 2000].

There are two different  $\text{N}_2\text{O}_{xs}/\text{AOU}$  relationships evident in our data. Therefore we have split the data into two parts: data points with potential densities  $< 27.5 \text{ kg m}^{-3}$  ( $< \sim 1000 \text{ m}$  or “shallow”) and data points with potential densities  $\geq 27.5 \text{ kg m}^{-3}$  ( $\geq \sim 1000 \text{ m}$  or “deep”).

Figure 2.6 presents these two least squares fits given by linear regression algorithms. The quantitative characteristics for all three approaches of  $[\text{N}_2\text{O}]_{xs}$  are listed in Table 2.1. The “contemporary” approach significantly overestimates  $[\text{N}_2\text{O}]_{eq}$  in middle-aged and older water masses by 8% – 13%. This results in a similar underestimation of  $[\text{N}_2\text{O}]_{xs}$ , whereas both methods, “contemporary” and “TTD” method, yield the same estimate of  $[\text{N}_2\text{O}]_{xs}$  for mixed layer sam-

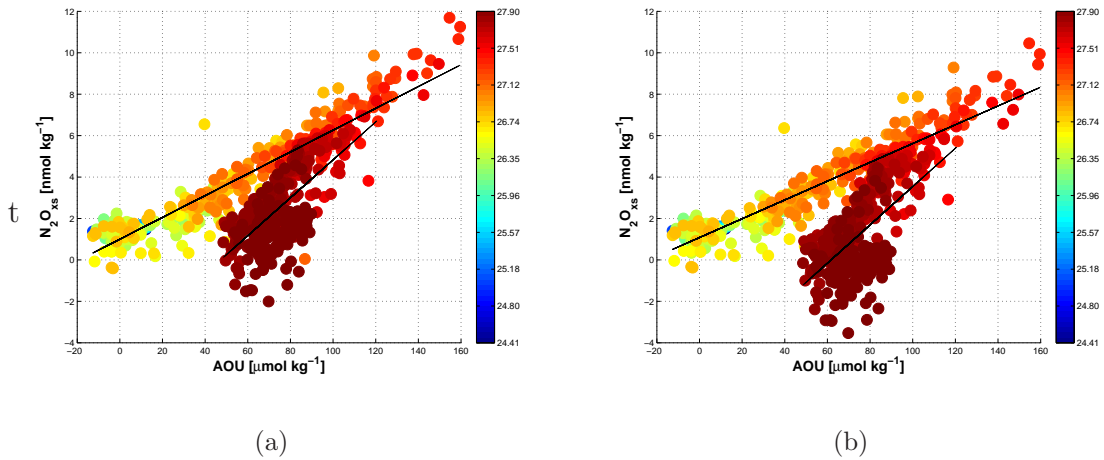


Figure 2.6:  $\text{N}_2\text{O}_{xs}$  concentrations ( $\text{nmol kg}^{-1}$ ) versus AOU concentrations ( $\mu\text{mol kg}^{-1}$ ),  $\sigma_\theta$  is colour coded in  $\text{kg m}^{-3}$ .  $[\text{N}_2\text{O}]_{xs}$  was calculated using the TTD method (a) and using only the contemporary mole fraction of 319 ppb (b).

ples. This gives rise to the steeper slope in the fit calculated using the “TTD” approach compared to the fit to the “shallow” data calculated using the contemporary atmospheric  $\text{N}_2\text{O}$  concentration. The slope for the “contemporary” approach is 14% smaller than the slope for the “TTD” approach. For the “deep” data points, the slope for the “contemporary” approach is 1% larger than that for the “TTD” approach. The difference in the “deep” water results from the fact, that the “contemporary” method underestimates  $[\text{N}_2\text{O}]_{xs}$  more strongly as the concerned water masses get older.

The “layer” method does not account for mixing and thus slightly underestimates  $[\text{N}_2\text{O}]_{eq}$  in old waters as it cannot reproduce the excess  $\text{N}_2\text{O}$  added to the respective water mass by mixing with younger waters enriched in  $\text{N}_2\text{O}$ .

For intermediate waters, the atmospheric mixing ratio used for the calculations was equivalent to the atmospheric  $\text{N}_2\text{O}$  mixing ratio from 1970. Therefore,  $[\text{N}_2\text{O}]_{eq}$  is underestimated for all water masses originating more recently than 1970, whereas it overestimates  $[\text{N}_2\text{O}]_{eq}$  for older water masses in this depth range. For “shallow” samples the slope for the “layer” approach is 3% smaller than the slope for the the “TTD” approach, indicating that most sampled intermediate water masses originated before 1970. For “deep” samples the slope for the “layer”

	“TTD”	“layer”	“contemporary”
slope ( $\sigma_\theta < 27.5$ )	0.0526	0.0512	0.0454
slope ( $\sigma_\theta \geq 27.5$ )	0.0916	0.0854	0.0924
intercept ( $\sigma_\theta < 27.5$ )	1.0005	1.3271	1.0797
intercept ( $\sigma_\theta \geq 27.5$ )	-4.3251	-3.7760	-5.7022

Table 2.1: Coefficients for a least squares fit of  $[\text{N}_2\text{O}]_{xs}$  regressed on [AOU].

approach is 7% smaller than the slope for the “TTD” approach. This implies that the age of intermediate water masses is underestimated, indicating that most sampled water masses between 1000 m and  $\sim 1500$  m originated before 1970.

#### 2.2.4 $\text{N}_2\text{O}$ Production Rates

To quantify sources and sinks of  $\text{N}_2\text{O}$ , it is not sufficient to look at  $[\text{N}_2\text{O}]_{xs}$  alone, but it is necessary to look at production rates. The  $[\text{N}_2\text{O}]_{xs}$  distribution, on its own, is not useful in revealing sources of  $\text{N}_2\text{O}$  as the water mass age distribution in the ocean interior is highly variable. Production rates ( $\text{N}_2\text{OPR}$ , see Section 2.1.6) can potentially shed more light on processes responsible for  $\text{N}_2\text{O}$  production.

In order to check whether our TTD-based estimates of  $\text{N}_2\text{OPR}$  are reasonable, we first calculated AOU rates from the same data set. AOUR varies between 0.1 and  $17 \mu\text{mol kg}^{-1} \text{yr}^{-1}$  (upper 500 m) and 0.1 and  $13 \mu\text{mol kg}^{-1} \text{yr}^{-1}$  (500 – 1000 m), respectively. These rates agreed reasonably well with prior estimates of AOUR of  $4 - 25 \mu\text{mol kg}^{-1} \text{yr}^{-1}$  (upper 500 m) and  $1 - 10 \mu\text{mol kg}^{-1} \text{yr}^{-1}$  (500 – 1000 m), respectively, based on  $^3\text{H}/^3\text{He}$  age determination for a similar region [*Jenkins and Wallace, 1992*]. The “TTD” approach was also used by *Tanhua et al. [2007]* to estimate anthropogenic carbon concentrations and was found to be in good agreement with independent methods. This suggests that the use of CFC-12 and  $\text{SF}_6$  as tracers is a good reliable basis for water mass age and hence rate calculations.

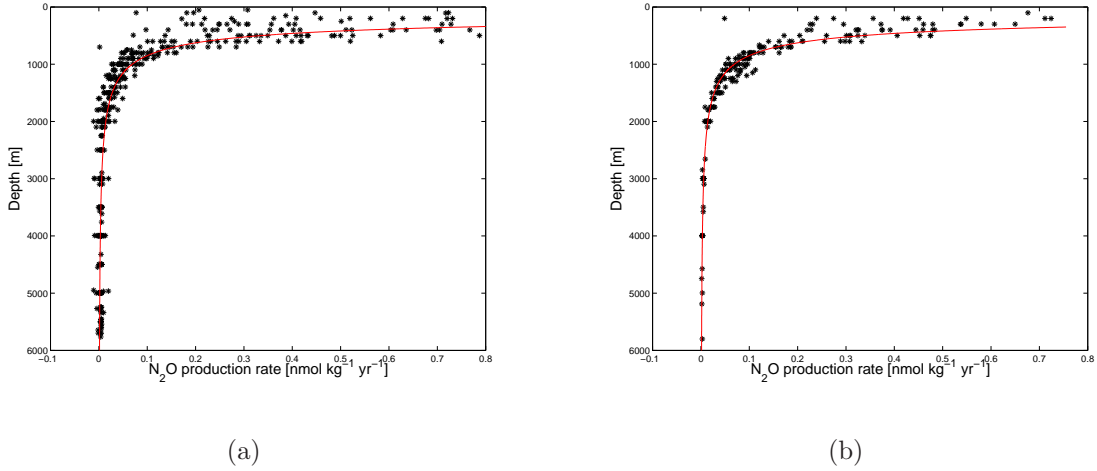


Figure 2.7: N<sub>2</sub>O production rates (nmol kg<sup>-1</sup> yr<sup>-1</sup>) versus depth (m) for the western (a) and eastern (b) basin of the North Atlantic Ocean. The red lines show a Martin curve fitted to the respective data (see Equation 2.10).

#### 2.2.4.1 Influence of Depth and Remineralisation

Figure 2.7 shows N<sub>2</sub>OPR plotted against depth. Maximum production rates occur just below the mixed layer, there is a lot of near-surface scatter, however. At most of the stations there is no subsurface maximum. Some stations between 30°N and 40°N in both basins display a small subsurface maximum, which mostly comprises just one sampled depth. The maximal production rate in the western basin of 1.9 nmol kg<sup>-1</sup> yr<sup>-1</sup> is only very slightly higher than the maximal production rate in the eastern basin of 1.7 nmol kg<sup>-1</sup> yr<sup>-1</sup>, and the general distribution is not significantly different, as is illustrated by the fitted curves displayed in red in Figure 2.7. Moreover, a paired t-test does not reject the hypothesis that both samples originate from distributions with equal mean and equal variance at the 1%-significance level.

The red line in Figure 2.7 represents a Martin curve fitted to the data. Following *Martin et al.* [1987], this fitted curve  $F(z)$  can be described as

$$F(z) = F_{100} \left( \frac{z}{100} \right)^b, \quad (2.10)$$

where  $F_{100}$  is the intercept of a log-log fit of the data,  $b$  is the slope of this log-log



fit and  $z$  denotes depth.

The parameters of the fit were determined using only the data from the eastern basin, but with the exception of the few very high rates, it fits the data from the western basin as well.

Especially in waters deeper than 2000 m there seems to be very little variation, neither within or between basins. However, the dissolved oxygen concentrations in the eastern basin of  $248 \pm 5 \mu\text{mol kg}^{-1}$  are lower than the concentrations of  $261 \pm 7 \mu\text{mol kg}^{-1}$  in the western basin, probably due to the effects of the thermohaline circulation. A t-test rejects the hypothesis that both oxygen-samples originate from a distribution with equal mean and equal variance at the 1%-significance level.

Oceanic  $\text{N}_2\text{O}$  is mainly produced by nitrification and denitrification [*Bange, 2008*]. Since the waters of the North Atlantic are well oxygenated and denitrification only occurs in low-oxygen environments, a significant nitrous oxide source originating from denitrification processes seems very unlikely. Together with the fact that a Martin curve fits the data so well, this suggests that  $\text{N}_2\text{O}$  production in deep waters is controlled by the flux of organic particles from above as this flux is typically parameterised by a Martin curve. This seems reasonable as nitrification is fuelled by organic particles, which are remineralised at depth.

#### 2.2.4.2 Influence of AOU and Temperature

As nitrification is supposed to be the main production mechanism, it is reasonable to quantify the  $\text{N}_2\text{O}$  yield per mole oxygen consumed  $\left(\frac{d\text{N}_2\text{O}}{-d\text{O}_2}\right)$ . *Nevison et al.* [2003] argued, that  $[\text{N}_2\text{O}]_{xs}/\text{AOU}$  may not be an adequate estimate of  $\frac{d\text{N}_2\text{O}}{-d\text{O}_2}$  due to the effects of mixing and advective transport. Mixing of water masses with different temperatures can create “virtual” super- or undersaturations as the solubility function of  $\text{N}_2\text{O}$  depends non-linearly on temperature. Following *Nevison et al.* [2003] we neglect this effect as it is probably small. We use  $\text{N}_2\text{OPR}/\text{AOUR}$  as an estimate of  $\frac{d\text{N}_2\text{O}}{-d\text{O}_2}$ . The influence of mixing on  $[\text{N}_2\text{O}]_{eq}$  in terms of mixing of water with different ages is accounted for by the TTD approach (see Section 2.1.5), which leaves the influence of mixing and advective transport on  $[\text{N}_2\text{O}]_{xs}$  to be dealt with. It is important to note that our approach to estimation of  $[\text{N}_2\text{O}]_{xs}$  integrates the effects of potentially varying production/decomposition

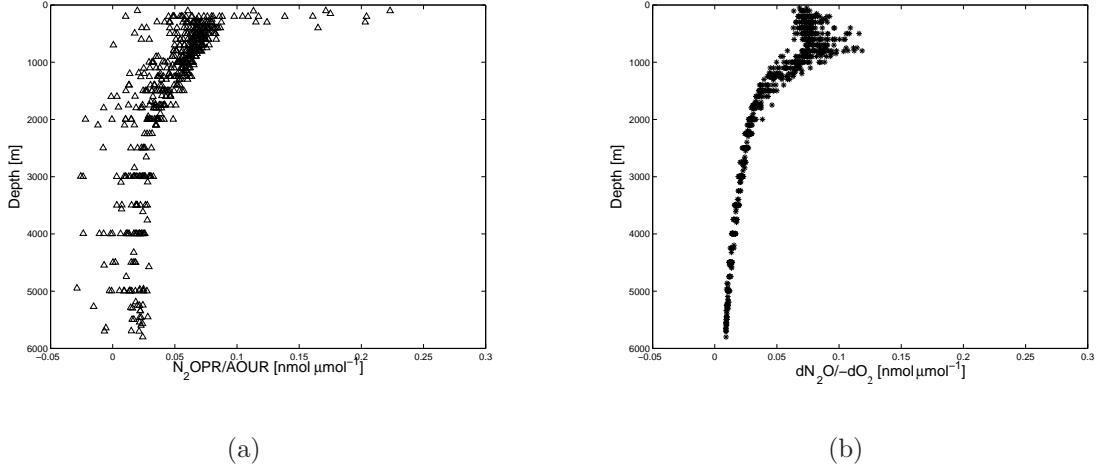


Figure 2.8: (a):  $N_2\text{OPR}/\text{AOUR}$  ( $\text{nmol } \mu\text{mol}^{-1}$ ) versus depth (m), ratios calculated from the M60/5 data. (b):  $\frac{dN_2O}{-dO_2}$  calculated using the parameterisation given by *Nevison et al.* [2003].

mechanisms along the transport path of a water mass. Hence our  $N_2\text{OPR}$  and  $\text{AOUR}$  estimates represent smoothed and averaged quantities along the transport pathway. They provide average rates which are not necessarily representative of instantaneous or local rates.

Figure 2.8 shows the ratio of  $N_2\text{OPR}$  to  $\text{AOUR}$ , both the ratios calculated from the M60/5 data and the ratios calculated according to the parameterisation given by *Nevison et al.* [2003]. The latter parameterised  $\frac{dN_2O}{-dO_2}$  as the  $N_2O$  yield of nitrification ( $\frac{dN_2O}{-dNO_3^-}$ ) based on laboratory experiments by *Goreau et al.* [1980], i. e.

$$\frac{dN_2O}{-dO_2} = R_{N:O_2} \frac{dN_2O}{-dNO_3^-}, \quad (2.11)$$

where  $R_{N:O_2}$  is the Redfield ratio. Noting the same exponential relationship we give in Equation 2.13, the parameterisation is extended to

$$\frac{dN_2O}{-dO_2} = R_{N:O_2} \frac{dN_2O}{-dNO_3^-} \exp\left(-\frac{z}{z_{scale}}\right), \quad (2.12)$$

where  $z$  denotes depth and  $z_{scale}$  is a scaling factor.

There seems to be a systematic difference between the two sets of ratios between 500 m and 1000 m. The parameterisation of *Nevison et al.* [2003] displays a clear

subsurface maximum in the production rates around 700 m. This is in general not reflected in our parameterisation. There are, however, a few stations which display a subsurface maximum in the concerned depth range, which is obscured by the scatter in Figure 2.8(a). This discrepancy could be due to the fact that the results of *Goreau et al.* [1980] were obtained by studying a single nitrifying organism.

The ratio of N<sub>2</sub>OPR to AOURL depends exponentially on depth, i.e. a relationship of the following type holds

$$\frac{\text{N}_2\text{OPR}}{\text{AOURL}} = a_1 \exp\left(-\frac{z}{z_{sc}}\right), \quad (2.13)$$

where  $a_1$  and  $z_{sc}$  are scaling factor and  $z$  denotes the depth. This seems to suggest that with greater depth the by-path in nitrification that produces N<sub>2</sub>O is less frequently used. This might be related to the general decline in temperature with depth or the decrease in the overall nitrification rate with depth. With the present data it is impossible to assign a reason for this trend, which could also be an effect of a change in community structure.

We used this relationship to develop a parameterisation of N<sub>2</sub>OPR against AOURL and depth. Using Equation 2.13 the best fit to our data can be described as

$$\text{N}_2\text{OPR}(\text{AOURL}, z) = \text{AOURL } a_1 \exp\left(-\frac{z}{z_{sc}}\right) + a_2, \quad (2.14)$$

where the coefficient values for the best fit are  $a_1 = 0.0658$ ,  $a_2 = -0.0065$ ,  $z_{sc} = 20000$  and  $z$  denotes the depth.

As depth is strongly correlated with temperature and the latter may have a stronger biological influence it seems reasonable to also develop a parameterisation of N<sub>2</sub>OPR based on temperature instead of depth. Equation 2.14 then translates into:

$$\text{N}_2\text{OPR}(\text{AOURL}, T) = \text{AOURL } a_1 \exp\left(-\frac{T}{T_{sc}}\right) + a_2, \quad (2.15)$$

where the coefficient values for the best fit are  $a_1 = 0.0665$ ,  $a_2 = -0.0032$ ,  $T_{sc} = 20000$  and  $T$  denotes the temperature.

Figure 2.9(a) shows the N<sub>2</sub>O production rates calculated from the M60/5-data. The fitted values according to Equation 2.14 (Figure 2.9(a)), and the correlation

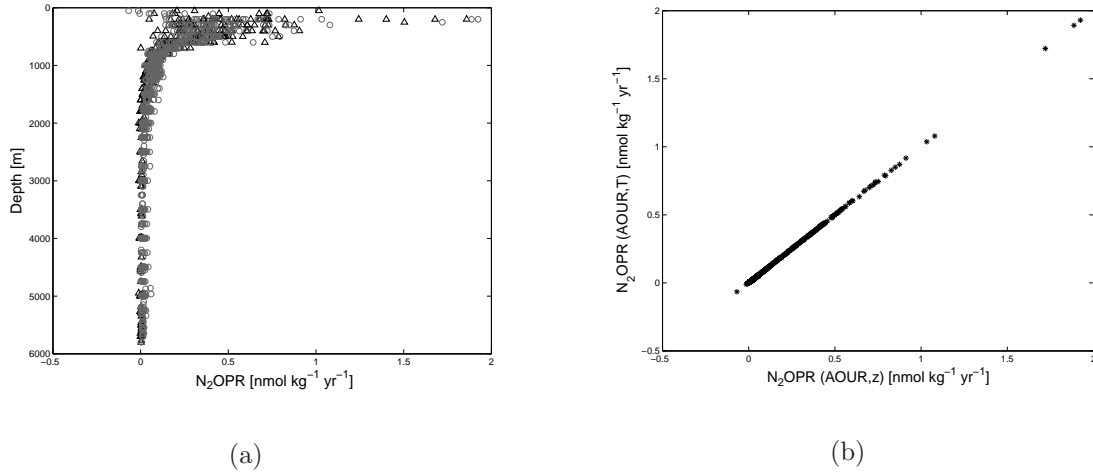


Figure 2.9: (a): N<sub>2</sub>O production rate (nmol kg<sup>-1</sup> yr<sup>-1</sup>) calculated from M60/data and (black triangles) fitted values given by Equation 2.14 (gray circles) versus depth (m). (b): Fitted values of N<sub>2</sub>OPR according to Equation 2.15 versus fitted values of N<sub>2</sub>OPR according to Equation 2.14.

between the fits given by Equation 2.14 and Equation 2.15, respectively, (Figure 2.9(b)) illustrate the goodness of our fits. Our parameterisations only account for N<sub>2</sub>O production by nitrification. However, due to lack of oxygen the AOURLs in anoxic zones will be very small. Therefore this parameterisation also effectively reproduces the decreasing to vanishing N<sub>2</sub>O production due to nitrification in suboxic to anoxic zones, which a parameterisation simply based on AOU is incapable of doing. Therefore this parameterisation can be used to calculate N<sub>2</sub>O production due to nitrification without having to introduce a somewhat artificial critical oxygen threshold. Our parameterisations can be used to calculate global N<sub>2</sub>O concentration fields with any coupled GCM/biogeochemical model, which allows for apparent oxygen utilisation rates to be calculated. Additionally, these parameterisations facilitate the calculation of global [N<sub>2</sub>O] fields using existing gridded tracer [Key *et al.*, 2004] and AOU data [Garcia *et al.*, 2006] (see Chapter 4).

## 2.3 Conclusions

1. The commonly employed method of using just the contemporary atmospheric mixing ratio of  $\text{N}_2\text{O}$  to calculate  $[\text{N}_2\text{O}]_{xs}$  underestimates the strength of possible  $\text{N}_2\text{O}$  sources. Due to this, the quantitative characteristics of the widely used correlation between AOU and  $[\text{N}_2\text{O}]_{xs}$  are biased. Especially as the quantitative characteristics of this relationship form the basis for calculation of  $\text{N}_2\text{O}$  production rates, it is of importance to estimate this relationship as accurately as possible. The TTD approach introduced here provides a way to calculate appropriately “age-corrected” excess  $\text{N}_2\text{O}$  concentrations. The difference in slopes of the correlation between AOU and  $[\text{N}_2\text{O}]_{xs}$  is up to 14% for the “contemporary” versus the “TTD” approach and up to 7% for the “layer” versus the “TTD” approach.
2.  $\text{N}_2\text{O}_{xs}^{TTD}$  concentrations found in the North Atlantic are similar to those found in previous studies. Largest concentrations of  $\text{N}_2\text{O}_{xs}$  are found between 700 m and 1000 m. This accumulation of  $\text{N}_2\text{O}_{xs}$  reflects a balance between production and water mass age.
3. We used TTDs to calculate AOURL and  $\text{N}_2\text{OPR}$ . AOURLs are similar to the rates found in earlier studies.  $\text{N}_2\text{OPR}$  correlates well with AOURL and correlates inversely with depth and/or temperature.
4. We developed a new parameterisation of  $\text{N}_2\text{OPR}$  in terms of AOURL and temperature/depth, which can be used in biogeochemical models and to calculate  $\text{N}_2\text{OPR}/[\text{N}_2\text{O}]$  from existing global gridded data like GLODAP/WOA. It differs from earlier parameterisations, as it parameterises a  $\text{N}_2\text{O}$  production rate per timestep in terms of an oxygen utilisation rate per timestep instead of a  $\text{N}_2\text{O}$  production rate per mole oxygen consumed. Our parameterisation can be applied to calculate the  $\text{N}_2\text{O}$  production due to nitrification in the entire ocean including the oxygen minimum zones, as AOURL, in contrast to AOU, tends to become very small at very low oxygen levels.



# Chapter 3

## North Atlantic Nitrous Oxide Emissions

Traditionally, the  $\text{N}_2\text{O}$  flux from the ocean is estimated as the product of the difference between the measured partial pressure of  $\text{N}_2\text{O}$  in surface water and the atmospheric equilibrium partial pressure, and the air-sea gas transfer coefficient. Several empirical models have been suggested to parameterise the gas transfer coefficient as a function of surface wind speed [e.g. *Liss and Merlivat, 1986; Wanninkhof, 1992*], with an estimated error of at least 50% [*Erickson, 1988*]. Generally,  $\text{N}_2\text{O}$  production is thought to take place only in the subsurface ocean. If this is the case, the sea-to-air flux of  $\text{N}_2\text{O}$  should be equal to the supply of  $\text{N}_2\text{O}$  to the mixed layer from below. In this chapter, we compare estimates of the  $\text{N}_2\text{O}$  flux across the air-sea interface with estimates of the  $\text{N}_2\text{O}$  flux to the mixed layer based on calculating the  $\text{N}_2\text{O}$  gradient and coupling it with the diapycnal mixing rate. Potential reasons for the differences between the flux estimates are discussed.

### 3.1 Methods

#### 3.1.1 Study Area and $\text{N}_2\text{O}$ Measurements

The data presented here were collected in the mid-latitude North Atlantic Ocean during spring 2004 on board the German research vessel RV Meteor [*Tanhua*

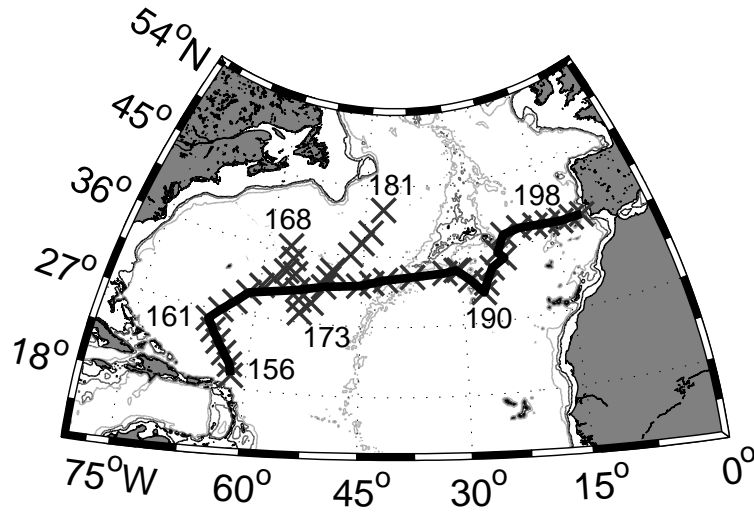


Figure 3.1: Cruise track of the M60/5 cruise in 2004. The crosses mark individual stations, and the black line marks the position of the section. Selected station numbers are indicated.

*et al.*, 2006; *Walter et al.*, 2006]. The cruise track of the Meteor cruise 60/5 was from Martinique to Lisbon, with a northernmost station at 42°N, 42°W so that the cruise included sampling of both the subtropical and cold-temperate gyres, as well as the western and eastern basins (see Figure 3.1).

Water samples for N<sub>2</sub>O analysis were collected at 37 stations in triplicate from various depths, taken with a 24-Niskin-bottle rosette, equipped with a CTD-sensor. Samples were then analysed by gas-chromatography using an electron capture detector. The analytical method applied for N<sub>2</sub>O analysis is described in detail by *Walter et al.* [2006]. For the two-point calibration procedure we used standard gas mixtures with  $311.8 \pm 0.2$  ppb and  $346.5 \pm 0.2$  ppb N<sub>2</sub>O in synthetic air, which have been calibrated against the NOAA (National Oceanic and Atmospheric Administration, Boulder, Co.) standard scale in the laboratories of the Air Chemistry Division of the Max Planck Institute for Chemistry, Mainz, Germany. The overall relative mean analytical error is estimated to be  $\pm 1.8$  %.

N<sub>2</sub>O concentrations are denoted by brackets and are generally reported in nmol kg<sup>-1</sup>. All measured profiles are displayed in Figure 3.2. Note: All error margins represent one standard deviation if not explicitly stated otherwise.



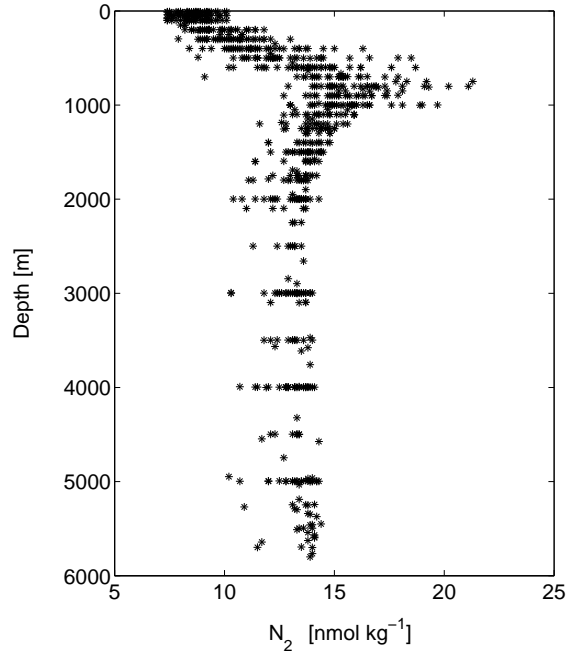


Figure 3.2:  $\text{N}_2\text{O}$  concentrations ( $\text{nmol kg}^{-1}$ ) measured during the M60/5 cruise.

### 3.1.2 Ocean-Atmosphere $\text{N}_2\text{O}$ flux

The flux of  $\text{N}_2\text{O}$  across the air-sea interface ( $F_{gasex}$ ) can be expressed as

$$F_{gasex} = k ([\text{N}_2\text{O}]_w - H_{T,S} X_{\text{N}_2\text{O}} P) \quad (3.1)$$

where  $k$  is the gas transfer velocity,  $[\text{N}_2\text{O}]_w$  is the  $\text{N}_2\text{O}$  concentration in the bulk of the water in the surface mixed layer,  $X_{\text{N}_2\text{O}}$  is the atmospheric mixing ratio of  $\text{N}_2\text{O}$  near the interface,  $P$  is the atmospheric pressure and  $H_{T,S}$  is the solubility of  $\text{N}_2\text{O}$  in seawater [Weiss and Price, 1980]. We used a compilation of surface  $\text{N}_2\text{O}$  data (see Table 3.1 for details) to calculate  $F_{gasex}$ . Monthly windspeed data from the ECMWF ERA-40 reanalysis ([http://data.ecmwf.int/data/d/era40\\_mnth/](http://data.ecmwf.int/data/d/era40_mnth/)) were used to calculate the gas transfer velocities. Two alternative relationships for  $k$ , as suggested by Liss and Merlivat [1986] (denoted by LM86) and Wanninkhof [1992] (relationship for climatological winds, denoted by W92) were used to give lower and upper boundaries for  $F_{gasex}$ , respectively.

Cruise	Time	Reference
AMT 7	09/1998-10/1998	<i>Rhee et al.</i> [2009]
INDOMED 11A	09/1978	<i>Weiss et al.</i> [1992]
INDOMED Leg 2	11/1977-12/1977	<i>Weiss et al.</i> [1992]
SAVE Transit	11/1987	<i>Weiss et al.</i> [1992]
TTO/NAS Leg 2	04/1981-05/1981	<i>Weiss et al.</i> [1992]
TTO/NAS Leg 3	05/1981-06/1981	<i>Weiss et al.</i> [1992]
TTO/NAS Leg 4	06/1981-07/1981	<i>Weiss et al.</i> [1992]
TTO/NAS Leg 7	09/1981-10/1981	<i>Weiss et al.</i> [1992]
TTO/TAS Leg 2	01/1983	<i>Weiss et al.</i> [1992]

Table 3.1: Data points used for flux calculations according to gas exchange models.

### 3.1.3 Cross-Thermocline N<sub>2</sub>O Flux

The total flux  $F_{\text{N}_2\text{O}}^{\text{grad}}$  from deeper parts of the water column into the mixed layer was calculated as

$$F_{\text{grad}} = k_z \text{grad}_{\text{N}_2\text{O}}, \quad (3.2)$$

where  $k_z$  is the diapycnal mixing coefficient and  $\text{grad}_{\text{N}_2\text{O}}$  is the concentration gradient of N<sub>2</sub>O between the lower boundary of the mixed layer and the depth of the subsurface N<sub>2</sub>O maximum (cf. Figure 3.2).

To calculate  $\text{grad}_{\text{N}_2\text{O}}$  the depth of the N<sub>2</sub>O maximum ( $d_{\text{N}_2\text{O}_{\text{max}}}$ ) was determined for every station from the depth profile. The mixed layer depth ( $d_{\text{ml}}$ ) was calculated from the temperature profile at every station using CTD data and the refined algorithm of *Kara et al.* [2000] with  $\Delta T = 0.2^\circ\text{C}$ , as this algorithm yielded the best results on comparison with manual inspection. To calculate the nitrous oxide concentration at the bottom of the mixed layer  $[\text{N}_2\text{O}]_{\text{ml}}$ , we used the measured N<sub>2</sub>O profile and the interpolation scheme of *Steffen* [1990]. Nitrous oxide concentrations were interpolated using two points of the profile above and one below the calculated mixed layer depth and then again using one point above and two points below. The mean of the two interpolated concentrations was used as

Lat. Box	Lower left corner	Upper right corner
A	19.4°N, 66.0°W	25.0°N, 45.0°W
B	25.0°N, 66.0°W	30.7°N, 16.2°W
C	30.7°N, 66.0°W	36,4°N, 10.3°W
D	36,4°N, 66.0°W	42.0°N, 10.1°W

Table 3.2: Definition of the latitudinal boxes.

an estimate of  $[\text{N}_2\text{O}]_{ml}$ . The  $\text{N}_2\text{O}$  gradient was then calculated as

$$\text{grad}_{\text{N}_2\text{O}} = \frac{[\text{N}_2\text{O}]_{max} - [\text{N}_2\text{O}]_{ml}}{d_{\text{N}_2\text{O}_{max}} - d_{ml}}, \quad (3.3)$$

where  $[\text{N}_2\text{O}]_{max}$  is the maximum  $\text{N}_2\text{O}$  concentration. Please note that this assumes the gradient to be linear, which is a simplification.

Following *Watson and Ledwell* [2000] we estimated the diapycnal mixing coefficient  $k_z$  as

$$k_z = 0.49 \overline{\text{bf}}, \quad (3.4)$$

where  $\overline{\text{bf}}$  is a mean buoyancy frequency for the respective station. This was calculated for the depth interval between the  $\text{N}_2\text{O}$  maximum (usually at a depth of c. 700 – 800 m) and the base of the mixed layer using CTD data.

Both  $\text{N}_2\text{O}$  fluxes were averaged over four geographical boxes (see Table 3.2 and Figure 3.3 for definition) to facilitate a more meaningful comparison between  $F_{gasex}$  and  $F_{grad}$ , with (w) denoting the western part of the box and (e) denoting the eastern part of the box as defined by the Mid Ocean Ridge. Effects influencing  $F_{grad}$  and  $F_{gasex}$  such as production and stratification are likely to vary following a roughly latitudinal pattern. The same holds for large scale windspeed patterns.

## 3.2 Results & Discussion

### 3.2.1 $\text{N}_2\text{O}$ Flux – Comparison of Gas Exchange and Gradient Method

$F_{gasex}$  is shown in Figure 3.3 and Figure 3.4. Extrapolating these daily fluxes to annual estimates yields mean annual fluxes of  $71 \pm 214 \mu\text{mol m}^{-2} \text{yr}^{-1}$  ( $2 \pm 6$

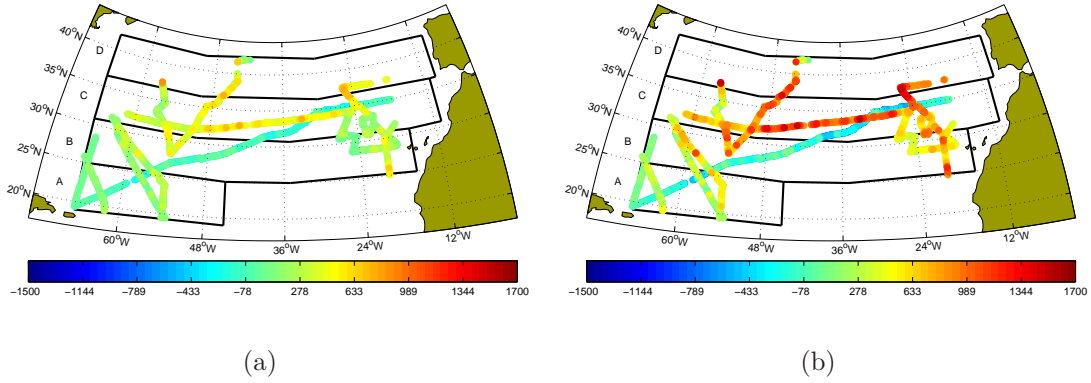


Figure 3.3:  $F_{gasex}$  ( $\text{nmol m}^{-2} \text{d}^{-1}$ , (a) LM86, (b) W92) calculated using supplementary surface  $\text{N}_2\text{O}$  data (see Table 3.1), mean monthly winds taken from the ERA40 reanalysis.

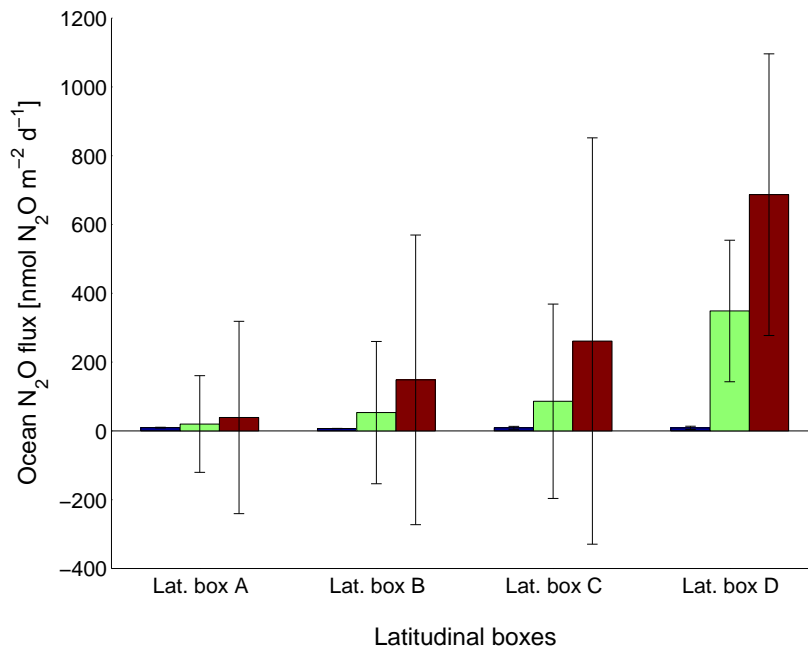


Figure 3.4: Fluxes ( $\text{nmol m}^{-2} \text{d}^{-1}$ )  $F_{grad}$  (blue),  $F_{gasex}^{LM86}$  (green), and  $F_{gasex}^{W92}$  (red) per latitudinal box.

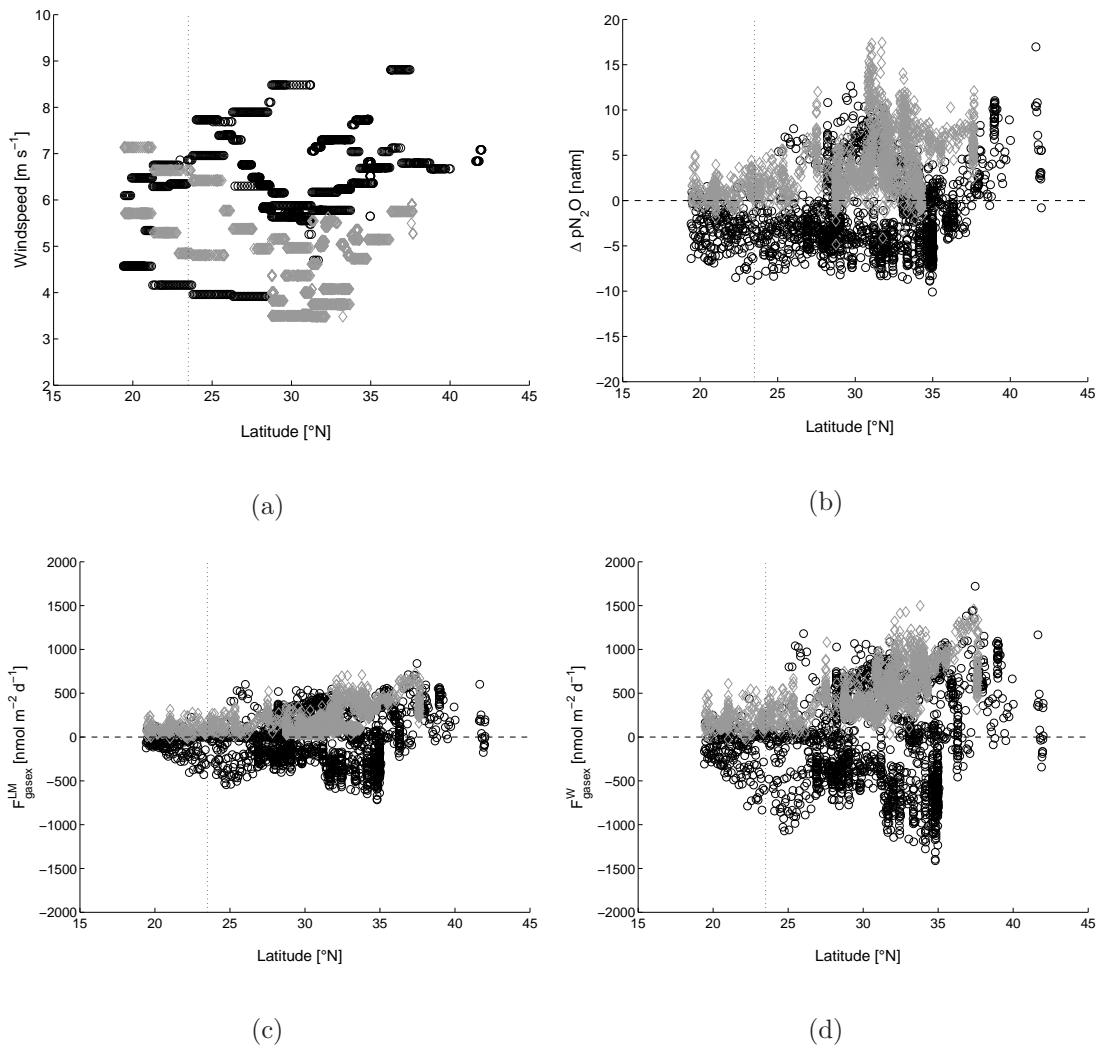


Figure 3.5: Windspeed ( $\text{m s}^{-1}$ , (a)),  $\Delta pN_2O$  (natm (b)), and  $F_{gasex}$  ( $\text{nmol m}^{-2} \text{d}^{-1}$ , (c) LM86, (d) W92) versus latitude. Gray diamonds denote spring/summer data points, black circles denote autumn/winter data points.

$\text{mg N m}^{-2} \text{yr}^{-1}$ ) (LM86) and  $143 \pm 428 \mu\text{mol m}^{-2} \text{yr}^{-1}$  ( $4 \pm 12 \text{mg N m}^{-2} \text{yr}^{-1}$ ) (W92). These compare well the range of  $0 - 8 \text{mg N m}^{-2} \text{yr}^{-1}$  for the mean annual flux calculated by *Nevison et al.* [1995] for this part of the Atlantic Ocean. This is, however, not surprising as *Nevison et al.* [1995] used almost the same data set and the parameterisations of *Liss and Merlivat* [1986] and *Wanninkhof* [1992] as well. *Forster et al.* [2009] calculated biogeochemical fluxes using in-situ  $N_2O$  data

Lat. Box	$F_{grad}$	$F_{gasex}^{LM86}$	$F_{gasex}^{W92}$
A	$9 \pm 1$	$20 \pm 144$	$39 \pm 279$
B (w)	$7 \pm 1$	$23 \pm 218$	$55 \pm 435$
B (e)	$7 \pm 1$	$92 \pm 184$	$268 \pm 369$
C (w)	$10 \pm 5$	$216 \pm 207$	$445 \pm 419$
C (e)	$6 \pm 1$	$8 \pm 293$	$151 \pm 648$
D (w)	$14 \pm 3$	$294 \pm 221$	$572 \pm 435$
D (e)	$5 \pm 1$	$428 \pm 150$	$854 \pm 301$

Table 3.3:  $F_{grad}$ ,  $F_{gasex}^{LM86}$ , and  $F_{gasex}^{W92}$  ( $\text{nmol m}^{-2} \text{d}^{-1}$ ) for the different latitudinal boxes. For details on the latitudinal boxes see Table 3.2 and Figure 3.6.

and in-situ wind speeds for several ‘‘Longhurst’’ provinces [Longhurst, 1998]. For the Longhurst provinces NAST(E) and NATR, which constitute the only overlap with our dataset, our average  $F_{gasex}$  of  $30 - 190 \text{ nmol m}^{-2} \text{d}^{-1}$  (NAST(E)) and  $270 - 540 \text{ nmol m}^{-2} \text{d}^{-1}$  (NATR) are reasonably similar to the ranges given by Forster *et al.*.  $F_{gasex}$  overall increases towards more northerly latitudes, which is in part maybe caused by the seasonal variability of windspeed and  $p\text{N}_2\text{O}$  and also partly by a seasonally biased sampling (cf. Figure 3.5). The influence of the seasonal cycle is discussed in the next section.

$F_{grad}$  calculated at every station of M60/5 is shown in Figure 3.6 and Figure 3.7. The mean  $F_{grad}$  equals  $9 \pm 4 \text{ nmol m}^{-2} \text{d}^{-1}$ .  $F_{grad}$  is distributed relatively uniformly throughout the North Atlantic with the exception of a few higher values towards the northern end of the sampled region of the western basin (see Figure 3.6). These high fluxes at northerly latitudes result from a particular configuration of a very deep mixed layer, a comparatively high diapycnal mixing rate and a fairly average  $[\text{N}_2\text{O}]_{max}$ . However, only data from a single expedition (M60/5) were used to calculate  $F_{grad}$  so there is no seasonal variability included in the estimates. Generally,  $[\text{N}_2\text{O}]_{xs}$  increases towards more tropical latitudes (cf. Figure 3.8). This increase in  $[\text{N}_2\text{O}]_{xs}$  was also found by Walter *et al.* [2006]. However, as  $F_{grad}$  displays no clearly discernible likewise trend, the strength of the  $\text{N}_2\text{O}$  maximum seems not to exert a major influence on  $F_{grad}$ . It is worth

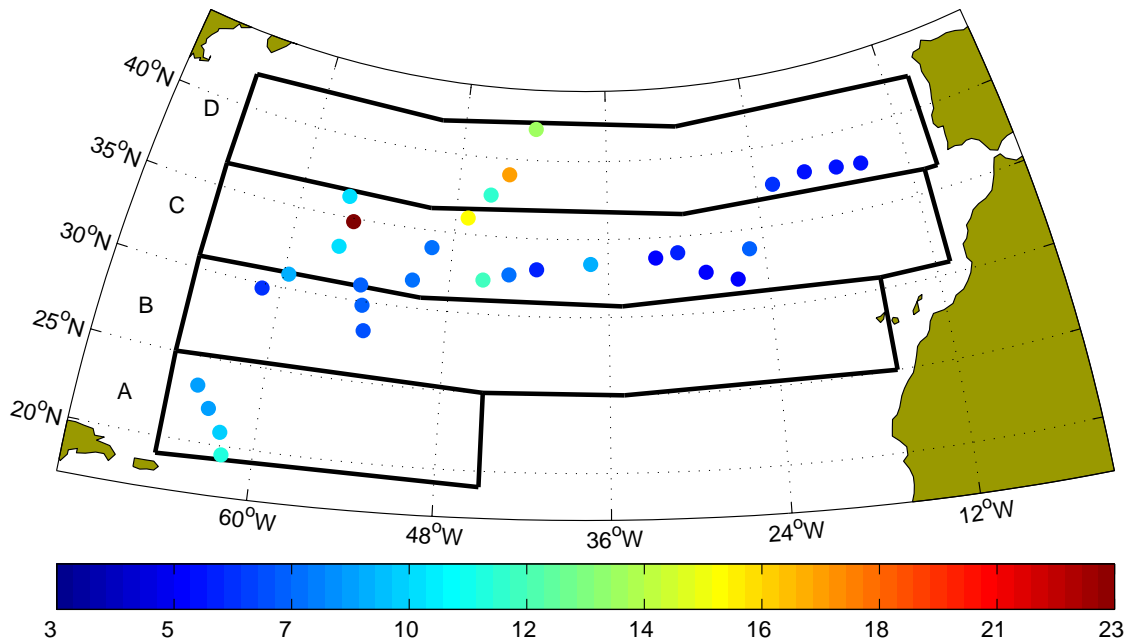


Figure 3.6:  $F_{grad}$  ( $\text{nmol m}^{-2} \text{d}^{-1}$ ) for M60/5 station data. For definition of the boxes see Table 3.2.

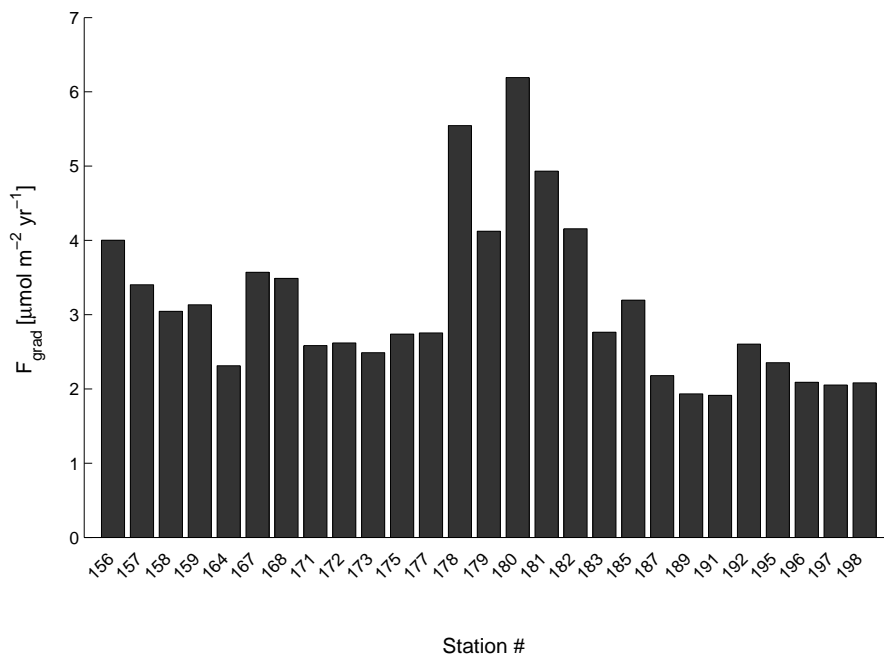


Figure 3.7:  $F_{grad}$  ( $\text{nmol m}^{-2} \text{d}^{-1}$ ) per station. For geographical information about the stations cf. Figure 3.1.

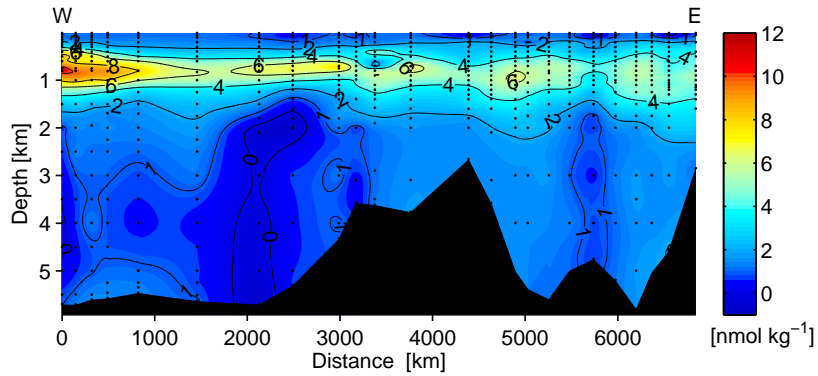


Figure 3.8: Section of excess  $\text{N}_2\text{O}$  ( $\text{nmol kg}^{-1}$ ) calculated with the TTD method. For definition of excess  $\text{N}_2\text{O}$  cf. Chapter 2 and for exact location of the section cf. Figure 3.1.

noting that there is almost no variability in the eastern basin (cf. also Table 3.3) and that a paired t-test rejects the hypothesis that  $F_{grad}$  (w) and  $F_{grad}$  (e) originate from normal distributions with equal mean and equal variance at the 99%-significance level, which means that the t-test suggests that there is a systematic difference between the eastern and the western basin.

The smallest values of  $F_{grad}$  ( $5 - 6 \text{ nmol m}^{-2} \text{ d}^{-1}$ ) occur in the eastern part of boxes C and D, while the largest values of  $F_{grad}$  occur in the western part of boxes C and D. It should be noted that box C (w) features two very high flux values, which influence the mean, while values at the other stations of the box are only slightly elevated. There are only 3 stations in box D (w), which all display elevated fluxes. The mean  $F_{gasex}$  displays a clear increasing trend towards the northerly latitudes, with the exception of box C (e). High values of  $F_{gasex}$  also occur in boxes C (w) and D (w). However, the highest values of  $F_{gasex}$  occur in box D (e), which features the lowest value of  $F_{grad}$ . Mainly due to the large variability in  $F_{gasex}$ , both  $F_{grad}$  and  $F_{gasex}$  agree within the range of one standard deviation for boxes A, B, C, although the mean  $F_{grad}$  is smaller than the mean  $F_{gasex}$  by a factor of 2 – 150 (cf. Table 3.3). Only for boxes C (w, only W92) and D is the mean  $F_{grad}$  smaller than the mean  $F_{gasex}$  within one standard deviation, even despite the considerable uncertainties of the latter.

There are two possible reasons for this difference between  $F_{gasex}$  and  $F_{grad}$ . Firstly, there could be seasonal variability in  $F_{gasex}$ , which is not captured by a seasonally-



Lat. Box	Number of Data Points				
	Spring	Summer	Autumn	Winter	Total
A	296	0	244	0	540
B (w)	183	0	445	0	628
B (e)	6	236	94	152	488
C (w)	256	0	391	0	647
C (e)	353	348	383	0	1084
D (w)	0	0	120	0	120
D (e)	0	82	0	0	82
Total	1094	666	1677	152	3589

Table 3.4: Seasonal breakdown of the N<sub>2</sub>O surface measurements.

biased sampling of surface waters (cf. Table 3.4 for a seasonal breakdown of our data points). This suggestion is supported by samples collected from similar locations showing ingassing and outgassing of N<sub>2</sub>O for different sampling times (cf. Figure 3.3). Additionally, depending on the type of function describing this seasonal cycle, a simple mean might not be a representative estimate of the net N<sub>2</sub>O flux, even if the seasonal cycle is adequately resolved. Secondly, there could be biological production of N<sub>2</sub>O in the mixed layer causing  $F_{gasex}$  to be greater than  $F_{grad}$ .

### 3.2.2 Seasonal Cycle

A typical North Atlantic N<sub>2</sub>O profile displays a maximum well below the mixed layer. This implies the existence of a gradient in direction of the surface (and towards the deep sea) and therefore the existence of a flux of N<sub>2</sub>O into the mixed layer. Profile data indicate that this profile structure is largely unaffected by seasonality, except in areas of deep convection (cf. Section 1.1.4). Therefore it is very unlikely that there is export of N<sub>2</sub>O out of the mixed layer into the deep ocean, again except in areas of deep convection. However, even if the mixed layer cannot be a source of N<sub>2</sub>O for the deep ocean, it can still act as a temporary source or sink for atmospheric N<sub>2</sub>O.

To investigate the seasonal cycle, the expeditions were broken down in four cate-

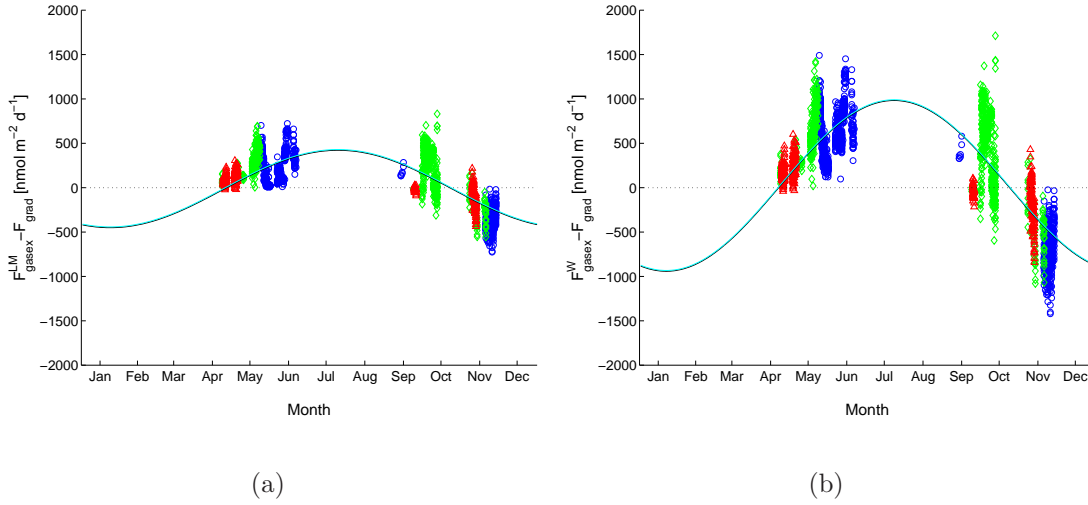


Figure 3.9: Tropical (red triangles), western subtropical (green diamonds) and eastern subtropical (blue circles)  $F_{gasex} - F_{grad}$  ( $\text{nmol m}^{-2} \text{d}^{-1}$ , (a) LM86, (b) W92) versus month. The solid lines denote a harmonic function of the type described in Equation 3.5 fitted to  $F_{gasex} - F_{grad}$  (black) and  $F_{gasex}$  (cyan), respectively.

gories: winter (December, January, February), spring (March, April, May), summer (June, July, August), autumn (September, October, November). The seasonal breakdown of the surface  $\text{N}_2\text{O}$  measurements is detailed in Table 3.4 and Figures 3.5, and 3.9. Overall, the 1760 spring/summer data points are reasonably balanced by the 1829 autumn/winter data points. A paired t-test rejects the hypothesis that the spring/summer and the autumn/winter surface  $p\text{N}_2\text{O}$  values are independent samples of normal distributions with equal mean and equal variance at the 99%-significance level for tropical latitudes, the subtropical part of the western basin, and the subtropical part of the eastern basin, respectively. It is worth noting, that a paired t-test yields the same results for windspeeds. For tropical latitudes average windspeeds are very similar in spring/summer and in autumn/winter ( $\sim 6 \pm 1 \text{ m s}^{-1}$ ). For subtropical latitudes, average windspeeds are higher in autumn/winter ( $\sim 7 \pm 1 \text{ m s}^{-1}$  (w, e)) than in spring/summer ( $\sim 5 \pm 1 \text{ m s}^{-1}$  (w), ( $\sim 4 \pm 1 \text{ m s}^{-1}$ )(e)). Therefore the same absolute  $\Delta p\text{N}_2\text{O}$  value tends to induce a higher flux in autumn/winter. The seasonally broken down difference between  $F_{gasex}$  and  $F_{grad}$  and the seasonal variability of  $F_{gasex}$  are il-

illustrated in Figure 3.9. A paired t-test rejects the hypothesis that  $F_{gasex} - F_{grad}$  in spring/summer and  $F_{gasex} - F_{grad}$  in autumn/winter originate from a normal distribution with identical mean and variance at the 99%-significance level, for both parameterisations (LM86, W92) and both basins, respectively. A paired t-test for  $F_{gasex}$  yields the same results. This supports the assertion that there is a seasonal effect on  $F_{gasex}$ , generally leading to a net positive flux in spring/summer and a net negative flux in autumn/winter.

There are three main potential controls of the behaviour of surface  $N_2O$  and thus the mixed layer source/sink:

1. Temperature. Temperature is subject to a seasonal cycle, which is more pronounced towards higher latitudes. A change in temperature induces a change in solubility. If this change happens faster than an adjustment of the equilibrium concentration can take place, large short-scale super-/undersaturations in the surface layer can result. The seasonal temperature change also induces a change in stratification, resulting in a deepening of the mixed layer during the onset of the cooling season. The ensuing entrainment of deeper  $N_2O$ -rich waters can cause temporary elevated surface  $pN_2O$ .
2. Biology. Oceanic  $N_2O$  is mainly produced by nitrification and denitrification (cf. Section 1.1.5). Since the mixed layer is well oxygenated and denitrification only occurs in low-oxygen environments [Devol, 2008], a significant nitrous oxide source in the mixed layer originating from denitrification processes is very unlikely. Therefore only production via nitrification could potentially exert an influence on mixed layer  $N_2O$  concentrations. Whether or not nitrification can take place in the mixed layer, is still debated controversially. It should be noted, that although temperature often influences biological processes, temperature is not a limiting factor for in-situ nitrification rates [Ward, 2008].
3. Mixing. With the data available, this effect cannot be distinguished. However, mixing and advection also change nutrient concentrations and are thus partly included in “biological” influence, while the temperature-induced seasonal mixed layer deepening is included in 1.

Therefore, following *Lüger et al.* [2004] we will only consider the two driving mechanisms temperature effects and “biology”.

Generally, spring and summer are characterised by an increase in sea-surface temperature (SST), while autumn and winter are characterised by a decline in SST. In spring, the temperature may often rise faster than an adjustment of the equilibrium concentration can take place, resulting in large short-scale supersaturations in the surface layer. In autumn, the process is reversed resulting in large short-scale undersaturations in the surface layer. However, the onset of sea-surface cooling induces a deterioration of stratification and thus often a deepening of the mixed layer. The ensuing entrainment of deeper,  $\text{N}_2\text{O}$ -enriched waters may cause elevated surface  $p\text{N}_2\text{O}$  values on short timescales, counteracting the solubility effect of decreasing SST. Any snapshot capturing some of these short-term features obviously does not necessarily represent a realistic estimate of an annual average surface  $p\text{N}_2\text{O}$  level.

In the case of “biology”, the picture is less clear. Until recently, nitrification was thought to be inhibited by light [*Horrigan et al.*, 1981] – making it a very unlikely occurrence in the mixed layer. The results of *Bange* [2004] are in line with this. He used a simple box model of the surface layer of the central Arabian Sea to calculate ocean-atmosphere  $\text{N}_2\text{O}$  fluxes based on the gas exchange models of *Liss and Merlivat* [1986], *Wanninkhof* [1992] and *Wanninkhof and McGillis* [1999]. The model results agreed well with existing data leading the author to conclude that the surface layer  $\text{N}_2\text{O}$  saturation in the Arabian Sea is mainly controlled by gas exchange, entrainment of  $\text{N}_2\text{O}$  from deeper layers and variability in the sea surface temperature.

On the other hand, model results by *Yool et al.* [2007] based on nitrification measurements suggest something very different. They suggest a significant nitrification activity in the euphotic zone, which would put nitrification in the picture as a possible nitrous oxide source in the mixed layer. *Clark et al.* [2008] measured  $\text{NH}_4^+$  and  $\text{NO}_2^-$  oxidation rates on a north-south transect through the Atlantic Ocean. Their data suggest that in the oligotrophic Atlantic Ocean there is nitrification in the photic zone which is of sufficient intensity to turn over the  $\text{NO}_3^-$ -pool in one day.

*Dore and Karl* [1996] used in-situ measurements of  $[\text{N}_2\text{O}]$  at the ALOHA station

in April and October, and the gas exchange model of *Wanninkhof* [1992] to calculate  $\text{N}_2\text{O}$  ocean-atmosphere fluxes. They calculated the flux to the euphotic zone using concentration gradients and an eddy-diffusivity coefficient of  $3.7 \times 10^{-5} \text{ m}^2 \text{ s}^{-1}$ . They used these flux estimates to calculate a net  $\text{N}_2\text{O}$  production rate in the euphotic zone of  $1.68 - 7.94 \mu\text{mol m}^{-2} \text{ d}^{-1}$ , which they attribute to in-situ nitrification. Assuming a  $\text{N}_2\text{O}$  yield of 0.5% during nitrification, nitrification estimates derived from the  $\text{N}_2\text{O}$  production rate were on the same order of magnitude as their directly measured nitrification rates. Even taking into account the probably rather large uncertainties involved in all the calculations, these results clearly point towards a significant  $\text{N}_2\text{O}$  production via nitrification in the euphotic zone. Slightly larger (super-) saturations of  $\text{N}_2\text{O}$  in the upper 40 m of the water column might even have suggested near-surface production.

*Morell et al.* [2001] used the whitecap model of *Erickson* [1993] and the gas exchange models of *Liss and Merlivat* [1986] and *Wanninkhof and McGillis* [1999] to calculate the air-sea  $\text{N}_2\text{O}$  flux based on their data from the Atlantic Ocean and the Caribbean Sea in the vicinity of Puerto Rico. They calculated the cross-thermocline flux using the eddy-diffusivity coefficient derived by *Pacanowski and Philander* [1981] for the tropical oceans. They also found a difference between cross-thermocline and air-sea  $\text{N}_2\text{O}$  fluxes in the range of *Dore and Karl* [1996]. They acknowledge that this difference might likely be due to nitrification as indicated by experimental evidence of *Dore and Karl* [1996] and *Dore et al.* [1998]. However, they also concede that large uncertainties, especially in gas-exchange models, might play a major role for the magnitude of the differences found. It should be noted that their calculations are only based on samples from April and June. The difference between their flux estimates might therefore well – at least partly – be due to seasonal thermal effects instead of biological effects. While the situation is unclear in case of  $p\text{N}_2\text{O}$ , the picture is a lot clearer for  $p\text{CO}_2$ , its seasonal variability and the driving forces. A comparison of surface  $\text{N}_2\text{O}$  and surface  $\text{CO}_2$  could be instructive in understanding the driving forces of the variability in surface  $\text{N}_2\text{O}$  and  $F_{\text{gasex}}$ . The harmonic function

$$x(t) = c_0 + c_1 \sin\left(2\pi \frac{t}{365}\right) + c_2 \cos\left(2\pi \frac{t}{365}\right) + c_3 \sin\left(4\pi \frac{t}{365}\right) + c_4 \cos\left(4\pi \frac{t}{365}\right), \quad (3.5)$$

where  $x$  is the seasonally varying quantity,  $t$  is the day of the year and  $c_1 - c_4$

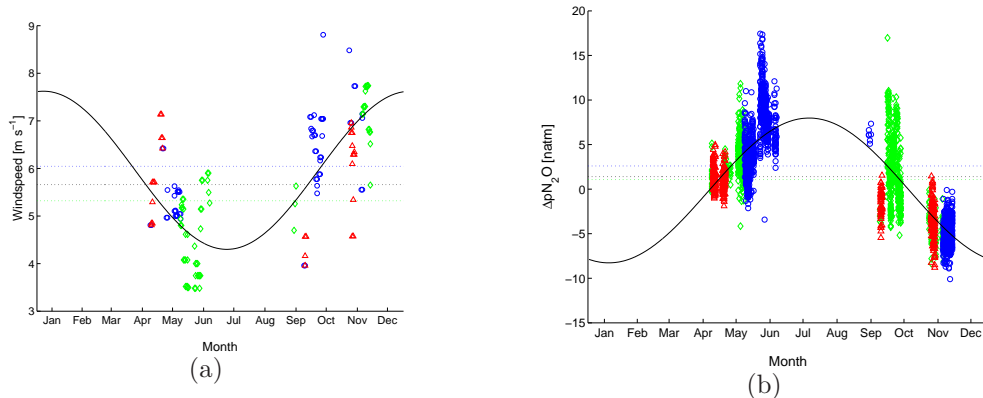


Figure 3.10: Tropical (red triangles), western subtropical (green diamonds) and eastern subtropical (blue circles) windspeed ( $\text{m s}^{-1}$ , (a)) and surface  $\Delta p\text{N}_2\text{O}$  (natm, (b)) data points versus month. The solid black line denotes a fitted harmonic function of the type described in Equation 3.5. The dotted lines denote the respective annual mean for all data points (black), the western (green) and the eastern (blue) basin.

are seasonal terms, has been found to adequately reflect the seasonality of SST and both seawater and atmospheric  $p\text{CO}_2$  [Zeng *et al.*, 2002; Lüger *et al.*, 2004]. It is therefore not completely unreasonable to assume that surface  $p\text{N}_2\text{O}$  is governed by some sort of harmonic function as well. However, as the maximum data gap must not exceed 3 months for a robust estimation of  $c_1 - c_4$  [Zeng *et al.*, 2002], the seasonal data coverage does not allow for a resolution of the full seasonal cycle for each latitudinal box, or even for each basin. Fitting the function given in Equation 3.5 to all available  $p\text{N}_2\text{O}$  data yields a reasonable fit (cf. Figure 3.10) explaining 61% of the systematic variability in  $p\text{N}_2\text{O}$  and featuring a significant overall F-test ( $p$ -value of 0) and significant t-tests ( $p$ -value of  $< 10^{-6}$  for each coefficient). This indicates that the components included in our regression model are highly significant in explaining the systematic variability in  $p\text{N}_2\text{O}$ , even if the  $r^2$ -value of 61% suggests that we are still missing some controlling factors. However, there is still a 4-month data gap from December-March. On comparison, it should be noted that a simple linear fit, assuming no seasonality, only explains 24% of the systematic variability in surface  $p\text{N}_2\text{O}$ . Nevison *et al.* [1995], who found the North Atlantic to be a weak source in summer and a weak sink

in winter, also acknowledged the existence of a seasonal temperature effect on  $F_{gase,x}$ .

### Seasonal Cycle of Surface $pN_2O$

*Lüger et al.* [2004] found a significant difference between  $pCO_2$  in the eastern and in the western basin. In the eastern basin, biological and temperature effects cancel, as the major phytoplankton blooms, during which  $pCO_2$  is lowered due to photosynthesis, occur at times when a purely temperature-controlled surface  $pCO_2$  displays seasonal maxima. This leads to a subdued annual cycle in the eastern basin. In the western basin there are no counteracting effects between “biology” and temperature, leading *Lüger et al.* to conclude that surface  $pCO_2$  in the western basin is strongly temperature controlled. However, it should be kept in mind that for surface  $pN_2O$ , the effects of “biology” and temperature would add up instead of cancel each other in the eastern basin, as high primary productivity leads to higher amounts of organic matter being recycled and thus potentially to higher rates of  $N_2O$  production. Therefore a mainly biologically controlled seasonal cycle of surface  $pN_2O$  should display more pronounced seasonal maxima in the eastern basin instead of the subdued seasonal cycle displayed by surface  $pCO_2$ .

A paired t-test rejects the hypothesis that the  $\Delta pN_2O$  values from the eastern and the western basin originate from a normal distribution with equal mean and equal variance, suggesting there is a systematic difference between the eastern and the western basin. However, there is very little seasonal overlap among samples from the western and the eastern basin (cf. Figure 3.10), which in presence of a seasonal cycle could explain the statistical results. Figure 3.10 rather suggests that there is good agreement between data from the eastern and the western basin sampled at a comparable time of year. The data points from the eastern basin for the time of intense biological activity between August-October do not indicate a more pronounced  $\Delta pN_2O$  peak, however, unfortunately, there are only very few data points for this period. In line with this, the overall shape of the fitted annual cycle indicates a mainly temperature-controlled behaviour of  $\Delta pN_2O$ .  $\Delta pN_2O$  also reflects the increasing amplitude of the seasonal cycle of SST increases towards higher latitudes (cf. Figure 3.5).

### Seasonal Variability of $F_{\text{gasex}}$ in the Latitudinal Boxes

$F_{\text{gasex}}$  also shows systematic (seasonal) variability, although the results for the individual boxes are sometimes biased due to seasonally-biased sampling. For box A there are no summer and no winter data points and there is no significant seasonal bias for either the warming or the cooling season (cf. Table 3.4). Also, box A comprises the tropical latitudes where the seasonal variation of SST is less pronounced. The mean spring  $\Delta p\text{N}_2\text{O}$  value is  $1 \pm 1$  natm, the mean autumn  $\Delta p\text{N}_2\text{O}$  value was  $-3 \pm 2$  natm. The ocean-atmosphere flux from box A was also reasonably well balanced (cf. Figure 3.9, Figure 3.4) and the resulting  $F_{\text{gasex}}$  of  $20 \pm 144$  nmol m<sup>-2</sup> d<sup>-1</sup> (LM86) and  $39 \pm 279$  nmol m<sup>-2</sup> d<sup>-1</sup> (W92), respectively, was comparatively small.

Box B (w) displays a clear seasonal bias towards autumn (cf. Table 3.4). In the warming season  $\Delta p\text{N}_2\text{O}$  was elevated ( $4 \pm 2$  natm), while in the cooling season  $\Delta p\text{N}_2\text{O}$  was mostly diminished ( $-2 \pm 4$  natm). The mean  $\Delta p\text{N}_2\text{O}$  was  $0 \pm 4$  natm. There is a comparatively small net N<sub>2</sub>O flux to the atmosphere of  $23 \pm 218$  nmol m<sup>-2</sup> d<sup>-1</sup> (LM86), and  $55 \pm 435$  nmol m<sup>-2</sup> d<sup>-1</sup> (W92)), respectively. The likely reason for this is the mixed layer deepening, as most data points originate from September. This is in line with the results of *Lüger et al.* [2004], who found high values of surface  $p\text{CO}_2$  in the western basin (between 34°N and 54°N) in September, which they attributed to temperature-induced changes.

In Box B (e), there is no clear seasonal bias, but within the cooling season there is a slight bias towards winter data points and within the warming season there is a clear bias towards summer data points (cf. Table 3.4). There are only data points from the warming season towards the northern end of Box B. In the warming season surface  $\Delta\text{N}_2\text{O}$  is almost never diminished ( $2 \pm 2$  natm), while in the cooling season  $\Delta p\text{N}_2\text{O}$  varies from  $-9 - 12$  natm. The mean  $\Delta p\text{N}_2\text{O}$  was  $0 \pm 4$  natm. Windspeeds are generally higher in the cooling season ( $7 \pm 1$  m s<sup>-1</sup> compared to  $4 \pm 1$  m s<sup>-1</sup>), attaching comparatively more weight to cooling season  $\Delta p\text{N}_2\text{O}$  when calculating mean fluxes. This results in a larger net ocean-atmosphere flux compared to box B (w) of  $92 \pm 184$  μmol m<sup>-2</sup> yr<sup>-1</sup> (LM86), and  $268 \pm 369$  μmol m<sup>-2</sup> yr<sup>-1</sup> (W92).

Box C (w) is slightly biased towards autumn and there are no summer or winter data points (cf. Table 3.4).  $\Delta p\text{N}_2\text{O}$  in the warming season is on average elevated



( $4 \pm 2$  natm). At an average  $\Delta p\text{N}_2\text{O}$  value of  $1 \pm 4$  natm, this is also the case in the cooling season. As all cooling season data points originate from October,  $\Delta p\text{N}_2\text{O}$  is likely strongly influenced by the seasonal mixed layer deepening. A paired t-test still rejects the hypothesis that  $\Delta p\text{N}_2\text{O}$  datasets originate from normal distributions with equal mean and equal variance at the 99%-significance level. Due to the overall elevated  $\Delta p\text{N}_2\text{O}$  values, the net air-sea  $\text{N}_2\text{O}$  flux in box C of  $216 \pm 207$  nmol  $\text{m}^{-2} \text{d}^{-1}$  (LM86) and  $445 \pm 419$  nmol  $\text{m}^{-2} \text{d}^{-1}$  (W92), respectively, is larger than that of box A and B.

Box C (e) is clearly biased towards the warming season and there are no winter data points (cf. Table 3.4).  $\Delta p\text{N}_2\text{O}$  is elevated on average in the warming season ( $6 \pm 4$  natm), and diminished in the cooling ( $-5 \pm 2\%$  natm). 376 of the 383 autumn data points originate from a single cruise in November and display negative  $\Delta p\text{N}_2\text{O}$  values. In connection with elevated mean wind speeds in autumn of  $7 \pm 1$   $\text{m s}^{-1}$  vs.  $4 \pm 1$   $\text{m s}^{-1}$  in spring/summer, the only half as many negative autumn  $\Delta p\text{N}_2\text{O}$  values still balance the elevated  $\Delta p\text{N}_2\text{O}$  values in the warming season. That high windspeeds exert a comparatively important influence in box C (e) is also reflected in the overall flux. For all other boxes, the W92-flux is roughly two times larger than the LM86-flux, while in box C (e) the mean W92-flux of  $151 \pm 648$  nmol  $\text{m}^{-2} \text{d}^{-1}$  is roughly 15 times larger than the LM86-flux of  $8 \pm 293$  nmol  $\text{m}^{-2} \text{d}^{-1}$ .

Box D (w) is not very representative. It only comprises 120 data points, which were only collected in autumn (cf. Table 3.4) during a single cruise in October. Surface waters mostly display elevated  $\Delta p\text{N}_2\text{O}$  values, with an average  $\Delta p\text{N}_2\text{O}$  value of  $4 \pm 4$  natm. Negative  $\Delta p\text{N}_2\text{O}$  values occur less frequent than positive  $\Delta p\text{N}_2\text{O}$  values, possibly due to seasonal mixed layer deepening. Additionally, although maximum windspeeds are not significantly larger than those for the other boxes, high windspeeds occur more frequently (cf. Figure 3.5). Together with the mainly non-negative  $\Delta p\text{N}_2\text{O}$  values, the frequently occurring high windspeeds (overall range  $7 - 9$   $\text{m s}^{-1}$ ) result in a net flux of  $294 \pm 221$  nmol  $\text{m}^{-2} \text{d}^{-1}$  (LM86) and  $572 \pm 435$  nmol  $\text{m}^{-2} \text{d}^{-1}$  (W92), respectively. This flux is considerably larger than that of boxes A-C. This is, however, a highly biased estimate as all of the data points originate from only a single cruise.

Box D (e) is probably the least representative. It only comprises 82 summer data

points (cf. Table 3.4). In line with the supposed seasonal cycle,  $\Delta p\text{N}_2\text{O}$  values are always positive and vary between 2–12 natm. Windspeeds are quite uniform, they only vary between 5 – 6 m s<sup>-1</sup>. The resulting net fluxes of  $428 \pm 150$  nmol m<sup>-2</sup> d<sup>-1</sup> (LM86) and  $854 \pm 301$  nmol m<sup>-2</sup> d<sup>-1</sup> (W92) are larger than for any other box.

### Seasonal Cycle of $F_{gasex}$

Comparing Figures 3.10 and 3.9 illustrates that the amplitude and especially the sign of the systematic variability of  $F_{gasex}$  is (mainly) controlled by the systematic variability of  $\Delta p\text{N}_2\text{O}$ . And since the seasonal cycle of  $p\text{N}_2\text{O}$  is mainly temperature-controlled, the same holds for  $F_{gasex}$ . However, due to the seasonal cycle of windspeed (cf. Figure 3.10), the same absolute  $\Delta p\text{N}_2\text{O}$  values on average result in higher fluxes during autumn/winter. Windspeed and  $\Delta p\text{N}_2\text{O}$  also show a systematic variation with latitude, which is also reflected in  $F_{gasex}$  (cf. Figure 3.5). On a regional level, this latitudinal trend likely influences the amplitude of the seasonal cycle of  $F_{gasex}$  (as discussed for the latitudinal boxes).

A harmonic function of the type given in Equation 3.5 explains 55% (LM86) and 67% (W92) of the systematic variability in  $F_{gasex}$ . The F-test and t-tests indicate that the components of this regression model contribute significantly to explaining the systematic variability in  $F_{gasex}$  (p-values  $< 10^{-138}$ ), although some of the controlling factors are still not accounted for. As explained, looking at latitudinal bands would probably increase the amount of systematic variability explained by this kind of harmonic function, as there is a latitudinal trend in windspeed and  $\Delta p\text{N}_2\text{O}$  (cf. Figure 3.5), but the data coverage unfortunately does not allow for this.

### Seasonal Cycle of $F_{grad}$

It should be noted that temperature-induced changes might affect  $F_{grad}$ , even if the overall profile structure is fairly unaffected by mixed layer seasonality. Temperature-driven seasonal mixed layer deepening has two counteracting effects on the gradient: deepening of the mixed layer results in a decrease of the denominator in Equation 3.3. But due to the lower SST and the thus enhanced

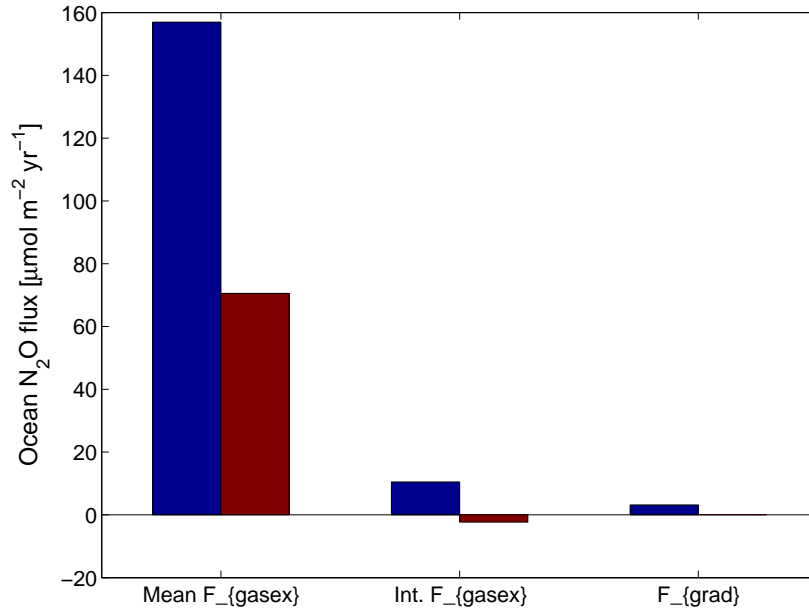


Figure 3.11: Annual mean  $F_{gasex}$  ( $\mu\text{mol m}^{-2}$ , W92 blue, LM86 dark red), integrated annual  $F_{gasex}$  ( $\mu\text{mol m}^{-2}$ , W92 blue, LM86 dark red) and extrapolated annual mean  $F_{grad}$  ( $\mu\text{mol m}^{-2}$ ).

solubility, part of the upmixed  $\text{N}_2\text{O}$  is kept in the mixed layer. Thus concentration in the mixed layer is enhanced compared to the more stratified case and the numerator in Equation 3.3 is also diminished. Additionally, any change in stratification induces a change in the diapycnal mixing rate and thus effects the estimation of  $F_{grad}$ .

Also, local phenomena like upwelling can have a significant effect on the diapycnal mixing rate. The diapycnal mixing rates calculated from our data only varied between  $6 \times 10^{-6} \text{ m}^2 \text{ s}^{-1}$  and  $2 \times 10^{-5} \text{ m}^2 \text{ s}^{-1}$ , but diapycnal mixing rates of up to  $10^{-4} \text{ m}^2 \text{ s}^{-1}$  have been found in the ocean [Moum and Osborn, 1986; Hibiya and Nagasawa, 2004]. Unfortunately, these effects cannot be resolved with our data, which only originate from a single cruise.

### Influence of the Seasonal Cycle on Flux Estimates

The discussed kind of seasonality is of consequence for estimating the average net flux. Depending on the type of function describing the seasonal cycle, a simple mean, especially a mean based on seasonally-biased sampling, cannot adequately

represent the net annual flux. Using the extrapolated mean daily  $\text{N}_2\text{O}$  flux results in an annual flux of  $71 \pm 211 \mu\text{mol}$  (LM86) and  $157 \pm 412 \mu\text{mol}$  (W92), respectively. In comparison, integrating Equation 3.5 over a full annual cycle to capture the full seasonal variability yields a net annual  $\text{N}_2\text{O}$  ocean-atmosphere flux of  $-2 \pm 1 \mu\text{mol m}^{-2}$  (LM86) and  $10 \pm 2 \mu\text{mol m}^{-2}$  (W92), respectively. The mean annual  $F_{grad}$  of  $3 \pm 1 \mu\text{mol m}^{-2}$  is about a factor of 3 smaller than  $F_{gasex}^{W92}$ . This is comparable to results from  $\text{N}_2\text{O}$  surface and microstructure measurements off the Mauritanian coast (Annette Kock, personal communication). It should be noted that the small net negative  $F_{gasex}^{LM86}$  is likely due to the 4-months data gap and resulting uncertainty in the fit. A true net negative annual flux is unlikely because of the vertical profile structure (cf. Section 1.2).

Assuming there is no seasonality in  $F_{grad}$ , the difference between both fluxes can also be calculated by integrating the fitted harmonic function illustrated in Figure 3.9 over a full annual cycle. This also results in an estimated difference of  $-5 \pm 1 \mu\text{mol m}^{-2} \text{ yr}^{-1}$  between  $F_{gasex}^{LM86}$  and  $F_{grad}$  and a difference of  $7 \pm 2 \mu\text{mol m}^{-2} \text{ yr}^{-1}$  between  $F_{gasex}^{W92}$  and  $F_{grad}$  (cf. Figure 3.11), which is not explained by the mainly temperature-controlled seasonal cycle of  $p\text{N}_2\text{O}/F_{gasex}$ . While the uncertainties in the fit due to 4-months data gap might be responsible for this difference, the existence of a biological  $\text{N}_2\text{O}$  source in the mixed layer cannot be ruled out. It should be noted, that compared to an annual subsurface  $\text{N}_2\text{O}$  production of  $14 \pm 10 \mu\text{mol m}^{-2} \text{ yr}^{-1}$  (calculated at the stations of M60/5, cf. Chapter 2), a mixed layer production of  $\text{N}_2\text{O}$  of  $7 \pm 2 \mu\text{mol m}^{-2} \text{ yr}^{-1}$  would constitute an important contribution to oceanic  $\text{N}_2\text{O}$  production.

### 3.3 Conclusions

1.  $p\text{N}_2\text{O}$ , as well as  $F_{gasex}$ , seem to follow a seasonal cycle similar to that of  $p\text{CO}_2$ , so that it can be described by a harmonic function. This seasonal cycle is mainly controlled by temperature.
2. The presence of such a harmonic seasonal cycle makes a mean flux, especially one calculated from a seasonally-biased dataset, a very poor estimate of the true annual net flux. Integrating the harmonic function over a full

annual cycle gives a much better estimate of the net annual flux. Using extrapolated mean fluxes,  $F_{grad}$  is significantly smaller than  $F_{gasex}$  in the North Atlantic Ocean. Using an integrated estimate accounting for the seasonal cycle considerably reduces the difference between the various flux estimates. It results in a net annual ocean-atmosphere  $N_2O$  flux of  $-2 \pm 1 \mu\text{mol m}^{-2}$  (LM86) and  $10 \pm 2 \mu\text{mol m}^{-2}$  (W92), respectively, which compares well to the annual mean  $F_{grad}$  of  $3 \pm 1 \mu\text{mol m}^{-2}$ .

3. Even though there is no conclusive evidence for a biologically-controlled seasonal cycle of surface  $pN_2O/F_{gasex}$ , the small difference between the two flux estimates of  $-5 \pm 1 \mu\text{mol m}^{-2} \text{ yr}^{-1}$  between  $F_{gasex}^{LM86}$  and  $F_{grad}$  and a difference of  $7 \pm 2 \mu\text{mol m}^{-2} \text{ yr}^{-1}$  between  $F_{gasex}^{W92}$  and  $F_{grad}$  indicates there could be biological effects on  $N_2O$  in the mixed layer. However, the difference between the flux estimates could also be due to the 4-months data gap in the seasonal fit, uncertainties in estimating the diapycnal mixing rate or an overestimation of the gas transfer velocity. As the seasonal/latitudinal resolution does not allow for a robust coefficient estimation, the possibility of biological effects on  $pN_2O/F_{gasex}$  cannot be ruled out. The small net negative  $F_{gasex}^{LM86}$  is likely due to the 4-months data gap and resulting uncertainty in the fit. A true net negative annual flux is unlikely because of the vertical profile structure.
4. Compared to an annual subsurface  $N_2O$  production of  $14 \pm 10 \mu\text{mol m}^{-2} \text{ yr}^{-1}$  calculated at the stations of M60/5, a mixed layer production of  $N_2O$  of  $7 \pm 2 \mu\text{mol m}^{-2} \text{ yr}^{-1}$  would constitute an important contribution to oceanic  $N_2O$  production.



# Chapter 4

## Global Subsurface Nitrous Oxide Production

The global oceanic emissions of  $\text{N}_2\text{O}$  are still rather poorly constrained [see compilation of estimates in *Denman et al.*, 2007; *Bange*, 2006] and there is no global database of  $\text{N}_2\text{O}$  comparable to e.g. the World Ocean Atlas. We use gridded World Ocean Atlas (WOA) temperature [*Locarnini et al.*, 2006], salinity [*Antonov et al.*, 2006] and oxygen [*Garcia et al.*, 2006] data together with gridded GLODAP CFC-12 data [*Key et al.*, 2004] and the parameterisation of an apparent  $\text{N}_2\text{O}$  production rate ( $\text{N}_2\text{OPR}$ ) developed in Chapter 2 to estimate the global annual production of  $\text{N}_2\text{O}$  below the mixed layer. These new data-based estimates are presented in this chapter. We also present an estimate of the global annual carbon remineralisation rate based on an estimate of the annual apparent oxygen utilisation rate.

### 4.1 Methods

#### 4.1.1 Mean Age and $\text{N}_2\text{O}$ Equilibrium Concentration

Following *Waugh et al.* [2003], it is assumed that the age distribution (TTD) of a water parcel, produced by different transport pathways and mixing, can be described as an inverse Gaussian function. In this case, this function can then be used to calculate the concentration of a conservative tracer at any given point in

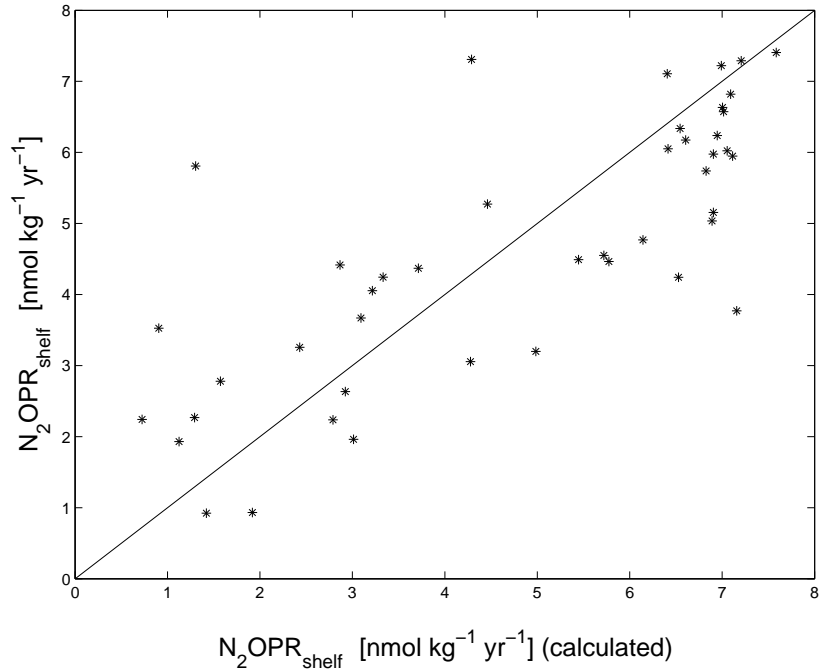


Figure 4.1: Shelf  $N_2O$  production rates ( $\text{nmol kg}^{-1} \text{yr}^{-1}$ ) calculated from  $N_2O$  data versus shelf  $N_2O$  production rates ( $\text{nmol kg}^{-1} \text{yr}^{-1}$ ) calculated using Equation 4.3.

space and any given time (cf. Section 2.1.4 for details).

To uniquely determine an inverse Gaussian age distribution one needs to determine its two parameters  $\Gamma$ , the mean age, and  $\Delta$ , the width of the distribution. In order to estimate these from observations of a single transient tracer, such as CFC-12 or  $SF_6$ , one needs to make an assumption about the ratio of  $\Gamma$  and  $\Delta$ . *Waugh et al.* [2004] analysed the effect of different  $\Gamma$  and  $\Delta$  ratios using a range of tracer and observations. Although they found that the  $\Gamma$  and  $\Delta$  ratio which best fits the observations varies for different oceanic sections, they conclude that the differences in  $\Gamma/\Delta$  from different oceanic sections are probably not significant given that larger differences result from varying the boundary conditions within uncertainties [*Waugh et al.*, 2004]. We used a ratio of  $\Gamma/\Delta = 1$ , which is consistent with the distribution of a range of different tracers.

Using the GLODAP  $1^\circ \times 1^\circ$  grid of CFC-12 data [*Key et al.*, 2004], we calculated a TTD age distribution and a mean age for every grid point. Since CFC-12 concentrations in the deep Pacific are too low to allow calculation of TTDs and



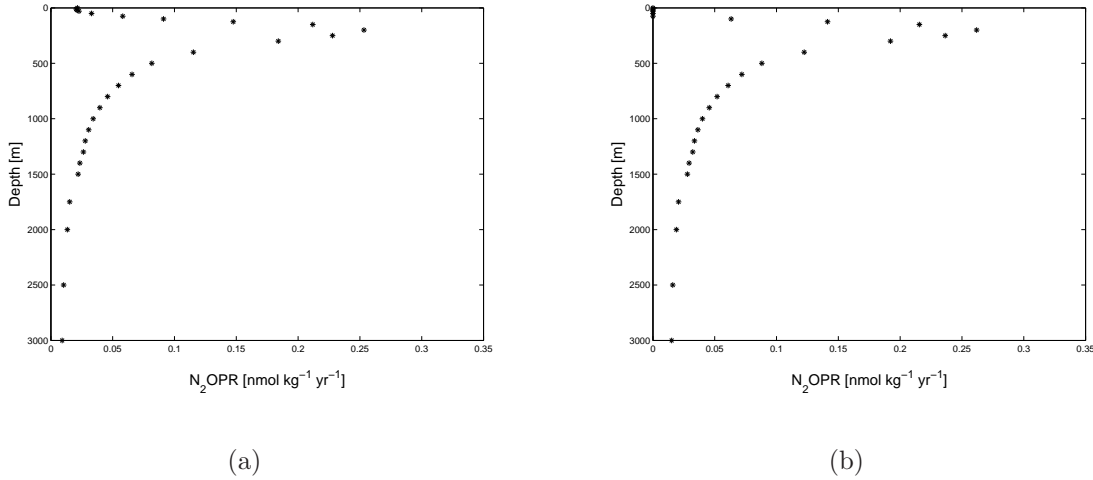


Figure 4.2:  $\text{N}_2\text{O}$  production rates ( $\text{nmol kg}^{-1} \text{yr}^{-1}$ ) used in the Arctic Ocean calculated using Equation 4.1 (a) and Equation 4.2 (b).

the highest calculated mean age is 731 yr, the mean age for every grid point with such a low CFC-12 concentration was set to 800 yr. This choice results in a realistically smooth age distribution and is in line with the results of *Matsumoto* [2007], who found using  $^{14}\text{C}$  the deep ocean to be characterised by centennial rather than millennial timescales.

In order to estimate the background  $\text{N}_2\text{O}$  signal ( $\text{N}_2\text{O}_{eq}$ ) in the ocean from the TTD we need to know the time dependent history of atmospheric concentrations. We used a synthesis of ice-core and firn data [*Machida et al.*, 1995; *Battle et al.*, 1996] merged with more recent air measurements. The data are available at <http://daac.ornl.gov> [*Holland et al.*, 2005]. We assume a constant atmospheric mixing ratio of  $\text{N}_2\text{O}$  of 275 ppb prior to year 1800 and used a polynomial fit of the data from 1800 to the present day. For details on the atmospheric history of  $\text{N}_2\text{O}$  used and the use of TTDs to calculate  $[\text{N}_2\text{O}]_{eq}$  see Sections 2.1.3 and 2.1.4.

#### 4.1.2 Open Ocean Apparent $\text{N}_2\text{O}$ Production Rate

The bottom depth at each grid point was determined using the 60 s-resolution ETOPO global elevation map distributed with the Ferret program (Information is available at <http://ferret.pmel.noaa.gov/Ferret/>). A grid point was defined as an open ocean grid point, if its bottom depth was  $> 200$  m. An appar-

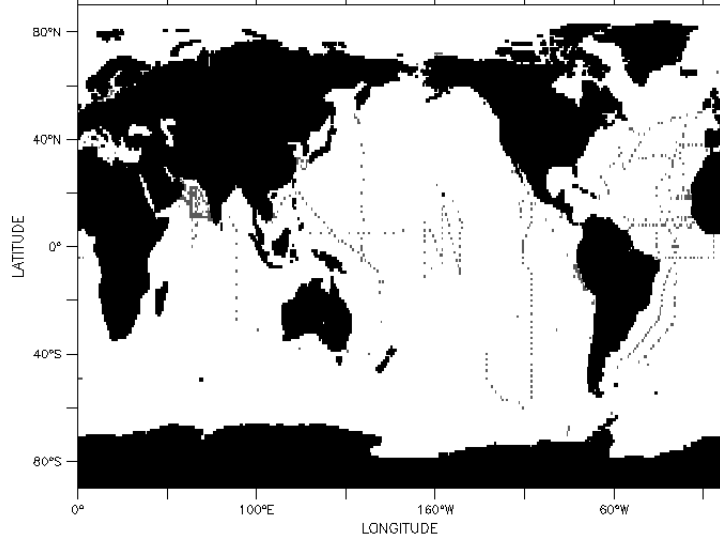


Figure 4.3: Available  $\text{N}_2\text{O}$  depth profiles.

ent  $\text{N}_2\text{O}$  production rate for open ocean grid points was calculated in two ways ( $\text{N}_2\text{OPR}_{depth}$  and  $\text{N}_2\text{OPR}_{temp}$ ) using the parameterisations developed in Section 2.2.4.2. An apparent  $\text{N}_2\text{O}$  production rate depending on an apparent oxygen utilisation rate (AOUR) and depth was calculated as

$$\text{N}_2\text{OPR}_{depth} = \text{AOUR} a_1 \exp\left(-\frac{z}{z_{sc}}\right) + a_2, \quad (4.1)$$

where the coefficient values for the best fit are  $a_1 = 0.0658$ ,  $a_2 = -0.0065$ ,  $z_{sc} = 20000$ ,  $z$  denotes the depth,  $\text{AOUR} = \frac{[\text{AOU}]}{\bar{t}}$ , and where  $\bar{t}$  is the mean age of the water parcel calculated using the TTD method.

An apparent  $\text{N}_2\text{O}$  production rate depending on AOUR and temperature was calculated as

$$\text{N}_2\text{OPR}_{temp} = \text{AOUR} a_1 \exp\left(-\frac{T}{T_{sc}}\right) + a_2, \quad (4.2)$$

where the coefficient values for the best fit are  $a_1 = 0.0665$ ,  $a_2 = -0.0032$ ,  $T_{sc} = 20000$ ,  $T$  denotes the temperature,  $\text{AOUR} = \frac{[\text{AOU}]}{\bar{t}}$ , and where  $\bar{t}$  is the mean age of the water parcel calculated using the TTD method.

To exclude any undue influence of short-term seasonal variations affecting the near-surface ocean in the estimates, all production rates were only calculated for grid fields below the mixed layer. The mixed layer depth was determined using the mixed layer climatology of *Montegut et al.* [2004]. The mixed layer depth is determined by an absolute change in temperature of 0.2°C compared to the temperature at 10 m depth. This parameterisation only accounts for N<sub>2</sub>O production by nitrification.

There are no CFC-12 data and thus there is no mean age information available for the Arctic Ocean in the GLODAP data set. A N<sub>2</sub>OPR for the Arctic Ocean (N<sub>2</sub>OPR<sup>arctic</sup>) was estimated using the 25%-quantile of the overall N<sub>2</sub>OPR. This takes into account, that in general the relevant biological productivity is comparatively low in the Arctic Ocean. Our estimates of N<sub>2</sub>OPR are displayed in Figure 4.2. These parameterisations only account for N<sub>2</sub>O production by nitrification.

### 4.1.3 Apparent N<sub>2</sub>O Production Rate on the Continental Shelves

A grid point was defined as a shelf grid point, if its bottom depth was  $\leq 200$  m. The bottom depth at each grid point was determined using the 60 s-resolution ETOPO global elevation map distributed with the Ferret program (Information is available at <http://ferret.pmel.noaa.gov/Ferret/>). An apparent shelf N<sub>2</sub>O production rate (N<sub>2</sub>OPR<sub>shelf</sub>) was calculated using 52 shelf data points from our N<sub>2</sub>O data base. Unlike for N<sub>2</sub>OPR there is a good correlation between N<sub>2</sub>OPR<sub>shelf</sub>/AOUR and depth but not between N<sub>2</sub>OPR<sub>shelf</sub>/AOUR and temperature. Therefore N<sub>2</sub>OPR<sub>shelf</sub> was estimated as

$$\text{N}_2\text{OPR}_{\text{shelf}} = \text{AOUR} a_1 \exp\left(-\frac{z}{z_{sc}}\right) + a_2, \quad (4.3)$$

where the coefficient values for the best fit are  $a_1 = 0.1795$ ,  $a_2 = 0.5374$ ,  $z_{sc} = 350$  and  $z$  denotes the depth. This parameterisation only accounts for N<sub>2</sub>O production by nitrification. The goodness of the fit is illustrated in Figure 4.1. Due to lack of data we did not attempt to calculate a shelf production rate for the Arctic Ocean.

Zone	Average oxygen age
Arabian Sea	5
ETNP	60
ETSP	5

Table 4.1: Average time of residence (years) per oxygen minimum zone.

#### 4.1.4 Denitrification

Denitrification can either produce or consume  $\text{N}_2\text{O}$ , depending on the surrounding conditions: it produces  $\text{N}_2\text{O}$  at the interface between suboxic and anoxic waters and it consumes  $\text{N}_2\text{O}$  under (close to) anoxic conditions when the complete process of denitrification is performed [Tiedje, 1988].

To estimate production due to denitrification, we used a global collection of  $\text{N}_2\text{O}$  depth profiles (see Figure 4.3) to determine the maximal and mean  $\text{N}_2\text{O}$  ( $[\text{N}_2\text{O}]_{max}^{omz}$  and  $[\text{N}_2\text{O}]_{mean}^{omz}$ ) concentration per depth and oxygen minimum zone. Following Codispoti et al. [1992] and Stramma et al. [2008] we defined suboxic zones as WOA fields with an oxygen content of less than  $10 \mu\text{mol kg}^{-1}$ . This results in three main oxygen minimum zones, in the Arabian Sea, in the Eastern Tropical North Pacific and the Eastern Tropical South Pacific, which is in good agreement with Paulmier et al. [2008]. The difference between  $[\text{N}_2\text{O}]_{max}^{omz}$  and  $[\text{N}_2\text{O}]_{mean}^{omz}$  and the estimated  $[\text{N}_2\text{O}]$  resulting from nitrification, respectively, was used as an estimate of the total amount of  $\text{N}_2\text{O}$  produced by denitrification. As using  $[\text{N}_2\text{O}]_{mean}^{omz}$  resulted in a negligible amount of  $\text{N}_2\text{O}$  production via denitrification,  $[\text{N}_2\text{O}]_{max}^{omz}$  and  $[\text{N}_2\text{O}]_{mean}^{omz}$  were used as an upper and lower boundary, respectively, for the total amount of  $\text{N}_2\text{O}$  produced via denitrification. The  $\text{N}_2\text{O}$  production rate due to denitrification ( $\text{N}_2\text{OPR}^{denit}$ ) was then calculated as

$$\begin{aligned} \text{N}_2\text{OPR}^{denit} = & \frac{1}{\bar{t}_{omz}} \left( [\text{N}_2\text{O}]_{max}^{omz} - \left( \text{N}_2\text{OPR} \bar{t} + [\text{N}_2\text{O}]_{eq} \right) \right) \\ & - \frac{1}{2\bar{t}_{omz}} \left( [\text{N}_2\text{O}]_{max}^{omz} - [\text{N}_2\text{O}]_{mean}^{omz} \right), \end{aligned} \quad (4.4)$$

where  $\bar{t}_{omz}$  is the average time a water parcel has already spent in the respective oxygen minimum zone [Naqvi and Shailaja, 1993; Olson et al., 1993; Karstensen et al., 2008, see Table 4.1].

To estimate consumption due to denitrification, we used a the same collection of N<sub>2</sub>O depth profiles (see Figure 4.3) to determine the minimal and mean N<sub>2</sub>O ( $[\text{N}_2\text{O}]_{min}^{omz}$  and  $[\text{N}_2\text{O}]_{mean}^{omz}$ ) concentration per depth and oxygen minimum zone. We used an oxygen content of 4  $\mu\text{mol kg}^{-1}$  as a threshold for an environment supporting a denitrification sink of N<sub>2</sub>O, which marks out parts of the oxygen minimum zones described above. The difference between the estimated  $[\text{N}_2\text{O}]$  resulting from nitrification and  $[\text{N}_2\text{O}]_{max}^{omz}$  and  $[\text{N}_2\text{O}]_{mean}^{omz}$ , respectively, was used as an estimate of the total amount of N<sub>2</sub>O consumed by denitrification. As using  $[\text{N}_2\text{O}]_{mean}^{omz}$  resulted in no N<sub>2</sub>O consumption via denitrification,  $[\text{N}_2\text{O}]_{max}^{omz}$  and  $[\text{N}_2\text{O}]_{min}^{omz}$  were used as an upper and lower boundary, respectively, for the total amount of N<sub>2</sub>O consumed by denitrification. The N<sub>2</sub>O consumption rate due to denitrification ( $\text{N}_2\text{OCR}^{denit}$ ) was then calculated as

$$\begin{aligned} \text{N}_2\text{OCR}^{denit} = & \frac{1}{\bar{t}_{omz}} \left( \left( \text{N}_2\text{OPR} \bar{t} + [\text{N}_2\text{O}]_{eq} \right) - [\text{N}_2\text{O}]_{min}^{omz} \right) \\ & - \frac{1}{2\bar{t}_{omz}} \left( [\text{N}_2\text{O}]_{mean}^{omz} - [\text{N}_2\text{O}]_{min}^{omz} \right), \end{aligned} \quad (4.5)$$

where  $\bar{t}_{omz}$  is the average time a water parcel has already spent in the respective oxygen minimum zone [Naqvi and Shailaja, 1993; Olson *et al.*, 1993; Karstensen *et al.*, 2008, see Table 4.1] and  $\bar{t}$  is the TTD mean age. Concentration differences in Equation 4.5 indicating production were discarded for the purpose of this calculation.

#### 4.1.5 Integrated Production Estimates

To estimate annual production rates per m<sup>2</sup>, the respective N<sub>2</sub>OPR was integrated over the water column. To estimate the magnitude of the global annual production of N<sub>2</sub>O, first the volume of each grid cell was determined by integrating over the three dimensions latitude, longitude and depth. The calculated volume was then multiplied by the respective N<sub>2</sub>OPR to calculate the annual N<sub>2</sub>O yield per grid cell. The sum of the annual N<sub>2</sub>O yield of all ocean grid cells was used to estimate the global annual N<sub>2</sub>O production.

The integrated volume of a grid cell  $V_{gc}$  in m<sup>3</sup> used in our calculations can be described as

$$V_{gc} = \frac{\phi_2 - \phi_1}{3} \left( (R_{earth} - D_1)^3 - (R_{earth} - D_2)^3 \right) (\sin(\theta_2) - \sin(\theta_1)), \quad (4.6)$$

Param.	Median	Mean
$N_2OPR_{depth}$	24%	34%
$N_2OPR_{temp}$	22%	34%
$N_2OPR_{shelf}$	42%	54%

Table 4.2: Average percental error in concentration estimates.

where  $\phi_1$ ,  $\phi_2$  and  $\theta_1$ ,  $\theta_2$ , with  $\theta_2 > \theta_1$ , are the longitudinal and latitudinal boundaries, respectively, of the respective grid cell in degrees,  $D_1$ ,  $D_2$ , with  $D_2 > D_1$ , are the depth boundaries of the respective grid cell in m and  $R_{earth}$  is the radius of the Earth in m.

#### 4.1.6 $N_2O$ concentration

$[N_2O]$  was predicted as

$$[N_2O] = [N_2O]_{eq} + N_2OPR \bar{t} + f([O_2]) N_2OPR^{denit} \bar{t}_{omz} - g([O_2]) N_2OCR^{denit} \bar{t}_{omz}, \quad (4.7)$$

where  $\bar{t}$  is the TTD mean age and  $\bar{t}_{omz}$  is the average time a water parcel has already spent in the respective oxygen minimum zone [Naqvi and Shailaja, 1993; Olson *et al.*, 1993; Karstensen *et al.*, 2008, see Table 4.1].  $f$  and  $g$  are switch functions, which determine whether denitrification contributes to  $[N_2O]$ . They are defined as

$$f([O_2]) = \begin{cases} 1 & \text{for } [O_2] < 10 \text{ nmol kg}^{-1} \\ 0 & \text{for } [O_2] \geq 10 \text{ nmol kg}^{-1} \end{cases} \quad (4.8)$$

and

$$g([O_2]) = \begin{cases} 1 & \text{for } [O_2] < 4 \text{ nmol kg}^{-1} \\ 0 & \text{for } [O_2] \geq 4 \text{ nmol kg}^{-1}. \end{cases} \quad (4.9)$$

#### 4.1.7 Error Estimates

The CFC-12, AOU and temperature measurements neither originate from the same water mass nor necessarily even from roughly the same time. Additionally, they represent some kind of average over latitude, longitude and depth. This is likely to dominate the error in our estimates. To estimate this error we used 5900

open ocean data points below the mixed layer and 46 shelf data points below the mixed layer from our data base. Using the gridded CFC concentrations from GLODAP we calculated the difference between the original  $[\text{N}_2\text{O}]$  and  $[\text{N}_2\text{O}]_{est}$ , with

$$[\text{N}_2\text{O}]_{est} = [\text{N}_2\text{O}]_{eq} + \bar{t} \text{ N}_2\text{OPR}, \quad (4.10)$$

where  $\bar{t}$  is the mean age. The mean and median of the absolute percental differences can be found in Table 4.2. It seems reasonable to use the median as a few very different data points can unduly influence the mean. It is likely that peculiar local conditions can lead to a considerable misfit but this does not adequately represent the overall goodness of fit. As the mean age is crucial for both terms in Equation 4.10, we assume that both terms contribute to the overall percental error in the same way. Table 4.2 suggests that the parameterisation based on temperature (see Equation 4.2) seems to do a slightly better job.

The amount of  $\text{N}_2\text{O}$  produced (consumed) by denitrification is estimated in a completely different fashion compared to nitrification rates (see Section 4.1.4). Using the mean  $[\text{N}_2\text{O}]$  from our data base, the fraction of denitrification with regard to total annual production becomes insignificant (see Table 4.3). We therefore assume that the rate calculations based on  $[\text{N}_2\text{O}]_{mean}^{OMZ} - [\text{N}_2\text{O}]$  and  $[\text{N}_2\text{O}]_{max}^{OMZ} - [\text{N}_2\text{O}]$  ( $[\text{N}_2\text{O}]_{min}^{OMZ} - [\text{N}_2\text{O}]$ ) (cf. Section 4.1.4 for details), respectively, represent reasonable lower and upper boundaries.

## 4.2 Results & Discussion

### 4.2.1 Concentration and Rate Estimates

#### 4.2.1.1 Oxygen Utilisation Rates

AOUR varies between 0.01 and 49  $\mu\text{mol kg}^{-1} \text{ yr}^{-1}$ , with an overall mean AOUR of  $2.9 \pm 0.5 \mu\text{mol kg}^{-1} \text{ yr}^{-1}$  ( $1\sigma$ ). The North Atlantic mean AOUR of  $3.6 \pm 0.9 \mu\text{mol kg}^{-1} \text{ yr}^{-1}$  ( $1\sigma$ ) compares well to prior estimates of AOUR of 1 – 25  $\mu\text{mol kg}^{-1} \text{ yr}^{-1}$  (0 – 1000 m) based on  $^3\text{H}/^3\text{He}$  age determination in the North Atlantic [Jenkins and Wallace, 1992]. The Pacific Ocean mean AOUR of  $4.3 \pm 0.7 \mu\text{mol kg}^{-1} \text{ yr}^{-1}$  (100 – 1000 m,  $1\sigma$ ) and  $0.6 \pm < 0.1 \mu\text{mol kg}^{-1} \text{ yr}^{-1}$  (below 1200 m,  $1\sigma$ )

agree reasonably well with the estimates given by *Feely et al.* [2004] of  $0.02 - 10 \mu\text{mol kg}^{-1} \text{ yr}^{-1}$  (100–1000 m) and  $\sim 0.1$  (below 1200 m)  $\mu\text{mol kg}^{-1} \text{ yr}^{-1}$  based on CFC age determination in the Pacific Ocean. The CFC-ages of *Feely et al.* [2004] were determined by comparing concentrations to a reconstructed atmospheric history and correcting for mixing bias using an advection-diffusion model.

Globally integrating our estimated AOURL and using a Redfield ratio of 117 : 170 for C:O [*Anderson and Sarmiento, 1994*], we estimate an export production of  $17.6 \text{ Pg C yr}^{-1}$ . This estimate agrees reasonably well with the export production estimate of  $\sim 11 - 16 \text{ Pg C yr}^{-1}$  by *Falkowski et al.* [2000, 1998]. It is within the range of  $11 - 21 \text{ Pg C yr}^{-1}$  *Laws et al.* [2000] derived from a suite of models. Our estimate is slightly higher than the data-based estimate of  $10.8 \pm 2.7 \text{ Pg C yr}^{-1}$  given by *Lee* [2001] and the estimate of  $\sim 10 \text{ Pg C yr}^{-1}$  given by *Schlitzer* [2004, 2002].

This good agreement of these estimates based on different methods with our estimates suggests that the use of a TTD-based mean age for rate calculations yields reliable rate estimates. Additionally, *Tanhua et al.* [2007] found TTD-based estimates of anthropogenic carbon concentrations to be in good agreement with independent methods, suggesting the use of CFC-12 and  $\text{SF}_6$  as tracers is a reliable basis for water mass age and hence estimation of background concentrations like  $[\text{N}_2\text{O}]_{eq}$ .

#### 4.2.1.2 Apparent $\text{N}_2\text{O}$ Production Rates

$\text{N}_2\text{OPR}$  varies between  $0 - 3.3 \text{ nmol kg}^{-1} \text{ yr}^{-1}$  with an overall mean  $\text{N}_2\text{OPR}$  of  $0.2 \pm 0.04 \text{ nmol kg}^{-1} \text{ yr}^{-1}$  ( $1 \sigma$ ). Between 100 – 500 m  $\text{N}_2\text{OPR}$  averages  $0.4 \pm 0.04 \text{ nmol kg}^{-1} \text{ yr}^{-1}$  ( $1 \sigma$ ), while below 500 m  $\text{N}_2\text{OPR}$  averages  $0.09 \pm 0.01 \text{ nmol kg}^{-1} \text{ yr}^{-1}$  ( $1 \sigma$ ), indicating that the largest amount of subsurface  $\text{N}_2\text{O}$  is produced in the upper 500 m of the water column. The estimates of the two parameterisations differ only in the second significant figure.

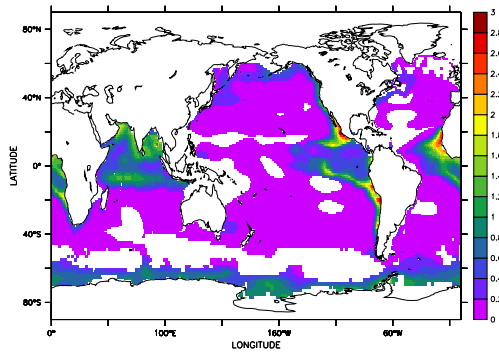
Figure 4.4 shows  $\text{N}_2\text{OPR}$  in 200 m depth. Both parameterisations generally show the same qualitative features, however,  $\text{N}_2\text{OPR}_{temp}$  is slightly higher than  $\text{N}_2\text{OPR}_{depth}$ . Above 125 m the eastern boundary upwelling systems and to a lesser extent the Bay of Bengal and the Arabian Sea display high  $\text{N}_2\text{OPR}$ .  $\text{N}_2\text{OPR}$  is lowest in the subtropical gyres and slightly elevated in the Southern Ocean.



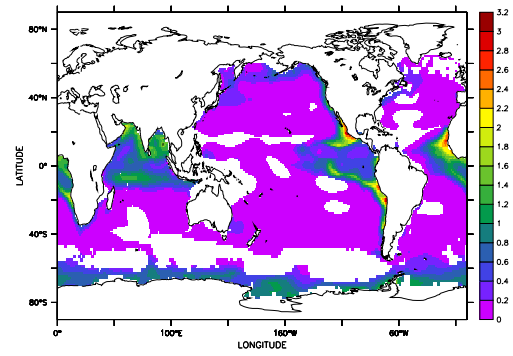
These patterns are mainly controlled by AOU as the mean age in these depths is relatively uniform, except for elevated mean ages in the Eastern Tropical Pacific upwelling system.  $N_2$ OPR is still high in the Eastern Tropical Pacific upwelling despite the elevated mean age.

Between  $\sim 125 - 400$  m  $N_2$ OPR is relatively uniform throughout the world ocean. Especially, there is no signal of elevated production in the oxygen minimum zones. This appears to be due to the relatively high AOU in these regions being “cancelled out” by the also elevated mean age (cf. Figure 4.5). There are elevated  $N_2$ OPR values around the horizontal rim of the oxygen minimum zones, which are most likely artefacts due to a slight mismatch between the CFC- and the AOU-datasets. In the AOU data set the oxygen minimum zones extend slightly further than in the CFC-data set, creating high  $N_2$ OPR. Below  $\sim 400$  m, elevated values of  $N_2$ OPR are mainly caused by a comparatively small mean age. Young waters lead to comparatively high  $N_2$ OPR in the deep ( $< 1000$  m) North Atlantic Ocean and some areas of the Southern Ocean, mostly close to the Polar Front ( $< 1000$  m). However, profile data from the North Atlantic [*Walter et al.*, 2006] suggest there is no significant  $N_2O$  production this deep. Considering that overall features of AOU are for the most part balanced by the same features in the mean age so that they cancel each other out yielding fairly uniform  $N_2$ OPR, it seems likely that high values of  $N_2$ OPR in the deep North Atlantic are artefacts of the method caused by a slight mismatch between the CFC12- and AOU-datasets.

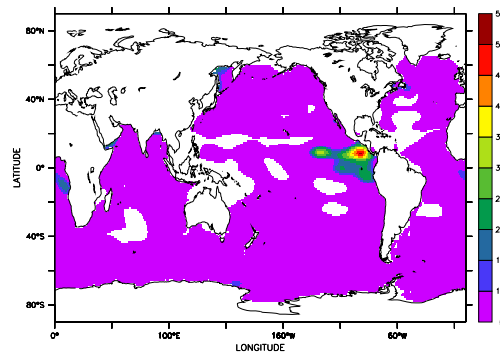
Modelling isotopic results from station ALOHA in the oligotrophic North Pacific gyre, *Popp et al.* [2002] found that approximately 40% – 75% of the net flux of  $N_2O$  to the atmosphere is produced between 100 m and 300 m depth. Comparing these results to a mean profile of  $N_2$ OPR averaged over the oligotrophic North Pacific gyre (see Figure 4.6), we find that  $N_2$ OPR also attains its maximum values between 100 m and 300 m. About 70% of the  $N_2O$  produced in the water column originate between 100 m and 500 m.



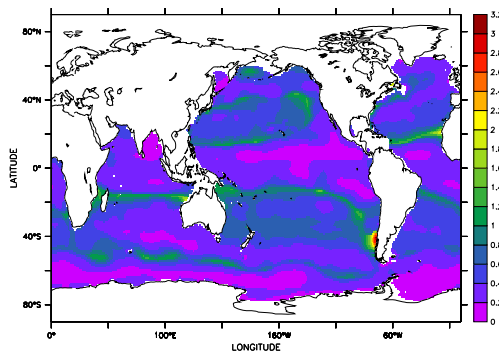
(a)



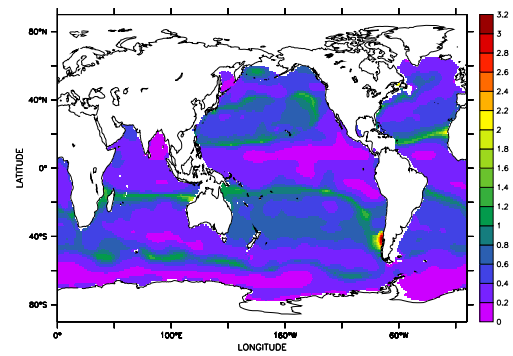
(b)



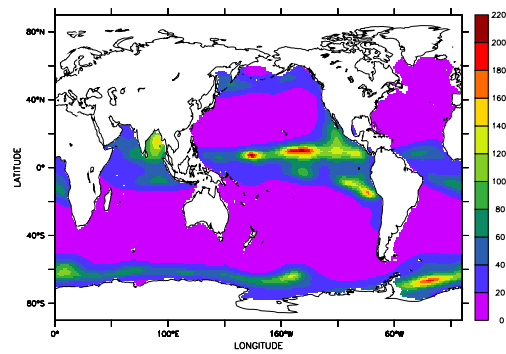
(c)



(d)



(e)



(f)

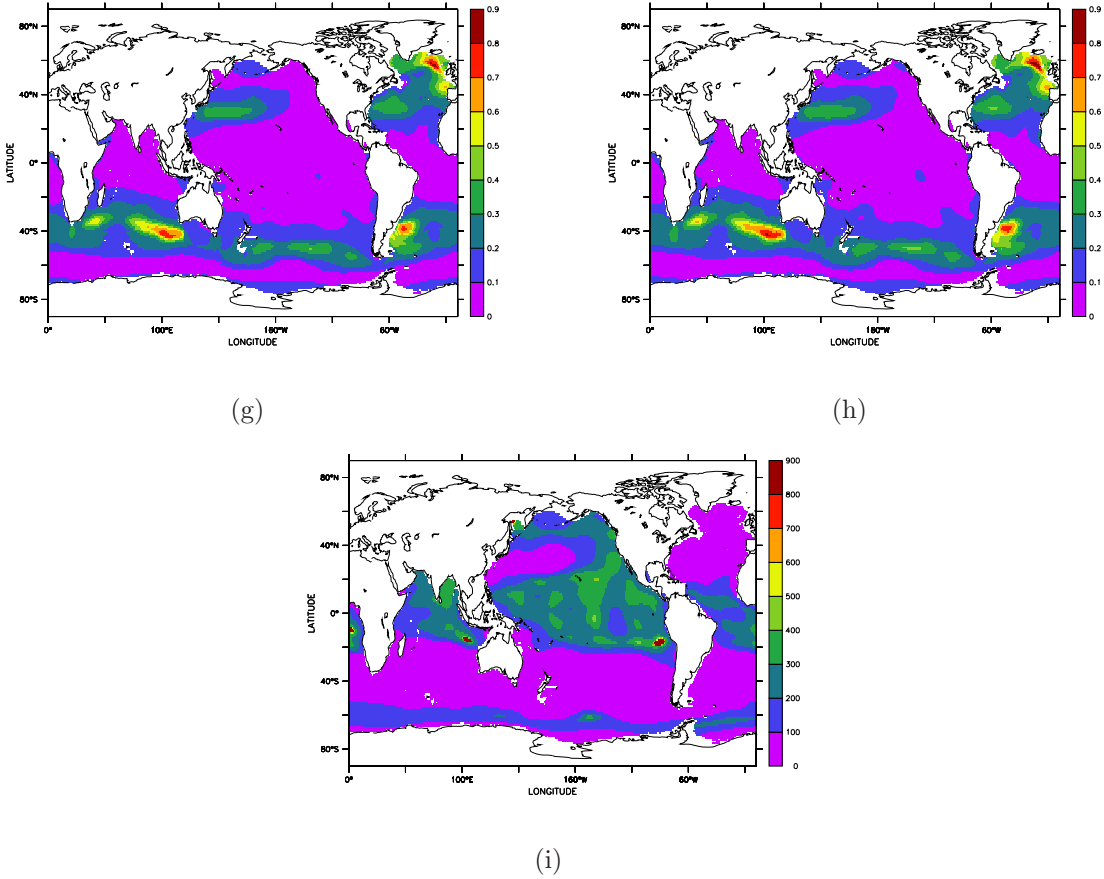


Figure 4.4: Global  $N_2OPR_{depth}$  ( $\text{nmol kg}^{-1} \text{ yr}^{-1}$ ) distribution,  $N_2OPR_{temp}$  ( $\text{nmol kg}^{-1} \text{ yr}^{-1}$ ) distribution and TTD mean age (yr) in 75 m ((a), (b), (c)), 250 m ((c), (d), (e)) and 700 m ((f), (g), (h)) depth.

#### 4.2.1.3 $N_2O$ concentration

The global distribution of predicted  $[N_2O]$  varies between  $4 - 31 \text{ nmol kg}^{-1}$  and, where measurement data exist, is qualitatively very similar to the measured  $[N_2O]$  of our database. Figure 4.7 shows a comparison of measured and predicted  $[N_2O]$  along  $110^\circ\text{W}$ . In the oligotrophic part, the predicted concentrations agree quite well with the measured  $N_2O$ , in the suboxic zone, the predicted  $[N_2O]$  clearly underestimates  $[N_2O]$ . This could be due to the use of annual mean dissolved  $[O_2]$ , which might not adequately reflect the location and extent of the oxygen minimum zone at the time of the data acquisition. Our parameterisation does not account for the export of  $[N_2O]_{xs}$  from highly productive regions, which might

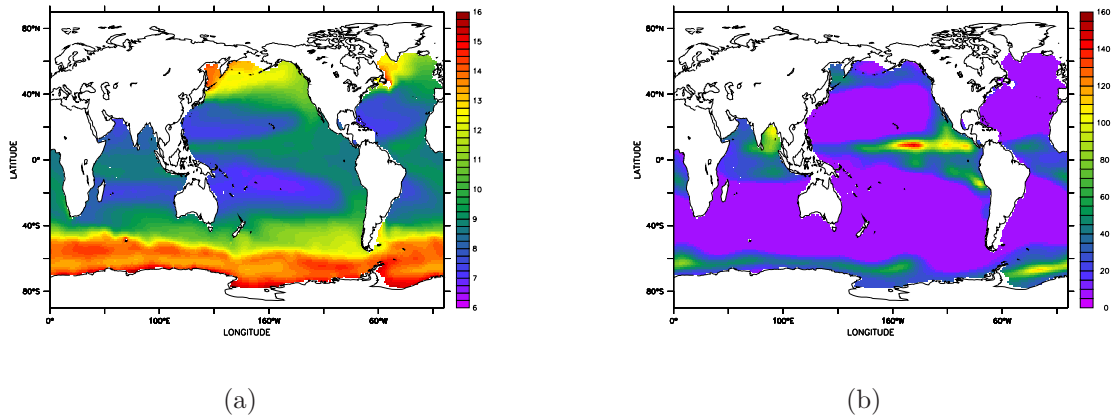


Figure 4.5: (a):  $[\text{N}_2\text{O}]_{eq}$  ( $\text{nmol kg}^{-1}$ ) in 200 m depth. (b): TTD mean age (yr) in 200 m depth.

also be a reason for the underestimation shown in Figure 4.7. Qualitative patterns are represented very well by our prediction.

Figure 4.8 shows the estimated  $[\text{N}_2\text{O}]$  distribution in 200 m depth. Concentrations exceeding  $40 \text{ nmol kg}^{-1}$ , which are only found in the Arabian Sea, are masked out in Figure 4.8 as not to obscure the overall qualitative patterns. The eastern boundary upwelling systems are clearly displayed. Concentrations in the Antarctic are slightly elevated, owing to the cold temperatures increasing solubility and thus elevated  $[\text{N}_2\text{O}]_{eq}$ . Highest concentrations  $90 \text{ nmol kg}^{-1}$  occur in the Arabian Sea. Concentrations are also comparatively high in the North Pacific Ocean and the Bay of Bengal. Considering the parameterisation was solely derived from North Atlantic data, the systematic features of  $[\text{N}_2\text{O}]$  in the world ocean are remarkably well displayed.

$[\text{N}_2\text{O}]$  is almost always exclusively determined by production via nitrification and  $[\text{N}_2\text{O}]_{eq}$ , with the exception of the three oxygen minimum zones. In the oxygen minimum zone in the Arabian Sea the fraction of  $\text{N}_2\text{O}$  produced via denitrification varies between 2% and 89% between 200 – 900 m. In the oxygen minimum zone of the Eastern Tropical North Pacific the average fraction of  $\text{N}_2\text{O}$  produced via denitrification per depth varies between 2% and 35% between 400 – 500 m. In the oxygen minimum zone of the Eastern Tropical South Pacific the average fraction of  $\text{N}_2\text{O}$  produced via denitrification per depth varies between 1% and 14% between 150 – 400 m.

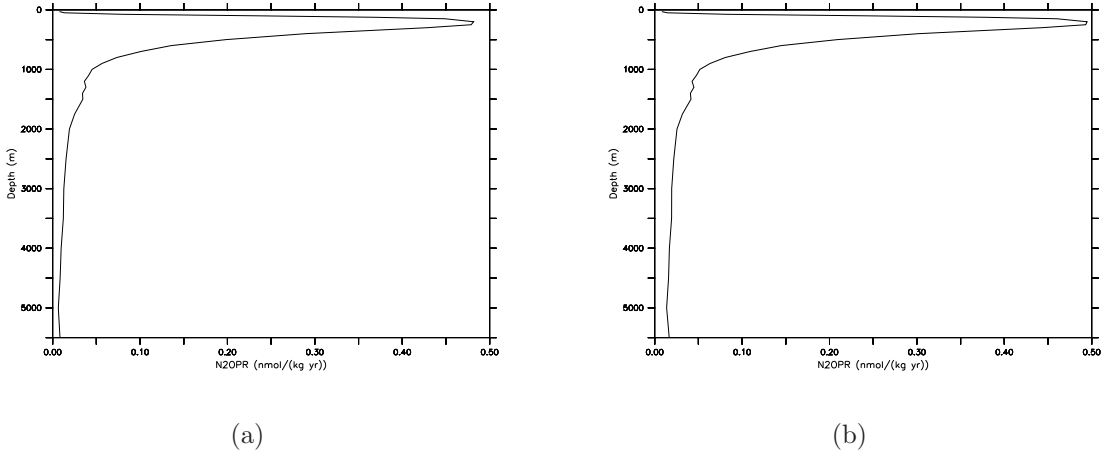


Figure 4.6: Average  $\text{N}_2\text{OPR}$  ( $\text{nmol kg}^{-1} \text{ yr}^{-1}$ ) in the oligotrophic North Pacific gyre estimated using Equation 4.1 (a) and Equation 4.2 (b).

#### 4.2.1.4 Influence of Temperature

It is worth noting, that the qualitative features of  $[\text{N}_2\text{O}]$  are not only controlled by the qualitative features of  $\text{N}_2\text{OPR}$  but also by temperature (via solubility).  $[\text{N}_2\text{O}]_{eq}$  shows patterns very similar to those displayed by  $[\text{N}_2\text{O}]$ , as is illustrated in Figure 4.5(a). Comparing Figure 4.5(a) and Figure 4.5(b) we find that  $[\text{N}_2\text{O}]_{eq}$  is strongly controlled by temperature. However, the qualitative features of  $\text{N}_2\text{OPR}$  mainly reflect AOU/mean age and not temperature.

## 4.2.2 Annual Subsurface $\text{N}_2\text{O}$ yield

The integrated annual  $\text{N}_2\text{O}$  production per  $\text{m}^2$  due to nitrification is displayed in Figure 4.9 and detailed in Table 4.3. The qualitative features are similar for both parameterisations.  $\text{N}_2\text{OPR}_{temp}$  estimates a slightly bigger  $\text{N}_2\text{O}$  yield but both parameterisations agree within the error margins. The error analysis suggests, that  $\text{N}_2\text{OPR}_{temp}$  estimates the production slightly more accurately (cf. Section 4.1.7, Table 4.2).

The largest amount of  $\text{N}_2\text{O}$  per  $\text{m}^2$  and  $\text{yr}^{-1}$  is produced in the North Atlantic Ocean and off Argentina, which is more likely due to the potential data mismatch in the deep, as discussed in Section 4.2.1.2 than to truly elevated production. However, even assuming true North Atlantic subsurface production only

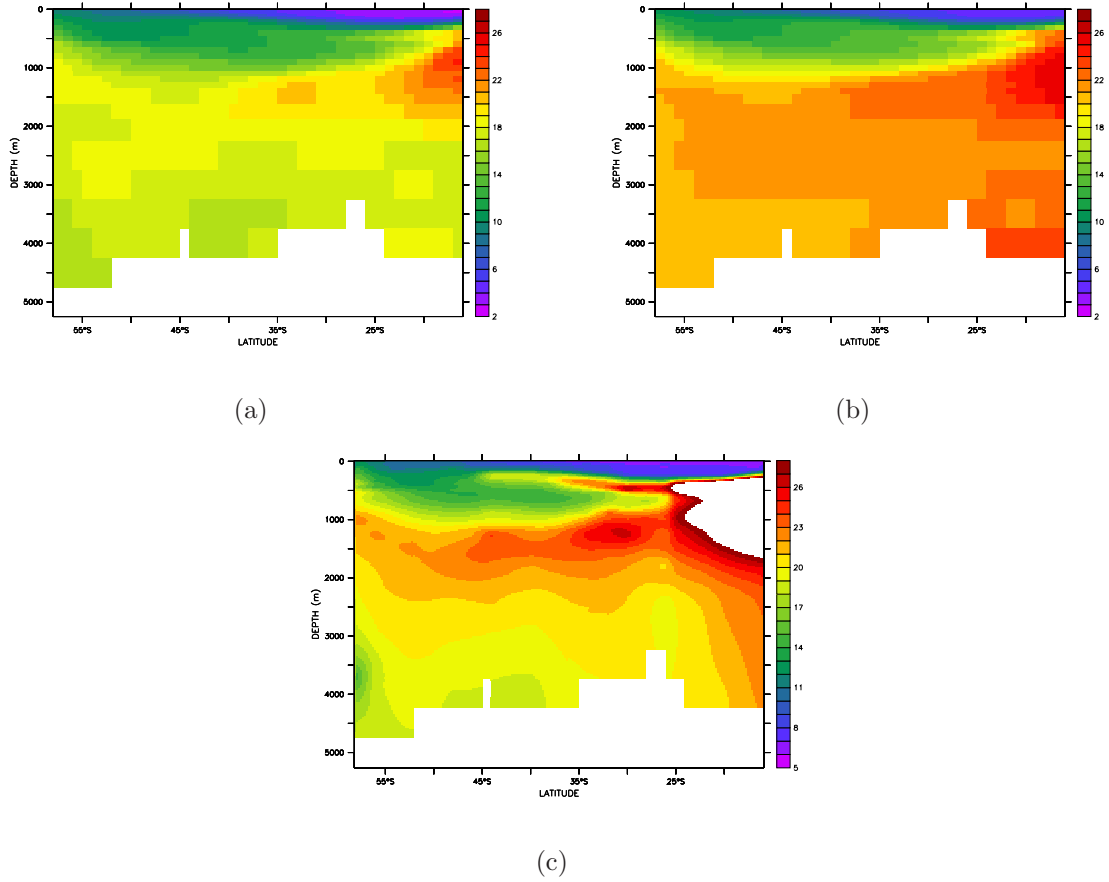


Figure 4.7: Section along  $110^{\circ}\text{W}$  (averaged between  $100^{\circ}\text{W}$ – $120^{\circ}\text{W}$ ). (a): Predicted  $[\text{N}_2\text{O}]$  ( $\text{nmol kg}^{-1}$ ) according to  $\text{N}_2\text{OPR}_{depth}$ . (b): Predicted  $[\text{N}_2\text{O}]$  ( $\text{nmol kg}^{-1}$ ) according to  $\text{N}_2\text{OPR}_{temp}$ . (c): Measured  $[\text{N}_2\text{O}]$  ( $\text{nmol kg}^{-1}$ ) from *James Butler* [RITS, 1989, unpublished] and *Farias et al.* [2007].

amounts to half of what is predicted by our method, would only change the global production estimate by  $\sim 5\%$ .

Production is also very high in the upwelling regions off Mauritania and Chile. Production is elevated in the North Pacific Ocean, the Southern Ocean and parts of the Indian Ocean. However, even if the  $\text{N}_2\text{O}$  yield per  $\text{m}^2$  is relatively high in the Southern Ocean, its overall contribution to the global annual production of  $\text{N}_2\text{O}$  is small due to the small area covered. Overall, the patterns of  $\text{N}_2\text{OPR}$  in the deep ocean, and therefore in our case the patterns in the mean age (cf. Figure 4.4), govern the  $\text{N}_2\text{O}$  yield of the water column. Larger water depth

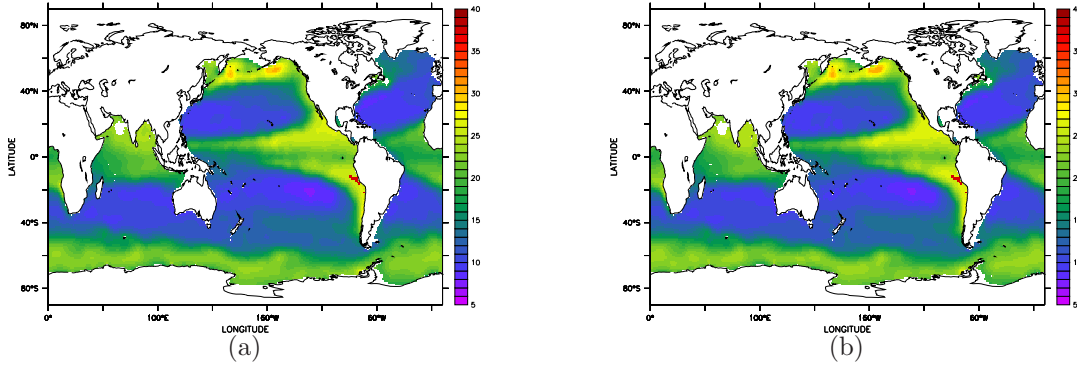


Figure 4.8: Global  $[\text{N}_2\text{O}]$  ( $\text{nmol kg}^{-1}$ ) distribution in 200 m depth estimated using Equation 4.1 (a) and Equation 4.2 (b). The white area in the Arabian Sea represents concentrations exceeding  $40 \text{ nmol kg}^{-1}$ .

does, however, also lead to a larger  $\text{N}_2\text{O}$  yield per  $\text{m}^2$  without  $\text{N}_2\text{OPR}$  being significantly higher for the involved grid cells.

It should be noted, that areas of extensive subsurface production must not necessarily coincide with areas of large sea to air fluxes because of the effects of advection. Also, the yield per  $\text{m}^2$  does not necessarily illustrate the respective contribution of the different oceanic regions to the overall  $\text{N}_2\text{O}$  source very well, as a high yield per  $\text{m}^2$  does not necessarily equal a large regional contribution, depending on the area of the respective region.

As denitrification is only relevant in suboxic and anoxic environments, it only has an impact on the  $\text{N}_2\text{O}$  yield of the suboxic zones in the Arabian Sea and in the Eastern Tropical Pacific. The production yield via denitrification is badly constrained (cf. Table 4.3) and probably also highly variable, but despite the locally limited influence of denitrification it yields on average  $\sim 7\%$  of the total amount of  $\text{N}_2\text{O}$  produced via nitrification (cf. Table 4.3). However, these results are to be viewed with caution as the estimation of  $\text{N}_2\text{OPR}^{\text{denit}}$  inherently depends on the predicted  $\text{N}_2\text{OPR}$ .

The overall global annual subsurface production of  $\text{N}_2\text{O}$  amounts to  $3.1 \pm 0.9 \text{ Tg N yr}^{-1}$  ( $110.1 \pm 31.8 \text{ Gmol N}_2\text{O yr}^{-1}$ ) and  $3.4 \pm 0.9 \text{ Tg N yr}^{-1}$  ( $121.7 \pm 32.2 \text{ Gmol N}_2\text{O yr}^{-1}$ ), respectively, and is detailed in Table 4.3. Recent estimates based on gas-exchange parameterisations, compiled in *Bange* [2006], estimate an oceanic source between 1.4 to 14  $\text{Tg N yr}^{-1}$  with a mean oceanic source of  $6.6 \pm 3.6$

<b>Param.</b>	<b>Depth</b>	<b>Temp.</b>
N <sub>2</sub> OPR	101.6 ± 24.4	113.2 ± 24.9
N <sub>2</sub> OPR <sup>denit</sup>	6.9 ± 6.9	6.8 ± 6.8
N <sub>2</sub> OCR <sup>denit</sup>	< 0.1 ± < 0.1	< 0.1 ± < 0.1
N <sub>2</sub> OPR <sup>arctic</sup>	1.2 ± 0.3	1.3 ± 0.3
N <sub>2</sub> OPR <sub>shelf</sub>	0.5 ± 0.2	0.5 ± 0.2
=	110.1 ± 31.8	121.7 ± 32.2
=	(3.1 ± 0.9)	(3.4 ± 0.9)

Table 4.3: Constituents of the annual production of N<sub>2</sub>O below the mixed layer in Gmol N<sub>2</sub>O yr<sup>-1</sup>. The annual subsurface N<sub>2</sub>O yield in Tg N yr<sup>-1</sup> is given in brackets.

Tg N yr<sup>-11</sup> (1  $\sigma$ ) based on gas-exchange parameterisation, surface measurements and models. *Rhee et al.* [2009] estimated a global N<sub>2</sub>O source of 0.9 – 1.7 Tg N yr<sup>-1</sup> based on extrapolation of measurements in the Atlantic Ocean. The annual production of N<sub>2</sub>O is obviously an upper boundary for the annual ocean-atmosphere flux, but our production estimate is clearly situated at the lower end of the given range. Also, we found the cross-thermocline flux of N<sub>2</sub>O in the North Atlantic Ocean calculated from in-situ N<sub>2</sub>O data to be an order of magnitude smaller than the N<sub>2</sub>O flux across the air-sea interface calculated using gas-exchange parameterisations (cf. Chapter 2). Together this indicates, that there either is a systematic bias in at least one of the calculational methods used or that there might be a considerable source of N<sub>2</sub>O in the mixed layer.

### 4.2.3 N<sub>2</sub>O source in the Mixed Layer?

Since the mixed layer is well oxygenated, a significant nitrous oxide source in the mixed layer originating from denitrification processes seems unlikely. Until recently, nitrification was thought to be inhibited by light [*Horrigan et al.*, 1981] – making it a very unlikely occurrence in the mixed layer. The results of *Bange* [2004], who concluded that the surface layer N<sub>2</sub>O saturation in the Arabian Sea is mainly controlled by gas exchange, entrainment of N<sub>2</sub>O from deeper layers and variability in the sea surface temperature, are in line with this.



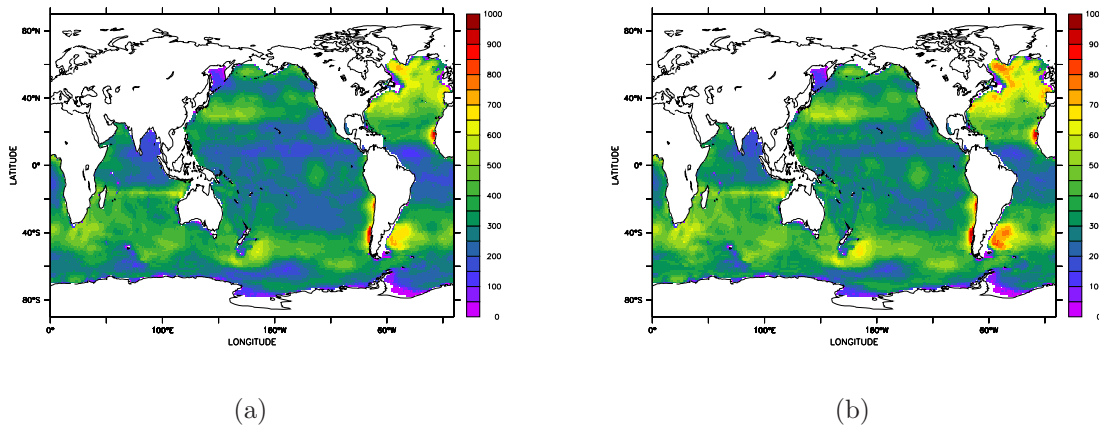


Figure 4.9: Annual  $\text{N}_2\text{O}$  production ( $\mu\text{mol m}^{-2} \text{yr}^{-1}$ ) via nitrification integrated over the water column estimated using Equation 4.1 (a) and Equation 4.2 (b).

It should be noted, however, that assuming a uniform mixed layer depth of 50 m and a ventilation time of  $\text{N}_2\text{O}$  of three weeks [Najjar, 1992], a mixed layer source of  $1 \text{ Tg N yr}^{-1}$  would only lead to an accumulation of  $\sim 0.09 \text{ nmol kg}^{-1}$  in the mixed layer. Assuming a uniform mixed layer depth of 20 m and a mixed layer source of  $1 \text{ Tg N yr}^{-1}$  would only lead to an accumulation of  $\sim 0.2 \text{ nmol kg}^{-1}$  in the mixed layer. These changes could probably not be distinguished from natural variability in the surface, even if the method's precision allowed for their detection.

Model results by Yool *et al.* [2007] based on nitrification measurements suggest something very different. They suggest a significant nitrification activity in the euphotic zone. Clark *et al.* [2008] measured  $\text{NH}_4^+$  and  $\text{NO}_2^-$  oxidation rates on a north-south transect through the Atlantic Ocean. Their data suggest that in the oligotrophic Atlantic Ocean there is nitrification in the photic zone which is of sufficient intensity to turn over the  $\text{NO}_3^-$ -pool in one day.

Dore and Karl [1996] used in-situ measurements of  $[\text{N}_2\text{O}]$  at the ALOHA station and the gas exchange model of Wanninkhof [1992] to calculate  $\text{N}_2\text{O}$  ocean-atmosphere fluxes. They calculated the flux to the euphotic zone using concentration gradients and an eddy-diffusivity coefficient of  $3.7 \cdot 10^{-5} \text{ m}^2 \text{ s}^{-1}$ . They used these flux estimates to calculate a net  $\text{N}_2\text{O}$  production rate in the euphotic zone of  $1.68 - 7.94 \mu\text{mol m}^{-2} \text{ d}^{-1}$ , which they attribute to in-situ nitrification. Assum-

ing a  $\text{N}_2\text{O}$  yield of 0.5% during nitrification, nitrification estimates derived from the  $\text{N}_2\text{O}$  production rate were on the same order of magnitude as their directly measured nitrification rates. Even taking into account the probably rather large uncertainties involved in all the calculations, these results clearly point towards a significant  $\text{N}_2\text{O}$  production via nitrification in the euphotic zone. Slightly larger (super-) saturations of  $\text{N}_2\text{O}$  in the upper 40 m of the water column might even have suggested near-surface production.

*Morell et al.* [2001] calculated the air-sea  $\text{N}_2\text{O}$  flux based on their data from the Atlantic Ocean and the Caribbean Sea in the vicinity of Puerto Rico. They also found a difference between cross-thermocline and air-sea  $\text{N}_2\text{O}$  fluxes in the range of *Dore and Karl* [1996]. They acknowledge that this difference might likely be due to nitrification as indicated by experimental evidence of *Dore and Karl* [1996] and *Dore et al.* [1998]. It should be noted that their calculations are only based on samples from April and June. The difference between their flux estimates might therefore well – at least partly – be due to seasonal thermal effects instead of biological effects (cf. Chapter 3).

While our results seem to point towards a significant  $\text{N}_2\text{O}$  production via nitrification in the euphotic zone, the probably rather large uncertainties involved in all these calculations need to be taken into account. It is worth noting, that commonly used gas exchange parameterisations are a measure of an instant sea to air flux. After the transfer of molecules, the concentration gradient between the surface water and the atmosphere changes, changing the gas transfer in turn. While this is of no consequence to the instant flux across the air-sea interface, it becomes important when an instant gas exchange flux is extrapolated over time. Lacking a term to account for the change in concentration over time, it is implicitly assumed in this kind of calculation that any amount of gas lost to the atmosphere is instantly replaced from below. This might result in an overestimation of the sea to air flux, partly explaining the discrepancy we encountered. Also, in view of the results of Chapter 3, flux estimates based on gas-exchange calculations could be distinctly overestimated as they fail to take the annual cycle of the  $\text{N}_2\text{O}$  flux across the air-sea interface into account. Such an overestimation is even more likely as the underlying datasets are mostly seasonally biased. Nevertheless the possibility of a nitrous oxide source in the mixed layer needs to be

addressed in future work.

### 4.3 Conclusions

1. Predicted apparent oxygen utilisation rates are similar to existing estimates. Using the Redfield ratio of *Anderson and Sarmiento* [1994], we estimate that 17.6 Pg of organic carbon are remineralised in the deep ocean per annum.
2. The predicted N<sub>2</sub>O production rates due to nitrification according to both our suggested parameterisations, N<sub>2</sub>OPR<sub>temp</sub> and N<sub>2</sub>OPR<sub>depth</sub>, show the same qualitative features. However, overall N<sub>2</sub>OPR<sub>temp</sub> estimates slightly higher production than N<sub>2</sub>OPR<sub>depth</sub>. N<sub>2</sub>OPR in the deep ocean is comparatively uniform.
3. The predicted [N<sub>2</sub>O] is qualitatively very similar to the measured [N<sub>2</sub>O] of our database. Concentrations in the Antarctic are slightly elevated, while highest concentrations occur in the North-Eastern Pacific Ocean. Temperature is an important control of qualitative features of [N<sub>2</sub>O] due to its effect on solubility.
4. Our estimates of N<sub>2</sub>O production via denitrification are badly constrained, but despite its locally limited influence, the production yield via denitrification on average amounts to ~ 7% of the total amount of N<sub>2</sub>O produced via nitrification.
5. The annual subsurface N<sub>2</sub>O yield amounts to  $3.1 \pm 0.9$  Tg N yr<sup>-1</sup> (N<sub>2</sub>OPR<sub>depth</sub>) and  $3.4 \pm 0.9$  Tg N yr<sup>-1</sup> (N<sub>2</sub>OPR<sub>temp</sub>), respectively. The annual yield of N<sub>2</sub>OPR<sub>temp</sub> is generally slightly larger than that of N<sub>2</sub>OPR<sub>depth</sub>. The error analysis suggests, that N<sub>2</sub>OPR<sub>temp</sub> estimates the production slightly more accurately.
6. Despite being an upper boundary for the annual air-sea flux of N<sub>2</sub>O, our estimate of the total annual N<sub>2</sub>O subsurface yield is situated at the lower end of the range of recent estimates based on gas exchange parameterisation.

This is likely due to a systematic bias in the gas exchange calculations or possibly to a mixed layer source of  $\text{N}_2\text{O}$ .

# Chapter 5

## Conclusions and Outlook

1. The commonly employed method of using just the contemporary atmospheric mixing ratio of  $\text{N}_2\text{O}$  to calculate the concentration of excess  $\text{N}_2\text{O}$  ( $[\text{N}_2\text{O}]_{xs}$ ) underestimates the strength of possible  $\text{N}_2\text{O}$  sources. Due to this, the quantitative characteristics of the widely used correlation between the apparent oxygen utilisation (AOU) and  $[\text{N}_2\text{O}]_{xs}$  are biased. Especially as the quantitative characteristics of this relationship form the basis for calculation of  $\text{N}_2\text{O}$  production rates, it is of importance to estimate this relationship as accurately as possible. The TTD approach introduced here provides a way to calculate appropriately “age-corrected” excess  $\text{N}_2\text{O}$  concentrations.
2.  $\text{N}_2\text{O}_{xs}^{TTD}$  concentrations found in the North Atlantic are similar to those found in previous studies. Largest concentrations of  $\text{N}_2\text{O}_{xs}$  are found between 700 m and 1000 m. This accumulation of  $\text{N}_2\text{O}_{xs}$  reflects a balance between production and water mass age.
3. We developed a new parameterisation of  $\text{N}_2\text{OPR}$  in terms of an apparent oxygen utilisation rate (AOUR) and temperature/depth and used it to calculate  $\text{N}_2\text{OPR}/[\text{N}_2\text{O}]$  from existing global gridded data (GLODAP/WOA). It differs from earlier parameterisations, as it parameterises a  $\text{N}_2\text{O}$  production rate per timestep in terms of an oxygen utilisation rate per timestep instead of a  $\text{N}_2\text{O}$  production rate per mole oxygen consumed. Our parameterisation can be applied to calculate the  $\text{N}_2\text{O}$  production due to nitrifi-

cation in the entire ocean including the oxygen minimum zones, as AO<sub>UR</sub>, in contrast to AO<sub>U</sub>, tends to become very small at very low oxygen levels.

4.  $p\text{N}_2\text{O}$ , as well as the  $\text{N}_2\text{O}$  flux across the air-sea interface ( $F_{gasex}$ ), seem to follow a seasonal cycle similar to that of  $p\text{CO}_2$ , so that it can be described by a harmonic function. This seasonal cycle is mainly controlled by temperature.
5. The presence of such a harmonic seasonal cycle makes a mean flux, especially one calculated from a seasonally-biased dataset, a very poor estimate of the true annual net flux. Integrating the harmonic function over a full annual cycle gives a much better estimate of the net annual flux. Using extrapolated mean fluxes, the  $\text{N}_2\text{O}$  flux into the mixed layer ( $F_{grad}$ ) is significantly smaller than  $F_{gasex}$  in the North Atlantic Ocean. Using an integrated estimate accounting for the seasonal cycle considerably reduces the difference between the various flux estimates. It results in a net annual ocean-atmosphere  $\text{N}_2\text{O}$  flux of  $-2 \pm 1 \mu\text{mol m}^{-2}$  (LM86) and  $10 \pm 2 \mu\text{mol m}^{-2}$  (W92), respectively, which compare well to the annual mean  $F_{grad}$  of  $3 \pm 1 \mu\text{mol m}^{-2}$ .
6. Even though there is no conclusive evidence for a biologically-controlled seasonal cycle of surface  $p\text{N}_2\text{O}/F_{gasex}$ , the small difference between the two flux estimates of  $-5 \pm 1 \mu\text{mol m}^{-2} \text{ yr}^{-1}$  between  $F_{gasex}^{LM86}$  and  $F_{grad}$  and a difference of  $7 \pm 2 \mu\text{mol m}^{-2} \text{ yr}^{-1}$  between  $F_{gasex}^{W92}$  and  $F_{grad}$  indicates there could be biological effects on  $\text{N}_2\text{O}$  in the mixed layer. However, the difference between the flux estimates could also be due to the 4-months data gap in the seasonal fit, uncertainties in estimating the diapycnal mixing rate or an overestimation of the gas transfer velocity. As the seasonal/latitudinal resolution does not allow for a robust coefficient estimation, the possibility of biological effects on  $p\text{N}_2\text{O}/F_{gasex}$  cannot be ruled out. The small net negative  $F_{gasex}^{LM86}$  is likely due to the 4-months data gap and the resulting uncertainty in the fit. A true net negative annual flux is unlikely because of the vertical profile structure.
7. Compared to an annual subsurface  $\text{N}_2\text{O}$  production of  $14 \pm 10 \mu\text{mol m}^{-2}$

$\text{yr}^{-1}$  calculated at the stations of M60/5, a mixed layer production of  $\text{N}_2\text{O}$  of  $7 \pm 2 \mu\text{mol m}^{-2} \text{yr}^{-1}$  would constitute an important contribution to oceanic  $\text{N}_2\text{O}$  production.

8. Predicted apparent oxygen utilisation rates are similar to existing estimates. Using the Redfield ratio of *Anderson and Sarmiento* [1994], we estimate that 17.6 Pg of organic carbon are remineralised in the deep ocean per annum.
9. The predicted  $\text{N}_2\text{O}$  production rates due to nitrification according to both our suggested parameterisations,  $\text{N}_2\text{OPR}_{temp}$  and  $\text{N}_2\text{OPR}_{depth}$ , show the same qualitative features. However, overall  $\text{N}_2\text{OPR}_{temp}$  estimates slightly higher production than  $\text{N}_2\text{OPR}_{depth}$ .  $\text{N}_2\text{OPR}$  in the deep ocean is comparatively uniform.
10. The predicted  $[\text{N}_2\text{O}]$  is qualitatively very similar to the measured  $[\text{N}_2\text{O}]$  of our database. Concentrations in the Antarctic are slightly elevated, while highest concentrations occur in the North-Eastern Pacific Ocean. Temperature is an important control of qualitative features of  $[\text{N}_2\text{O}]$  due to its effect on solubility.
11. Our estimates of  $\text{N}_2\text{O}$  production via denitrification are badly constrained, but despite its locally limited influence, the production yield via denitrification on average amounts to  $\sim 7\%$  of the total amount of  $\text{N}_2\text{O}$  produced via nitrification.
12. The annual subsurface  $\text{N}_2\text{O}$  yield amounts to  $3.1 \pm 0.9 \text{ Tg N yr}^{-1}$  ( $\text{N}_2\text{OPR}_{depth}$ ) and  $3.4 \pm 0.9 \text{ Tg N yr}^{-1}$  ( $\text{N}_2\text{OPR}_{temp}$ ), respectively. The annual yield of  $\text{N}_2\text{OPR}_{temp}$  is generally slightly larger than that of  $\text{N}_2\text{OPR}_{depth}$ . The error analysis suggests that  $\text{N}_2\text{OPR}_{temp}$  estimates the production slightly more accurately.
13. Despite being an upper boundary for the annual air-sea flux of  $\text{N}_2\text{O}$ , our estimate of the total annual  $\text{N}_2\text{O}$  subsurface yield is situated at the lower end of the range of recent estimates based on gas exchange parameterisations.

This is likely due to a systematic bias in the gas exchange calculations or possibly to a mixed layer source of  $\text{N}_2\text{O}$ .

Our findings emphasise that the marine  $\text{N}_2\text{O}$  cycling, production and emissions are still not well understood, and several important issues need to be investigated further. Air-sea fluxes are usually estimated using empirical air-sea gas exchange parameterisations, which introduces large uncertainties into source estimates. A suite of rather different parameterisations exists, which all fit some experimental dataset, showing that gas exchange itself is highly variable and the governing mechanisms are not yet fully understood. There is, however, also an inherent problem with using any kind of gas-exchange model involving the air-sea gradient of some species to estimate long-term average fluxes. Commonly used gas exchange parameterisations are a measure of an instant sea to air flux. After the transfer of molecules, the concentration gradient between the surface water and the atmosphere changes, changing the gas transfer in turn. While this is of no/little consequence to the instant/short-term flux across the air-sea interface, it becomes important when an instant gas exchange flux is extrapolated over time. Lacking a term to account for the change in concentration over time, it is implicitly assumed in this kind of calculation that any amount of gas lost to the atmosphere from surface waters is instantly replaced from below. Additionally, the use of a simple mean of extrapolated annual fluxes can result in a highly biased flux estimate, if the surface concentrations of the respective species are subject to a seasonal cycle. Both these effects can result in an overestimation of the sea to air flux, partly explaining the slight discrepancy we encountered in Chapters 3 and 4. Additionally, considering the non-linear dependence on wind speed of almost all gas exchange parameterisations, it is at least questionable if the use of averaged wind speeds results in a reasonable estimate of the average air-sea flux.

Independent of a potential bias in the calculational methods, the possibility of a significant source of  $\text{N}_2\text{O}$  in the mixed layer needs to be investigated. The production pathways of  $\text{N}_2\text{O}$  are still poorly understood (cf. Section 1.1.5). It is unclear, how exactly  $\text{N}_2\text{O}$  is produced during bacterial nitrification. *Horrigan et al.* [1981] found that nitrification was inhibited by light, making it an unlikely occurrence in the euphotic zone. Therefore, the  $\text{N}_2\text{O}$  production in the euphotic



zone has been assumed to be zero in virtually all existing (modelling) studies. Lately, observational evidence and model results by *Dore and Karl* [1996], *Dore et al.* [1998], *Morell et al.* [2001], *Yool et al.* [2007] and in Chapters 3 and 4 suggest that this long-prevailing view might have to be questioned. In view of this evidence, estimates of the total oceanic N<sub>2</sub>O source and results concerning the magnitude of local N<sub>2</sub>O production need to be critically reviewed.

Additionally, the existence of diel cycles needs to be investigated. Even if nitrification is inhibited by light, there might still be a significant amount of nitrification during the night time. It should be noted, however, that assuming a uniform mixed layer depth of 50 m and a ventilation time of N<sub>2</sub>O of three weeks [*Najjar*, 1992], a mixed layer source of 1 Tg N yr<sup>-1</sup> would only lead to an accumulation of  $\sim 0.09$  nmol kg<sup>-1</sup> in the mixed layer. Assuming a uniform mixed layer depth of 20 m and a mixed layer source of 1 Tg N yr<sup>-1</sup> would only lead to an accumulation of  $\sim 0.2$  nmol kg<sup>-1</sup> in the mixed layer. These changes could probably not be distinguished from natural variability in the surface, even if the method's precision allowed for their detection. At the moment, laboratory experiments seem to be the only promising available means to investigate this issue.

Also, the oxygen-dependence of bacterial nitrification, which is usually taken for granted, has hardly been investigated. Suggested parameterisations of the N<sub>2</sub>O production during nitrification often [*Nevison et al.*, 2003; *Suntharalingam et al.*, 2000] rely on the only available laboratory study conducted by *Goreau et al.* [1980], who examined a single marine nitrifying organism. As the bacterial community in the ocean probably never consists of only a single organism, it seems rather unlikely that this study accurately captures the characteristics of any ocean regime. Additionally, archaea have lately been suggested as an important producer of N<sub>2</sub>O via nitrification.

Likewise, there is no clear understanding of the oxygen-dependence of denitrification as a source or a sink for N<sub>2</sub>O. While several rather different oxygen thresholds have been suggested, it seems likely that the structure of the bacterial community also wields an important influence on whether denitrification locally acts as a source or a sink for N<sub>2</sub>O. Besides the net behaviour of denitrification as either a source or a sink and the controlling mechanisms, the influence of transport of N<sub>2</sub>O from highly productive regions is still debated controversially [*Nevison et al.*,

2003; *Suntharalingam et al.*, 2000]. Also, the absolute oxygen concentrations in these oxygen minimum zones is changing as well as their volume [*Stramma et al.*, 2008], which might significantly affect the strength of the marine  $\text{N}_2\text{O}$  source.

Coastal areas seem to be important, as they are probably highly productive and as shallow depths allow for  $\text{N}_2\text{O}$  from the sediments to reach the atmosphere. However, they are not included in most existing (modelling) studies, as data in coastal areas is sparse and likely almost completely determined by local conditions. Additionally, it seems unlikely that coastal areas are sufficiently similar to employ extrapolation techniques (as has been done for the open ocean). It therefore seems most important to investigate the role of coastal and riverine areas more closely and collect a sound data base, which in turn facilitates the useful employment of models to investigate cause-effect relationships. This is a central issue of the just started MEMENTO initiative [*Bange et al.*, 2009].

A coherent understanding of production mechanisms, their controlling features and interdependence is needed to model cause-effect relationships. While it is possible to use model data fitted to a sufficiently large set of observations to estimate e.g. the total ocean  $\text{N}_2\text{O}$  source, this type of modelling does not allow to predict the system's reaction to (anthropogenic) perturbations in a changing climate and a changing environment. It therefore seems imperative to better understand the underlying processes and their sensitivities, ideally using a combination of laboratory and open ocean experiments.

# Acknowledgements

I would like to thank Prof. Dr. Wallace for making this thesis possible and for always trying to make time for science, even if his schedule did not really allow for it. Particularly, I am indebted to him for his ideas, which never failed to resolve the particular scientific problem in question.

I am grateful to Dr. Bange for his optimism (and putting up with my scepticism) and his amazing knowledge of literature. He was always up for a discussion and willing to share his knowledge and his ideas. Also, I am incredibly grateful he trusted a mathematician with his lab equipment and made it possible for me to participate in three research cruises, thereby introducing me to the exciting area of oceanographic field work.

Thanks to Dr. Tanhua for sharing his tracer data, his considerable store of helpful MATLAB scripts and for supporting my TTD ambitions, as well as Dr. Walter for sharing her N<sub>2</sub>O data and her views.

There are several other people I would like to thank:

Netti, who was always up for the latest plot (yet another one), a discussion of the newest scientific problem and my lamenting – or just an explanation of some chemical detail I had always wanted to know about.

Anke, who spent several hours discussing the somehow elusive characteristics of TTDs with me – several times all over again.

Tobi, who graciously shared his expertise on  $p\text{CO}_2$  in the North Atlantic and also saved me many hours on literature research.

Axel, who solved my various L<sup>A</sup>T<sub>E</sub>X- and analysis-queries in virtually no time and provided an unfailing incentive for me to work reasonably effectively.

Tessi, who proof-read the complete thesis within one single morning and even spotted lots of typos in the already published manuscript, which had escaped all

the authors' scrutiny before.

Thanks to everyone in FB2-CH, despite being rather “exotic” among chemical oceanographers, I was made to feel welcome among all the chemists, biologists (and an occasional physicist) and never made to feel I was asking stupid questions – although I probably was.

And, of course, thanks to the various people who gracefully listened to my almost constant fretting about this whole Ph.D.-thing and still encouraged me to see it through!

ECMWF ERA-40 data used in this study have been obtained from the ECMWF data server. I wish to acknowledge use of the Ferret program for graphics in this thesis. Ferret is a product of NOAA's Pacific Marine Environmental Laboratory. (Information is available at [http://ferret.pmel.noaa.gov/Ferret/.](http://ferret.pmel.noaa.gov/Ferret/))

This study was supported by the German Science Foundation (DFG) by research grants DFG BA 1990/7, DFG WA 1434/5 and BMBF grant 03F0462A.

# Bibliography

- Alley, R. B., Wally was right: Predictive ability of the North Atlantic “Conveyor belt” hypothesis for abrupt climate change, *Annual Review of Earth and Planetary Sciences*, 35, 241–272, 2007.
- Anderson, L. A., and J. L. Sarmiento, Redfield Ratios of Remineralization Determined by Nutrient Data-Analysis, *Global Biogeochemical Cycles*, 8(1), 65–80, 1994.
- Antonov, J. I., R. A. Locarnini, T. P. Boyer, A. V. Mishonov, and H. E. Garcia, World Ocean Atlas 2005, Volume 2: Salinity, *S. Levitus, Ed. NOAA Atlas NESDIS 62, U.S. Government Printing Office, Washington, D.C.*, p. 182 pp., 2006.
- Bange, H. W., Air-sea exchange of nitrous oxide and methane in the Arabian Sea: A simple model of the seasonal variability, *Indian Journal Of Marine Sciences*, 33(1), 77–83, 2004.
- Bange, H. W., New Directions: The importance of oceanic nitrous oxide emissions, *Atmospheric Environment*, 40(1), 198–199, doi:10.1016/j.atmosenv.2005.09.030, 2006.
- Bange, H. W., Gaseous nitrogen compounds (NO, N<sub>2</sub>O, N<sub>2</sub>, NH<sub>3</sub>) in the Ocean, in *Nitrogen in the Marine Environment, 2nd Edition*, edited by D. G. Capone, D. A. Bronk, M. R. Mulholland, and E. J. Carpenter, pp. 51–94, Elsevier, 2008.
- Bange, H. W., and M. O. Andreae, Nitrous oxide in the deep waters of the world’s oceans, *Global Biogeochemical Cycles*, 13(4), 1127–1135, 1999.

- Bange, H. W., S. Rapsomanikis, and M. O. Andreae, Nitrous oxide in coastal waters, *Global Biogeochemical Cycles*, 10(1), 197–207, 1996.
- Bange, H. W., T. G. Bell, M. Cornejo, A. Freing, G. Uher, R. C. Upstill-Goddard, and G. Zhang, MEMENTO: a proposal to develop a database of marine nitrous oxide and methane measurements, *Environmental Chemistry*, 6(3), 195–197, doi:10.1071/EN09033, 2009.
- Barnett, T. P., D. W. Pierce, K. M. AchutaRao, P. J. Gleckler, B. D. Santer, J. M. Gregory, and W. M. Washington, Penetration of human-induced warming into the world's oceans, *Science*, 309(5732), 284–287, doi:10.1126/science.1112418, 2005.
- Battle, M., et al., Atmospheric gas concentrations over the past century measured in air from firn at the South Pole, *Nature*, 383, 231–235, 1996.
- Bonin, P., C. Tamburini, and V. Michotey, Determination of the bacterial processes which are sources of nitrous oxide production in marine samples, *Water Research*, 36(3), 722–733, 2002.
- Bouwman, A., K. Van der Hoek, and J. Olivier, Uncertainties in the global source distribution of nitrous oxide, *Journal of Geophysical Research*, 100(D2), 2785–2800, 1995.
- Broecker, W. S., Thermohaline circulation, the Achilles heel of our climate system: Will man-made CO<sub>2</sub> upset the current balance?, *Science*, 278(5343), 1582–1588, 1997.
- Broecker, W. S., and T.-H. Peng, Comparison of <sup>39</sup>Ar and <sup>14</sup>C ages for waters in the deep ocean, *Nuclear Instruments and Methods in Physics Research B*, 172, 473–478, 2000.
- Bullister, J., and R. Weiss, Determination of CCl<sub>3</sub>F and CCl<sub>2</sub>F<sub>2</sub> in seawater and air, *Deep-Sea Research Part A*, 35(5), 839–853, 1988.
- Bullister, J., D. Wisegarver, and F. Menzia, The solubility of sulfur hexafluoride in water and seawater, *Deep-Sea Research Part I*, 49(1), 175–187, 2002.

- Butler, J. H., J. W. Elkins, C. M. Brunson, K. B. Egan, T. M. Thompson, T. J. Conway, and B. D. Hall, Trace gases in and over the west Pacific and the east Indian Oceans during the *El Niño* southern oscillation event of 1987, *NOAA Data Report ERL ARL-16*, National Oceanic and Atmospheric Administration, Boulder, Colorado, 1988.
- Butler, J. H., J. W. Elkins, and T. M. Thompson, Tropospheric and dissolved  $N_2O$  of the west Pacific and east Indian Oceans during the *El Niño* southern oscillation event of 1987, *Journal of Geophysical Research*, *94*(D12), 14,865–14,887, 1989.
- Cabello, P., M. D. Roldan, and C. Moreno-Vivian, Nitrate reduction and the nitrogen cycle in archaea, *Microbiology-SGM*, *150*(Part 11), 3527–3546, doi:10.1099/mic.0.27303-0, 2004.
- Chen, M., S. Tsay, K. Chen, Y. Shi, Y. Lin, and G. Lin, *Pseudoxanthomonas taiwanensis* sp nov., a novel thermophilic,  $N_2O$ -producing species isolated from hot springs, *International Journal of Systematic and Evolutionary Microbiology*, *52*(Part 6), 2155–2161, doi:10.1099/ij.s.0.02306-0, 2002.
- Clark, D. R., A. P. Rees, and I. Joint, Ammonium regeneration and nitrification rates in the oligotrophic Atlantic Ocean: Implications for new production estimates, *Limnology and Oceanography*, *53*(1), 52–62, 2008.
- Codispoti, L. A., J. W. Elkins, T. Yoshinari, G. E. Friederich, C. M. Sakamoto, and T. T. Packard, On the nitrous oxide flux from productive regions that contain low oxygen waters, in *Oceanography of the Indian Ocean*, edited by B. N. Desai, pp. 271–284, Oxford and IBH, New Delhi, India, 1992.
- Codispoti, L. A., J. A. Brandes, J. P. Christensen, A. H. Devol, S. W. A. Naqvi, H. W. Paerl, and T. Yoshinari, The oceanic fixed nitrogen and nitrous oxide budgets: Moving targets as we enter the anthropocene?, *Scientia Marina*, *65*(Suppl. 2), 85–105, 2001.
- Cohen, Y., Consumption of Dissolved Nitrous-Oxide in an Anoxic Basin, Saanich Inlet, British-Columbia, *Nature*, *272*(5650), 235–237, 1978.

- Cohen, Y., and L. I. Gordon, Nitrous-Oxide in the Oxygen Minimum of the Eastern Tropical North Pacific – Evidence for its Consumption During Denitrification and Possible Mechanisms for its Production, *Deep-Sea Research*, 25(6), 509–524, 1978.
- Crutzen, P. J., The influence of nitrogen oxides on the atmospheric ozone content, *Quarterly Journal of the Royal Meteorological Society*, 96, 320–325, 1970.
- Crutzen, P. J., and U. Schmailzl, Chemical Budgets of the Stratosphere, *Planetary and Space Science*, 31(9), 1009–1032, 1983.
- DeLong, E. F., Oceans of Archaea, *ASM News*, 69(10), 503–511, 2003.
- Denman, K., et al., Couplings Between Changes in the Climate System and Biogeochemistry, in *Climate Change 2007: The Physical Science Basis. Contribution of Working Group I to the Fourth Assessment Report of the Intergovernmental Panel on Climate Change*, edited by S. Solomon, D. Qin, M. Manning, Z. Chen, M. Marquis, K. B. Averyt, T. M., and H. Miller, Cambridge University Press, Cambridge, United Kingdom and New York, NY, USA, 2007.
- Devol, A. H., Denitrification Including Anammox, in *Nitrogen in the Marine Environment, 2nd Edition*, edited by D. G. Capone, D. A. Bronk, M. R. Mulholland, and E. J. Carpenter, pp. 263–301, Elsevier, 2008.
- Dore, J. E., and D. M. Karl, Nitrification in the euphotic zone as a source for nitrite, nitrate, and nitrous oxide at Station ALOHA, *Limnology and Oceanography*, 41(8), 1619–1628, 1996.
- Dore, J. E., B. N. Popp, D. M. Karl, and F. J. Sansone, A large source of atmospheric nitrous oxide from subtropical North Pacific surface waters, *Nature*, 396, 63–66, 1998.
- Duce, R. A., et al., Impacts of Atmospheric Anthropogenic Nitrogen on the Open Ocean, *Science*, 320, 893–897, 2008.
- Elkins, J. W., S. C. Wofsy, M. B. McElroy, C. E. Kolb, and W. A. Kaplan, Aquatic Sources and Sinks for Nitrous-Oxide, *Nature*, 275(5681), 602–606, 1978.



- Erickson, D. J., Simulation of the global air-sea transfer velocity-field of helium, *Geophysical Research Letters*, 15(13), 1495–1498, 1988.
- Erickson, D. J., A stability dependent theory for air-sea gas exchange, *Journal of Geophysical Research*, 98(C5), 8471–8488, 1993.
- Falkowski, P., et al., The global carbon cycle: A test of our knowledge of earth as a system, *Science*, 290(5490), 291–296, 2000.
- Falkowski, P. G., R. T. Barber, and V. Smetacek, Biogeochemical controls and feedbacks on ocean primary production, *Science*, 281(5374), 200–206, 1998.
- Farias, L., A. Paulmier, and M. Gallegos, Nitrous oxide and N-nutrient cycling in the oxygen minimum zone off northern Chile, *Deep Sea Research I*, 54(2), 164–180, 2007.
- Feely, R. A., C. L. Sabine, R. Schlitzer, B. J. L., S. Mecking, and D. Greeley, Oxygen Utilization and Organic Carbon Remineralization in the Upper Water Column of the Pacific Ocean, *Journal of Oceanography*, 60, 45–52, 2004.
- Flückiger, J., E. Monnin, B. Stauffer, J. Schwander, T. F. Stocker, J. Chappellaz, D. Raynaud, and J. M. Barnola, High-resolution Holocene N<sub>2</sub>O ice core record and its relationship with CH<sub>4</sub> and CO<sub>2</sub>, *Global Biogeochemical Cycles*, 16(1), doi:10.1029/2001GB001417, 2002.
- Flückiger, J. e. a., N<sub>2</sub>O and CH<sub>4</sub> variations during the last glacial epoch: Insight into global processes, *Global Biogeochemical Cycles*, 18, GB1020, doi:10.1029/2003GB002122, 2004.
- Flückinger, J., A. Dallenbach, T. Blunier, B. Stauffer, T. F. Stocker, D. Raynaud, and J. M. Barnola, Variations in atmospheric N<sub>2</sub>O concentrations during abrupt climatic changes, *Science*, 285, 227–230, 1999.
- Forster, G., R. C. Upstill-Goddard, N. Gist, C. Robinson, G. Uher, and E. M. S. Woodward, Nitrous oxide and methane in the Atlantic Ocean between 50°N and 52°S: Latitudinal distribution and sea-to-air-flux, *Deep Sea Research II*, doi:10.1016/j.dsr2.2008.12.0002, 2009.

- Forster, P., et al., Changes in Atmospheric Constituents and in Radiative Forcing, in *Climate Change 2007: The Physical Science Basis. Contribution of Working Group I to the Fourth Assessment Report of the Intergovernmental Panel on Climate Change*, edited by S. Solomon, D. Qin, M. Manning, Z. Chen, M. Marquis, K. B. Averyt, T. M., and H. Miller, Cambridge University Press, Cambridge, United Kingdom and New York, NY, USA, 2007.
- Francis, C. A., J. M. Beman, and M. M. M. Kuypers, New processes and players in the nitrogen cycle: the microbial ecology of anaerobic and archaeal ammonia oxidation, *ISME Journal*, *1*(1), 19–27, doi:10.1038/ismej.2007.8, 2007.
- Garcia, H. E., R. A. Locarnini, T. P. Boyer, and J. I. Antonov, World Ocean Atlas 2005, Volume 3: Dissolved Oxygen, Apparent Oxygen Utilization and Oxygen Saturation, *S. Levitus, Ed. NOAA Atlas NESDIS 63, U.S. Government Printing Office, Washington, D.C.*, p. 342 pp., 2006.
- Goldstein, B., F. Joos, and T. F. Stocker, A modeling study of oceanic nitrous oxide during the Younger Dryas cold period, *Geophysical Research Letters*, *30*(2), doi:10.1029/2002GL016418, 2003.
- Goreau, T. J., W. A. Kaplan, S. C. Wofsy, M. B. McElroy, F. W. Valois, and S. W. Watson, Production of  $\text{NO}_2^-$  and  $\text{N}_2\text{O}$  by Nitrifying Bacteria at Reduced Concentrations of Oxygen, *Applied and Environmental Microbiology*, *40*(3), 526–532, 1980.
- Hibiya, T., and M. Nagasawa, Latitudinal dependence of diapycnal diffusivity in the thermocline estimated using a finescale parameterization, *Geophysical Research Letters*, *31*(1), doi:10.1029/2003GL017998, 2004.
- Holland, E. A., J. Lee-Taylor, C. Nevison, and J. Sulzman, Fluxes and  $\text{N}_2\text{O}$  mixing ratios originating from human activity, data set., <http://daac.ornl.gov/>, 2005.
- Horrigan, S. G., A. F. Carlucci, and P. M. Williams, Light inhibition of nitrification in sea-surface films, *Journal of Marine Research*, *39*(3), 557–565, 1981.

- Houghton, J., G. Jenkins, and J. Ephraums (Eds.), *Climate Change: The Intergovernmental Panel on Climate Change Scientific Assessment*, 364 pp. pp., Cambridge University Press, Cambridge, United Kingdom and New York, NY, USA, 1990.
- Jansen, E., et al., Palaeoclimate, in *Climate Change 2007: The Physical Science Basis. Contribution of Working Group I to the Fourth Assessment Report of the Intergovernmental Panel on Climate Change*, edited by S. Solomon, D. Qin, M. Manning, Z. Chen, M. Marquis, K. B. Averyt, T. M., and H. Miller, Cambridge University Press, Cambridge, United Kingdom and New York, NY, USA, 2007.
- Jenkins, W. J., and D. W. R. Wallace, Tracer Based Inferences of New Primary Production in the Sea, in *Primary Productivity and Biogeochemical Cycles in the Sea*, edited by P. G. Falkowski and A. D. Woodhead, pp. 299–316, Plenum Press, New York, 1992.
- Jin, X., and N. Gruber, Offsetting the radiative benefit of ocean iron fertilization by enhancing N<sub>2</sub>O emissions, *Geophysical Research Letters*, 30(24), doi: 10.1029/2003GL018458, 2003.
- Kara, A. B., P. A. Rochford, and H. E. Hurlburt, An optimal definition for ocean mixed layer depth, *Journal of Geophysical Research*, 105(C7), 16,803–16,821, 2000.
- Karl, D., et al., Dinitrogen fixation in the world's oceans, *Biogeochemistry*, 57(1), 47–98, 2002.
- Karstensen, J., L. Stramma, and M. Visbeck, Oxygen minimum zones in the eastern tropical Atlantic and Pacific oceans, *Progress in Oceanography*, 77(4), 331–350, doi:10.1016/j.pocean.2007.05.009, 2008.
- Kartal, B., M. M. M. Kuypers, G. Lavik, J. Schalk, H. J. M. O. den Camp, M. S. M. Jetten, and M. Strous, Anammox bacteria disguised as denitrifiers: nitrate reduction to dinitrogen gas via nitrite and ammonium, *Environmental Microbiology*, 9(3), 635–642, doi:10.1111/j.1462-2920.2006.01183.x, 2007.

- Key, R. M., et al., A global ocean carbon climatology: Results from Global Data Analysis Project (GLODAP), *Global Biogeochemical Cycles*, 18(4), doi:10.1029/2004GB002247, 2004.
- Knowles, R., Denitrification, *Microbiological Reviews*, 46, 43–70, 1982.
- Könneke, M., A. E. Bernhard, J. R. de la Torre, C. B. Walker, J. B. Waterbury, and D. A. Stahl, Isolation of an autotrophic ammonia-oxidizing marine archaeon, *Nature*, 437(7058), 543–546, doi:10.1038/nature03911, 2005.
- Körtzinger, A., J. Schimanski, U. Send, and D. W. R. Wallace, The ocean takes a deep breath, *Science*, 306(5700), 1337, 2004.
- Kroeze, C., and S. Seitzinger, The impact of land use on  $\text{n}_2\text{o}$  emissions from water-sheds draining into the northeastern Atlantic Ocean and European Seas, *Environmental Pollution*, 102, 149–158, 1998.
- Kroeze, C., and S. P. Seitzinger, Nitrogen inputs to rivers, estuaries and continental shelves and related nitrous oxide emissions in 1990 and 2050: a global model, *Nutrient Cycling in Agroecosystems*, 52(2-3), 195–212, 1998.
- Kroeze, C., E. Dumont, and S. P. Seitzinger, New estimates of global emissions of  $\text{n}_2\text{o}$  from rivers and estuaries, *Journal of Integrative Environmental Sciences*, 2(2-3), 159–165, doi:10.1080/15693430500384671, 2005.
- Kuypers, M. M. M., A. O. Sliemers, G. Lavik, M. Schmid, B. B. Jorgensen, J. G. Kuenen, J. S. S. Damste, M. Strous, and M. S. M. Jetten, Anaerobic ammonium oxidation by anammox bacteria in the Black Sea, *Nature*, 422(6932), 608–611, doi:10.1038/nature01472, 2003.
- Law, C., and R. D. Ling, Nitrous oxide flux and response to increased iron availability in the Antarctic Circumpolar Current, *Deep-Sea Research II*, 48, 2509–2527, 2001.
- Laws, E. A., F. G., W. O. Smith, J. R. H. Ducklow, and J. J. McCarthy, Temperature effects on export production in the open ocean, *Global Biogeochemical Cycles*, 14, 1231–1246, 2000.

- Lee, K., Global net community production estimated from the annual cycle of surface water total dissolved inorganic carbon, *Limnology and Oceanography*, 46(6), 1287–1297, 2001.
- Levitus, S., J. Antonov, and T. Boyer, Warming of the world ocean, 1955 – 2003, *Geophysical Research Letters*, 32(2), doi:10.1029/2004GL021592, 2005.
- Liss, P. S., and L. Merlivat, Air-sea gas exchange rates: Introduction and synthesis, in *The Role of Air-Sea Exchange in Geochemical Cycling*, edited by P. B. Menard, pp. 113–127, D. Reidel, Norwell, Mass., 1986.
- Locarnini, R. A., A. V. Mishonov, J. I. Antonov, T. P. Boyer, and H. E. Garcia, World Ocean Atlas 2005, Volume 1: Temperature, *S. Levitus, Ed. NOAA Atlas NESDIS 61, U.S. Government Printing Office, Washington, D.C.*, p. 182 pp., 2006.
- Longhurst, A., *Ecological Geography of the Sea*, 398 pp. pp., Academic Press, New York, 1998.
- Lüger, H., D. W. R. Wallace, A. Körtzinger, and Y. Nojiri, The  $p\text{CO}_2$  variability in the midlatitude North Atlantic Ocean during a full annual cycle, *Global Biogeochemical Cycles*, 18(3), doi:10.1029/2003GB002200, 2004.
- MacFarling Meure, C., D. Etheridge, C. Trudinger, P. Steele, R. Langenfelds, T. van Ommen, A. Smith, and J. Elkins, Law Dome  $\text{CO}_2$ ,  $\text{CH}_4$  and  $\text{N}_2\text{O}$  ice core records extended to 2000 years BP, *Geophysical Research Letters*, 33(14), doi:10.1029/2006GL026152, 2006.
- Machida, T., T. Nakazawa, Y. Fujii, S. Aoki, and O. Watanabe, Increase in the atmospheric nitrous oxide concentration during the last 250 years, *Geophysical Research Letters*, 22(21), 2921–2924, 1995.
- Maiss, M., and C. Brenninkmeijer, Atmospheric  $\text{SF}_6$ : Trends, sources, and prospects, *Environmental Science & Technology*, 232(20), 3077–3086, 1998.
- Martin, J. H., G. A. Knauer, D. M. Karl, and W. W. Broenkow, VERTEX - Carbon cycling in the Northeast Pacific, *Deep-Sea Research Part A*, 34(2), 267–285, 1987.

- Matsumoto, K., Radiocarbon-based circulation age of the world oceans, *Journal of Geophysical Research – Oceans*, 112(C9), doi:10.1029/2007JC004095, 2007.
- Montegut, C., G. Madec, A. Fischer, A. Lazar, and D. Iudicone, Mixed layer depth over the global ocean: An examination of profile data and a profile-based climatology, *Journal of Geophysical Research–Oceans*, 109(C12), doi:10.1029/2004JC002378, 2004.
- Morell, J. M., J. Capella, A. Mercado, J. Bauzá, and J. E. Corredor, Nitrous oxide fluxes in Carribean and tropical Atlantic waters: evidence for near surface production, *Marine Chemistry*, 74(2-3), 131–143, 2001.
- Mosier, A., C. Kroeze, C. Nevison, O. Oenema, S. Seitzinger, and O. van Cleemput, Closing the global N<sub>2</sub>O budget: nitrous oxide emissions through the agricultural nitrogen cycle - OECD/IPCC/IEA phase II development of IPCC guidelines for national greenhouse gas inventory methodology, *Nutrient Cycling in Agroecosystems*, 52(2-3), 225–248, 1998.
- Moum, J. N., and T. R. Osborn, Mixing in the main thermocline, *Journal of Physical Oceanography*, 16(7), 1250–1259, 1986.
- Najjar, R. G., Marine biogeochemistry, in *Climate System Modeling*, edited by K. E. Trenberth, pp. 241–280, Cambridge University Press, Cambridge, UK, 1992.
- Naqvi, S. W. A., and M. S. Shailaja, Activity of the Respiratory Eelectron-Transport System and Respiration Rates within the Oxygen Minimum Layer of the Arabian Sea, *Deep-Sea Research Part II-Topical Studies In Oceanography*, 40(3), 687–695, 1993.
- Nevison, C., R. F. Weiss, and D. J. Erickson III, Global oceanic emissions of nitrous oxide, *Journal of Geophysical Research*, 100(C8), 809–815, 1995.
- Nevison, C., J. H. Butler, and J. W. Elkins, Global distribution of N<sub>2</sub>O and the  $\Delta$ N<sub>2</sub>O-AOU yield in the subsurface ocean, *Global Biogeochemical Cycles*, 17(4), 1119, doi:10.1029/2003GB002068, 2003.

- Nevison, C. D., T. J. Lueker, and R. F. Weiss, Quantifying the nitrous oxide source from coastal upwelling, *Global Biogeochemical Cycles*, *18*(1), doi:{10.1029/2003GB002110}, 2004.
- Nicol, G. W., and C. Schleper, Ammonia-oxidising Crenarchaeota: important players in the nitrogen cycle?, *Trends in Microbiology*, *14*(5), 207–212, doi:10.1016/j.tim.2006.03.004, 2006.
- Olson, D. B., G. L. Hitchcock, R. A. Fine, and B. A. Warren, Maintenance of the Low-Oxygen Layer in the Central Arabian Sea, *Deep-Sea Research Part II-Topical Studies In Oceanography*, *40*(3), 673–685, 1993.
- Oudot, C., P. Jean-Baptiste, E. Fourré, C. Mormiche, M. Guevel, J.-F. o. Ternon, and P. Le Corre, Transatlantic equatorial distribution of nitrous oxide and methane, *Deep Sea Research – Part I*, *49*(7), 1175–1193, 2002.
- Pacanowski, R. C., and S. G. H. Philander, Parameterization of vertical mixing in numerical models of tropical oceans, *Journal of Physical Oceanography*, *11*(11), 1443–1451, 1981.
- Paulmier, A., D. Ruiz-Pino, and V. Garçon, The oxygen minimum zone (OMZ) off Chile as intense source of CO<sub>2</sub> and N<sub>2</sub>O, *Continental Shelf Research*, *28*(20), 2746–2756, doi:10.1016/j.csr.2008.09.012, 2008.
- Popp, B. N., et al., Nitrogen and oxygen isotopomeric constraints on the origins and sea-to-air flux of N<sub>2</sub>O in the oligotrophic subtropical North Pacific gyre, *Global Biogeochemical Cycles*, *16*(4), doi:{10.1029/2001GB001806}, 2002.
- Prinn, e. a., R.G., The ale/gage/agage network: Db1001, *Carbon Dioxide Information and Analysis World Data Center*, <http://cdiac.esd.ornl.gov/ndps/alegage.html>, 2005.
- Prinn, R., et al., A history of chemically and radiatively important gases in air deduced from ALE/GAGE/AGAGE, *Journal of Geophysical Research*, *105*(D14), 17,751–17,792, 2000.

- Punshon, S., and R. M. Moore, Nitrous oxide production and consumption in a eutrophic coastal embayment, *Marine Chemistry*, *91*(1-4), 37–51, doi:10.1016/j.marchem.2004.04.003, 2004.
- Rhee, T., A. Kettle, and M. Andreae, Methane and nitrous oxide emissions from the ocean: A re-assessment using basin-wide observations in the Atlantic, *Journal of Geophysical Research*, doi:10.1029/2008JD011662, 2009.
- Schlitzer, R., Carbon export fluxes in the Southern Ocean: results from inverse modeling and comparison with satellite-based estimates, *Deep-Sea Research Part II—Topical Studies in Oceanography*, *49*(9-10), 1623–1644, 2002.
- Schlitzer, R., Export production in the equatorial and North Pacific derived from dissolved oxygen, nutrient and carbon data, *Journal of Oceanography*, *60*(1), 53–62, 2004.
- Schmittner, A., and E. D. Galbraith, Glacial greenhouse-gas fluctuations controlled by ocean circulation changes, *Nature*, *456*(7220), 373–376, 2008.
- Schmittner, A., A. Oschlies, H. D. Matthews, and E. D. Galbraith, Future changes in climate, ocean circulation, ecosystems and biogeochemical cycling simulated for a business-as-usual CO<sub>2</sub> emission scenario until year 4000 ad, *Global Biogeochemical Cycles*, *22*, GB1013, doi:10.1029/2007GB002953, 2008.
- Shapleigh, J. (Ed.), *The denitrifying prokaryotes*, Springer Verlag, New York, 2001.
- Steffen, M., A simple method for monotonic interpolation in one dimension, *Astronomy and Astrophysics*, *239*, 443–450, 1990.
- Stramma, L., G. C. Johnson, J. Sprintall, and V. Mohrholz, Expanding oxygen-minimum zones in the tropical oceans, *Science*, *320*(5876), 655–658, doi:10.1126/science.1153847, 2008.
- Suntharalingam, P., and J. Sarmiento, Factors governing the oceanic nitrous oxide distribution: Simulations with an ocean general circulation model, *Global Biogeochemical Cycles*, *14*(1), 429–454, 2000.



- Suntharalingam, P., J. Sarmiento, and J. R. Toggweiler, Global significance of nitrous-oxide production and transport from oceanic low-oxygen zones: A modeling study, *Global Biogeochemical Cycles*, *14*(4), 1353–1370, 2000.
- Tanhua, T., A. Biastoch, A. Körtzinger, H. Lüger, C. Böning, and D. Wallace, Changes of anthropogenic CO<sub>2</sub> and CFCs in the North Atlantic between 1981 and 2004, *Global Biogeochemical Cycles*, *20*(4), GB4017, doi:10.1029/2006GB002695, 2006.
- Tanhua, T., A. Körtzinger, K. Friis, D. Waugh, and D. Wallace, An estimate of anthropogenic CO<sub>2</sub> inventory from decadal changes in oceanic carbon content, *Proceedings of the National Academy of Sciences of the United States of America*, *104*(9), 3037–3042, doi:10.1073/pnas.0606574104, 2007.
- Tanhua, T., D. Waugh, and D. Wallace, Use of SF<sub>6</sub> to estimate anthropogenic CO<sub>2</sub> in the upper ocean, *Journal of Geophysical Research*, *113*(C4), C04,037, doi:10.1029/2007JC004416, 2008.
- Tanhua, T., K. Bulsiewicz, and M. Rhein, Spreading of overflow water from the Greenland to the Labrador Sea, *Geophysical Research Letters*, *32*(10), L10,605, doi:10.1029/2005GL022700, 2005.
- Tiedje, J., Ecology of denitrification and dissimilatory nitrate reduction to ammonium, in *Biology of Anaerobic Microorganisms*, Wiley-Liss, Wageningen, NL, 1988.
- Treusch, A. H., S. Leininger, A. Kletzin, S. C. Schuster, H. P. Klenk, and C. Schleper, Novel genes for nitrite reductase and Amo-related proteins indicate a role of uncultivated mesophilic crenarchaeota in nitrogen cycling, *Environmental Microbiology*, *7*(12), 1985–1995, doi:10.1111/j.1462-2920.2005.00906.x, 2005.
- Walker, S., R. Weiss, and P. Salameh, Reconstructed histories of the annual mean atmospheric mole fractions for the halocarbons CFC-11, CFC-12, CFC-113, and carbon tetrachloride, *Journal of Geophysical Research*, *105*(C6), 14,285–14,296, 2000.

- Walter, S.,  $N_2O$  in the Atlantic Ocean and in the Baltic Sea, Ph.D. thesis, IFM-GEOMAR, Kiel, 2006.
- Walter, S., I. Peeken, K. Lochte, A. Webb, and H. W. Bange, Nitrous oxide measurements during EIFEX, the european iron fertilization experiment in the subpolar south atlantic ocean, *Geophysical Research Letters*, *32*, L23,613, 2005.
- Walter, S., H. W. Bange, U. Breitenbach, and D. W. R. Wallace, Nitrous oxide in the North Atlantic Ocean, *Biogeosciences*, *3*(4), 607–619, 2006.
- Wanninkhof, R., Relationship between wind speed and gas exchange over the ocean, *Journal of Geophysical Research*, *97*(C5), 7373–7382, 1992.
- Wanninkhof, R., and W. McGillis, A cubic relationship between air-sea  $CO_2$  exchange and wind speed, *Geophysical Research Letters*, *26*(13), 1889–1892, 1999.
- Ward, B. B., Nitrification in Marine Systems, in *Nitrogen in the Marine Environment, 2nd Edition*, edited by D. G. Capone, D. A. Bronk, M. R. Mulholland, and E. J. Carpenter, pp. 199–262, Elsevier, 2008.
- Warner, M. J., and R. F. Weiss, Solubilities of chlorofluorocarbons 11 and 12 in water and sea water, *Deep Sea Research Part I*, *32*(12), 1485–1497, 1985.
- Watson, A. J., and J. R. Ledwell, Oceanographic tracer release experiments using sulphur hexafluoride, *Journal of Geophysical Research*, *105*(C6), 14,325–14,337, 2000.
- Waugh, D. W., T. M. Hall, and T. W. N. Haine, Relationships among tracer ages, *Journal of Geophysical Research*, *108*(C5), 3138, 2003.
- Waugh, D. W., T. M. Hall, and T. W. N. Haine, Transport times and anthropogenic carbon in the subpolar North Atlantic Ocean, *Deep-Sea Research Part I*, *51*(11), 1475–1491, 2004.
- Weiss, R., and B. Price, Nitrous oxide solubility in water and seawater, *Marine Chemistry*, *8*(4), 347–359, 1980.

- Weiss, R., F. A. Van Woy, and P. K. Salameh, Surface water and atmospheric carbon dioxide and nitrous oxide observations by shipboard automated gas chromatography: Results from expeditions between 1977 and 1999, *Report – Scripps Institution of Oceanography, Reference 92-11*, 1992.
- Wuchter, C., et al., Archaeal nitrification in the ocean, *Proceedings of the National Academy of Sciences of the United States of America*, *103*(33), 12,317–12,322, doi:10.1073/pnas.0600756103, 2006.
- Yamagishi, H., N. Yoshida, S. Toyoda, B. N. Popp, M. B. Westley, and S. Watanabe, Contributions of denitrification and mixing on the distribution of nitrous oxide in the North Pacific, *Geophysical Research Letters*, *32*(4), doi:10.1029/2004GL021458, 2005.
- Yool, A., A. P. Martin, C. Fernandez, and D. R. Clark, The significance of nitrification for oceanic new production, *Nature*, *447*, 999–1002, doi:10.1038/nature05885, 2007.
- Yoshinari, T., Nitrous oxide in the sea, *Marine Chemistry*, *4*, 189–202, 1976.
- Zeng, J., Y. Nojiri, P. P. Murphy, C. Wong, and Y. Fujinuma, A comparison of  $\delta pCO_2$  distributions in the northern north pacific using results from a commercial vessel in 1995 – 1999, *Deep-Sea Research Part II*, *49*, 5303–5315, 2002.



# Eidesstattliche Versicherung

Ich versichere an Eides statt, dass ich die von mir vorgelegte Dissertation – abgesehen von der Beratung durch meinen Betreuer – selbstständig und ohne unerlaubte Hilfe angefertigt habe und alle benutzten Quellen und Hilfsmittel vollständig angegeben habe. Die Zusammenarbeit mit anderen Wissenschaftlern habe ich kenntlich gemacht. Die Arbeit ist unter Einhaltung der Regeln guter wissenschaftlicher Praxis der Deutschen Forschungsgemeinschaft entstanden. Ferner habe ich weder diese noch eine ähnliche Arbeit an einer anderen Abteilung oder Hochschule im Rahmen eines Prüfungsverfahrens vorgelegt, veröffentlicht oder zur Veröffentlichung vorgelegt.

Kiel, November 13, 2009

---

(Alina Freing)



## Curriculum Vitae

Alina Freing

born 6. Juni 1980 in Hamburg

German

### Publications & Presentations

- 07/09 Freing, A., Wallace, D. W. R., Tanhua, T., Walter, S. und Bange, H. W. (2009), North Atlantic production of nitrous oxide in the context of changing atmospheric Levels, *Global Biogeochemical Cycles*, 23, GB4015, doi: 10.1029/2009GB003472.
- 06/09 Bange, H. W., Bell, T. G., Cornejo, M., Freing, A., Uher, G., Upstill-Goddard, R. C. and Zhang, G., MEMENTO: a proposal to develop a database of marine nitrous oxide and methane measurements, *Environmental Chemistry*, doi: 10.1071/EN09033
- 01/09 Invited talk, *A Global N<sub>2</sub>O Databasse*, COST Action 735 Meeting, Kiel
- 12/07 Invited talk, *A Global Oceanic Nitrous Oxide Databasse*, University of East Anglia, Norwich, United Kingdom
- 10/07 Freing, A. und Bange, H. W., Towards a global database of oceanic nitrous oxide measurements, *IMBER Update*, Issue No. 8

### Research

- 02/08 COST Action Short Term Scientific Mission with Prof. Dr. Nicolas Gruber, ETH Zurich, Switzerland
- 02/07 *Poseidon 348* cruise, Tropical Atlantic
- 07/06-08/06 *Meteor 68/3* cruise, Tropical Atlantic
- 04/06 *Sonne 187/2* cruise, South China Sea

### **Summer Schools**

- 10/07-11/07 “Third international SOLAS Summer School”, Cargese, Corsica,  
France
- 09/07 Eur-Oceans/CarboOcean Summer School “Combining data and  
models – statistical analysis and data assimilation in biogeochemi-  
cal oceanography ”, Kiel

### **University Education**

- since 12/05: Postgraduate studies at the Leibniz-Institute of Marine Sciences  
(IFM-GEOMAR) at the University of Kiel
- 04/05 - 07/05 Research internship at the University of Gent, Belgium
- 10/99 - 02/05 Undergraduate studies in mathematics at the University of  
Würzburg
- 02/05 Degree: Diplom
- 10/02 - 07/03 Undergraduate studies in mathematics at the University of Exeter,  
United Kingdom

### **School Education**

- 08/90 - 07/99 Secondary school, Otto-Hahn-Gymnasium in Geesthacht
- 08/86 - 07/90 Primary school in Geesthacht